Design of a Processing Plant for Direct Lithium Extraction from Geothermal Brines from the Salton Sea Region

A Technical Report submitted to the Department of Chemical Engineering

Presented to the Faculty of the School of Engineering and Applied Science

University of Virginia • Charlottesville, Virginia

In Partial Fulfillment of the Requirements for the Degree

Bachelor of Science, School of Engineering

Beatrice Tremblay

Spring, 2024

Technical Project Team Members
Anna Harris
Lynsey Patterson
Sunya Qamar
Madison Stone

On my honor as a University Student, I have neither given nor received unauthorized aid on this assignment as defined by the Honor Guidelines for Thesis-Related Assignments

Advisor

Eric Anderson, Department of Chemical Engineering

Table of Contents

Executive Summary

Traditional methods of lithium extraction are highly energy, land, and freshwater intensive. Furthermore, much of the lithium in the U.S. is imported, despite the country demonstrating high amounts of domestic lithium reserves. To decrease reliance on externally sourced and often harmful traditional extraction techniques, a new method of lithium sourcing, direct lithium extraction (DLE), is currently being developed. Indeed, Team TELEPORT at the University of Virginia, consisting of Chemical Engineering Professors Geoff Geise, Gaurav "Gino" Giri, and Gary Koenig, have developed a novel sorbent, iron phosphate (FP), that selectively extracts lithium from geothermal brine containing several other competing ions. To assess process viability and direct further research efforts, this project needs to be modeled and analyzed on an industrial scale. Thus, in the following work, we present a design of a processing plant for direct lithium extraction from geothermal brine in the Salton Sea region of California.

In this process, four major unit operations were designed to selectively obtain lithium ions from geothermal brine and generate lithium hydroxide monohydrate. These units consist of adsorption and regeneration, electrodialysis, a fuel cell, and crystallization. In adsorption and regeneration, lithium ions are extracted from the brine, which is obtained from an existing geothermal power plant, and concentrated in a regenerated solution that is sent to electrodialysis. Electrodialysis then uses an applied voltage to promote ionic transfer and form aqueous lithium hydroxide. Hydrogen gas, produced as a side product in electrodialysis, is delivered to a fuel cell that produces electricity to be used in the process. Finally, aqueous lithium hydroxide is crystallized, filtered, and dried in the crystallization unit, which produces the final product: battery grade lithium hydroxide monohydrate.

In the first unit operation, the initial adsorption obtains 99% of the lithium in the provided geothermal brine. To further enrich the stream with lithium ions before it is sent to electrodialysis, subsequent adsorptions are used for previously regenerated solution, which leads to an overall lithium recovery of 81%. In summary, the series of unit operations detailed above work to produce 9,639,139 kg of lithium hydroxide monohydrate annually, leading to a net present value of more than $2 billion USD and a 162% annual return on investment. Current demand for lithium hydroxide monohydrate and the evident economic gain observed from the production of such supports the construction and operation of this plant. This said, we recommend further data collection and process optimization prior to the establishment of large-scale operation.

Section 1: Introduction

Amid growing vehicle electrification efforts, the global market for lithium, a key component in lithium-ion batteries, is projected to rise dramatically. The World Economic Forum estimates that the global demand for lithium will reach more than 3 million metric tons by 2030, a prediction significantly higher than current production capacities (Ying Shan, 2023). With such a rapidly scaling market, the International Energy Agency predicts there will be a global lithium shortage in as few as 2 years (Shine, 2023). Furthermore, while the U.S. has among the highest demonstrated lithium reserves, much of these resources are untapped, with almost the entirety of the lithium in the U.S. being imported. Coupling rapid market growth with significant foreign dependance, the U.S. Department of Energy Geothermal Technologies Office has identified lithium as a "critical mineral" essential to the economic security of the U.S. (Department of Energy, n.d.).

Traditional methods of lithium extraction, including underground or open pit mining, are highly energy, land, and freshwater intensive. Furthermore, current lithium production efforts are concentrated primarily in South America and China where there are less stringent labor laws, leading to human rights violations (Earnshaw-Olser, 2023).

To decrease reliance on externally sourced and often harmful traditional extraction techniques, a new method of lithium sourcing, direct lithium extraction (DLE), is currently being researched by multiple groups. DLE is designed to retrofit to geothermal energy plants, selectively extracting lithium from underground brines before they are reinjected. By incorporating into existing processes, DLE has an added benefit in that it requires less land disturbance than traditional lithium extraction methods (NREL, 2021). Furthermore, water requirements are reduced by relying on the closed loop circulation of underground water.

Presently, DLE has only been executed at small-scales, so the current challenge lies in scaling-up the process to achieve market viability. That said, the focus of this project is to design a commercial-scale lithium extraction process utilizing DLE technology. The process will be designed to retrofit to a geothermal power plant in the Salton Sea region of California. Sometimes described as a "Lithium Valley", this region has the potential to meet over 40% of global lithium demand. Successful lithium production will bring additional revenue to geothermal plants, creating new jobs and making the operation of geothermal plants much more cost-effective (Chao, 2020). The forthcoming proposed process produces battery-grade lithium hydroxide monohydrate ($LiOH \bullet H_2O$), through a series of operations including lithium adsorption and regeneration, electrodialysis, and crystallization.

Section 2: Prior Works

In the past many decades, several direct lithium extraction methods have been proposed, researched, and to some degree, developed. Though existing methods vary widely, most modern approaches fall under one of 5 broad categories: chemical precipitation, solvent extraction, membrane-based separation, electrochemical capture, or selective sorption. Though each method has its benefits, each also has its challenges, particularly regarding scaling up.

Chemical precipitation (CP) is achieved by doping lithium-containing brines with reagents that force supersaturation via chemical reactions. Once supersaturation has been achieved, sequential crystallization can be used to remove competing metal compounds, leaving a high-purity lithium compound as the final product (Murphy and Haji, 2022). Like traditional precipitation extraction, CP's low-cost and ease of industrialization are quite attractive. This said, CP requires large volumes of chemicals, generates large quantities of waste "sludge", and is not suitable for brines with high concentrations of competing salts (Li et al., 2019).

Solvent extraction (SE) separates compounds based on solubility. In this technique, an organic solvent is added to aqueous, lithium-containing brine, at which point organic lithium complexes form. These complexes (along with trace organic impurities) move to the organic phase, which can then be scrubbed, stripped, and then re-extracted. Compared to other DLE methods, SE is attractive in that it can concentrate lithium up to its saturation limit (Murphy and Haji, 2022). That said, SE often requires costly pretreatment to remove impurities that interfere with the efficiency of the extraction process and the purity of recovered lithium. The magnitude of waste generation, and the large volumes of corrosive solvents used are also barriers to using SE (Li et al., 2019). Though these obstacles are important to consider, in terms of scalability, the

paramount barrier is the high cost of effective lithium extraction solvents (Murphy and Haji, 2022).

Membrane-based lithium separation (MBLS) processes, such as nanofiltration, garner praise for their high energy efficiency and ability to operate continuously (Li et al., 2019). Primarily driven by Donnan exclusion, MBLS utilizes engineered membranes to selectively allow lithium ions to permeate while blocking other ions or impurities. This said, the selective transport of lithium compared to competing ions (particularly Mg^{2+} and Na^{+}) becomes challenging in scenarios where the Mg^{2+}/Li^{+} or Na^{+}/Li^{+} ratios are high. Additionally, high capital investments and operating costs along with membrane fouling issues remain as barriers to scaling MBLS (Li et al., 2019).

Electrochemical lithium extraction technologies such as Selective Electrodialysis (ED) rely on electrical potential difference as a driving force for moving ions. By employing alternating monovalent anion and cation exchange membranes and applying a voltage, monovalent anions (primarily Cl^{-}) and cations (predominantly Li^{+}, Na^{+}, and K^{+}) are transported to and concentrated at cells near the anode and cathode, respectively. While selective ED is lauded for its sustainability, recovery capacity, scalability, and efficiency, it is less effective than nanofiltration at monovalent and divalent separations and struggles to distinguish between monovalent cations - a considerable challenge in brines with high Na^{+} to Li^{+} ratios (Li et al., 2019).

Lithium-selective sorbents can be broken down into two main categories: metal compound sorbents and ion imprinted polymers (IEPs). While IEPs have generated some buzz in the academic and industrial communities, their price and synthetic complexity serve as substantial barriers to scalability. Metal compound sorbents, on the other hand, can be

synthesized via simpler processes, and provide impressive lithium selectivity and uptake (Safari et al., 2020). For these reasons, along with a minimal need for brine pretreatment and a limited environmental footprint, metal compound sorption processes are regarded as one of the most suitable candidates for direct lithium recovery (Safari et al., 2020). Among common metal-based sorbents, lithium–manganese oxide and iron phosphate stand out as perhaps the most promising. The direct lithium extraction process proposed in this report is supported and based on research conducted by University of Virginia Chemical Engineering professors Geoffrey Geise, Gaurav Giri, and Gary Koenig. Together with PowerTech water, an industrial partner, they have developed a DLE process which utilizes iron (III) phosphate as a lithium-selective sorbent, and iron chloride to control the redox state of the iron phosphate. While this project is still in the beginning stages of research and development, in September of 2023, the team was awarded one of three DOE American-Made Geothermal Lithium Extraction Prizes. In the Spring of 2023, 2 student-led teams developed and analyzed a process design based on the UVA team's proposed technique. Though important progress was made, data availability limitations posed a real constraint. The process outlined in the coming sections aims to improve upon the previous year's designs by building off their conclusions and utilizing improved data.

Section 3: Discussion

3.0 Process Overview

The following work describes a process for direct extraction of lithium from geothermal brine in the Salton Sea region of southern California. The final product, lithium hydroxide monohydrate ($LiOH \bullet H_2O$), is collected through a series of operations including lithium adsorption and regeneration, electrodialysis, and crystallization. Figure 3.0-1 depicts the block flow diagram to accompany the process.

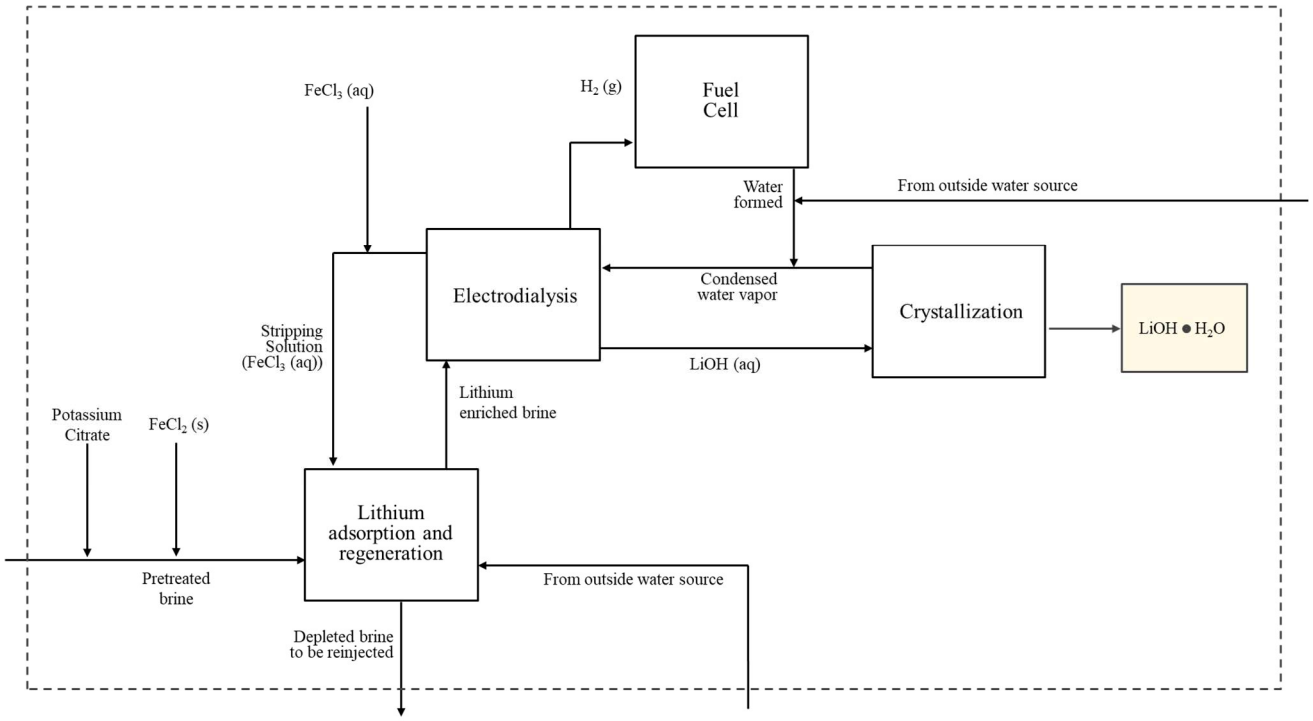

Figure 3.0-1. Generalized process flow diagram.

Geothermal brine is pumped out of underground wells. Due to the drop in pressure as the brine approaches the wellhead, it flashes and produces steam. The steam is sent to be used for power generation, which is outside the scope of this process. The saturated liquid brine is then sent to silica pre-treatment, where silica solids are separated from the brine to prevent scaling in

subsequent unit operations and pipes. Geothermal power plants must treat the brine prior to reinjection, so silica pre-treatment will also not be designed in the above process. As such, the brine entering our process, at 6000 gal/min with a 1:78 molar ratio of lithium ions to sodium ions, will be considered silica-treated at its saturation temperature and atmospheric pressure. The composition of the feed post-silica pre-treatment is depicted in *Table 3.0-1*. The treated brine is first sent to an adsorption and regeneration block where lithium ions are concentrated. The brine, now consisting primarily of lithium and iron chloride, is then directed to electrodialysis where lithium chloride is converted into dilute lithium hydroxide. Finally, the saturated lithium hydroxide undergoes crystallization to produce the product of lithium hydroxide monohydrate. Greater details on the theoretical basis and selected operation conditions for each of the blocks are discussed in the sections to follow.

Table 3.0-1. The components and mass flow rates of the components in the initial feed stream.

Component	Concentration (ppm)	Mass Flow (kg/min)
H_2O	711,364	16,157.00
Cl	154,590	3511.00
Na	58,443	1,327.00
Ca	26,992	613.00
K	14,918	339.00
Fe	1,148	26.10
Mn	1,025	23.30
Mg	736	16.70
Sr	434	9.86
B	332	7.54
Li	287	6.52
Ba	214	4.86

3.1 Lithium Adsorption and Regeneration

3.1.1 Reactions Overview

The adsorbent material used for each packed bed reactor (PBR) is iron phosphate (FP), currently one of the few lithium-ion intercalation materials. Indeed, FP has shown promise with its ion channels providing favorable uptake of lithium ions (J. Wang, personal communication, 2024). Furthermore, FP is extremely useful for selective extraction from geothermal brines specifically, as it can selectively adsorb lithium ions when other divalent ions, such as Mg^{2+}, are present in relatively high concentrations (G. Geise, personal communication, February 12, 2024). The overall reaction occurring across adsorption and regeneration is shown below, with each species' charged state included for reference.

$$Li^+(aq) + Fe^{2+}(aq) + Fe^{3+}PO_4(s) \leftrightarrow LiFe^{2+}PO_4(s) + Fe^{3+}(aq) \text{ (R. 3.1-1)}$$

The direction of the reaction, meaning whether a bed is in the adsorption or regeneration stage, is controlled through the concentrations of iron (II) and iron (III) ions. Such an idea can be explained further by examining each stage individually. The forward reaction, or the adsorption step, can be written in terms of its oxidation and reduction reactions as shown below.

$$\text{Oxidation: } Fe^{2+}(aq) \rightarrow Fe^{3+}(aq) + e^- \text{ (R.3.1-2)}$$

$$\text{Reduction: } Li^+(aq) + Fe^{3+}PO_4(s) + e^- \rightarrow LiFe^{2+}PO_4(s) \text{ (R.3.1-3)}$$

First, iron (II) ions are oxidized, transferring the lost electron to the iron (III) ions present in the FP solid. Due to the charge imbalance, where the FP solid now has a net charge of negative one, a lithium ion is absorbed onto the solid. Regeneration follows a very similar process, with *Reactions 3.1-4 and 5* showing the respective oxidation and reduction reactions.

Oxidation: $LiFe^{2+}PO_4(s) \rightarrow Li^+(aq) + Fe^{3+}PO_4(s) + e^-$ *(R.3.1-4)*

Reduction: $Fe^{3+}(aq) + e^- \rightarrow Fe^{2+}(aq)$ *(R.3.1-5)*

Like adsorption, regeneration begins with an electron transfer step. The iron (II) in FP sorbent releases an electron that is gained by the iron (III) ions present in solution. With an overall positive one charge, the FP releases the lithium ion to regain charge neutrality.

3.1.2 Mixing Unit Design

Mixing tanks help facilitate the addition of solid powder to a previously well-mixed aqueous solution. Multiple mixing tanks were designed for the addition of iron (II) chloride, potassium citrate, and iron (III) chloride powders at varying steps in the process. Iron (II) chloride powder is added to the feed to ensure there are enough iron (II) ions to reduce the iron (III) phosphate sorbent in the primary reactors. Potassium citrate powder is added to the feed and the effluent from primary regeneration to increase the chemical potential and spontaneity of the initial reduction reaction, which is described in further detail in an upcoming section, *3.1.2 Kinetic and Equilibrium Considerations*. Iron (III) chloride powder is added to a stream of water to supplement the recycled aqueous iron (III) chloride from electrodialysis for regeneration of the adsorption beds. The steps and calculations used to design the mixing tanks are detailed throughout the rest of this section.

For the iron (II) chloride and potassium citrate mixing tanks, the expected volumetric flow rate of feed needed to dissolve the solid powder was found using *Equation 3.1-1* below, where $\dot{m}_{solid}$ is the mass flow rate of the solid to be dissolved (g/min), $solubility$ is the solubility of the solid in water at a temperature close to that of the aqueous solution in the

process (g/ml), and $V_{feed,\dot{}mixing}$ is the volumetric flow rate of the feed to send into the mixing tank (ml/min):

$$\frac{\dot{m}_{solid}}{solubility} = \dot{V}_{feed,mixing} \text{ (E 3.1-1)}$$

The volumetric flow rate of water sent into the iron (III) chloride mixing tank was found differently. The difference between the water flow rate provided from electrodialysis to the iron (III) chloride recycle stream and the total water needed to maintain the proper molarity and flow rate of the aqueous iron (III) chloride solution to the regeneration stages was found. That amount of water was used in place of the variable $\dot{V}_{feed,mixing}$ for determining the volume of the iron (III) chloride tank in the equation introduced below.

Additionally, a 10-minute residence time in the mixing tank was assumed based off an advisor's recommendation (E. Anderson, personal communication, March 13th, 2024). The volume of the mixing tank was found using *Equation 3.1-2* below, where V_{mix} is the volume of the mixing tank (m^3), $\dot{V}_{feed,mixing}$ is the volumetric flow rate of the feed or water sent into the mixing tank (m^3/min), and τ is the residence time (min):

$$V_{mix} = \dot{V}_{feed,mixing} \cdot \tau \text{ (E 3.1-2)}$$

All final total mixing tank volumes, including their diameters and heights, were adjusted to the sizes of actual tanks that are available for sale through Protecoplas, a company who provides industrially sized mixing tanks. More information on the final dimensions and number of mixing tanks needed is provided in a forthcoming section on mixing tank design.

3.1.2.1 Impeller Choice and Design

Different impellers are best suited for mixing solutions with varying ranges of viscosities. The feed in this process has a low viscosity like that of water. However, one of the solid components that is added to the feed, specifically potassium citrate, is not very soluble. Potassium citrate is added to the feed at a rate in which its concentration in solution is 50 mM, a value chosen based off research recommendations (J. Wang, personal communication, 2024). Therefore, a pitched blade turbine was chosen for use because it produces a medium shear force in the fluid and is used to mix solutions containing solids (King, 2022). The diameter of the impeller was found using a reported ratio of the diameter of the impeller to the diameter of the tank for a pitched blade turbine in *Equation 3.1-3*, where $d_{impeller}$ is the diameter of the impeller (m) and d_{mixing} is the diameter of the mixing tank (m) found previously (King, 2022):

$$d_{impeller} = d_{mixing} \cdot 0.5 \quad \textit{(E 3.1-3)}$$

3.1.2.2 Mixing Tank Power Requirements

After the size of the mixing tanks and impeller diameters were found, the power to operate each of these tanks was calculated. First, the mass percent of solids in the solution within the mixing tank was found in *Equation 3.1-4*, where $\dot{m}_{solid}$ is the inlet mass flow rate of the solid to be dissolved (kg/min), $\dot{V}_{feed,mixing}$ is the volumetric flow rate of the feed (or water) to send into the mixing tank (m^3/min), and ρ_{fluid} is the density of the fluid to be mixed (kg/m^3):

$$\frac{\dot{m}_{solid}}{2 \cdot \dot{V}_{feed,mixing} \cdot \rho_{fluid} + \dot{m}_{solid}} \cdot 100 = mass\ percent\ of\ solid \quad \textit{(E 3.1-4)}$$

Figure 3.1-1 depicts the minimum required revolutions per minute according to the Zwietering equation, which correlates the minimum speed for solid suspension to other relevant

variables (Ayranci & Kresta, 2014). Lines “SG”, “R”, and “LG” are a series of different solid materials. After analyzing the paper, “R” was determined to be the most like solid powders in this process and therefore was the correlation line used to interpolate for the minimum required revolutions per minute of the impellers.

Impeller speed was based off an extrapolation of *Figure 3.1-1* using the $mass\ percent\ of\ solid$. This decision was discussed and approved by a colleague with industrial experience because mixing power and costs were found to be most sensitive to impeller speed. Due to the significant effect that one variable, impeller speed, had on mixing power and cost, an engineering decision was made to cut the value by half of what would be expected from *Figure 3.1-1*. If this is not done, the economics of this project are still favorable but much less so. The choice to decrease impeller speed by this factor decreased the cost of mixing by approximately $78,000,000 per year and increased the annual return on investment by 47%. It was decided that this engineering decision was best for both conserving power and costs while still promoting production.

A series of assumptions were made to support the decision to decrease chosen impeller speeds. The “R” line portrays a steep downward curve at the beginning of the x-axis, which can be assumed to continually decrease in a vertical fashion before the visible start of the line. Since most of the mixing tanks contained a percent of solids on the lower half of the x-axis, impeller speeds were chosen to be approximately half of what the graph in *Figure 3.1-1* reports. The mixing tanks are operating under the assumption of turbulent flow within the tank, which will also promote solid mixing in aqueous solution. Therefore, impeller speed was decreased due to these points and the need to conserve both energy and costs as much as possible.

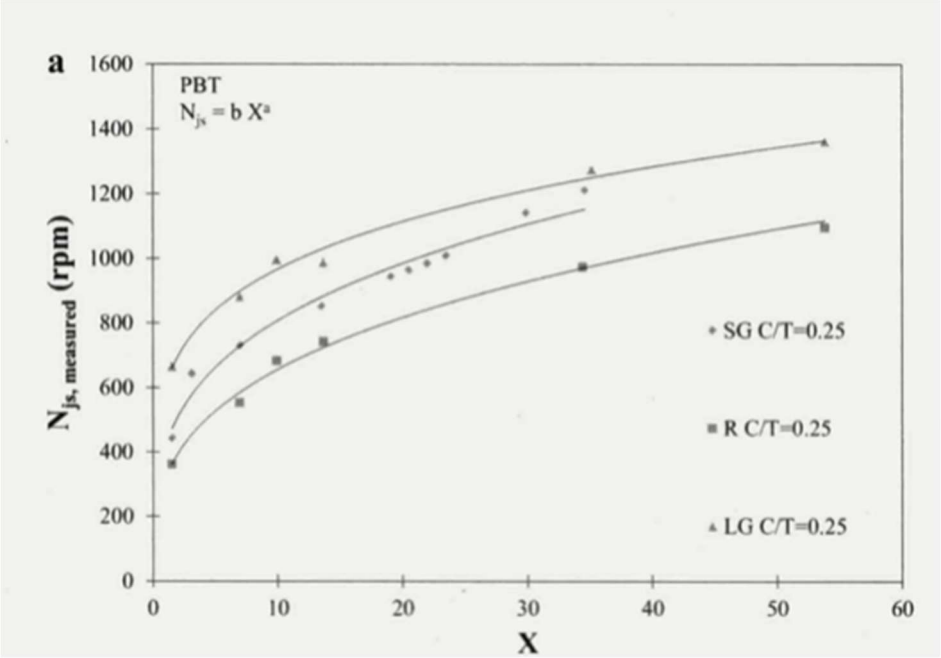

Figure 3.1-1. Recommended impeller speeds versus mass percent of solid in solution for a series of materials that are specified in detail in the literature source that published this graph (Ayranci & Kresta, 2014).

After estimating the speed of the impellers, the Reynolds number for mixing was found in *Equation 3.1-5*, where N_{Re} is the Reynolds number for mixing, n is the impeller speed (rev/s), $d_{impeller}$ is the impeller diameter (m), ρ_{fluid} is the density of the fluid to be mixed (kg/m^3), and μ_{fluid} is the viscosity of the fluid to be mixed (Pa·s):

$$N_{Re} = \frac{n{d_{impeller}}^2 \rho_{fluid}}{\mu_{fluid}} \quad (E\ 3.1\text{-}5)$$

The Reynolds number for mixing was used with the graph in *Figure 3.1-2* that specifies Power number versus Reynolds number for mixing for a pitched blade turbine impeller. *Equation 3.1-6* depicts the Power number for mixing from which the power was found, where N_P is the power number for mixing, P is the power (W), and n , $d_{impeller}$, and ρ_{fluid} are as defined for the previous equation:

$$N_P = \frac{P}{n^3 {d_{impeller}}^5 \rho_{fluid}} \text{ (E 3.1-6)}$$

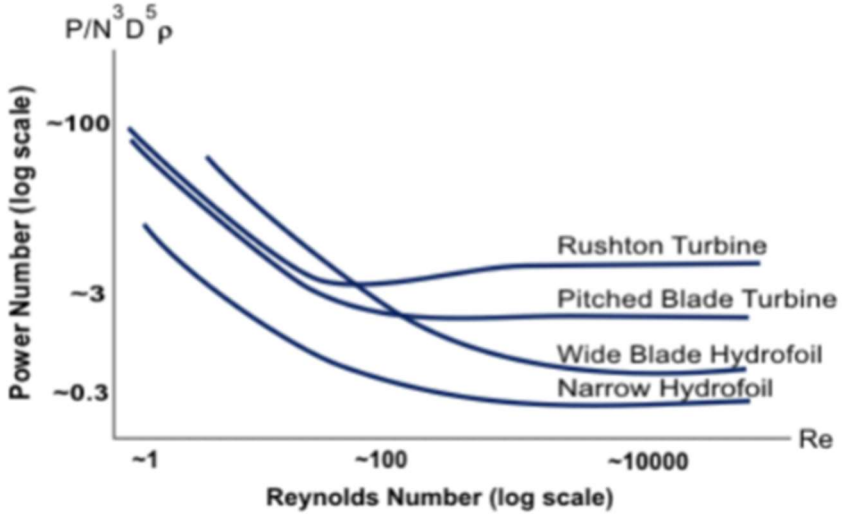

Figure 3.1-2. Power Number versus Reynolds Number for Select Turbine Styles.

3.1.3 Packed Bed Reactor Network Design

3.1.3.1 Primary Reactor Design

Designing a packed bed reactor involves optimizing reactor size and materials cost while considering the velocity of the fluid traveling into the vessel and overall pressure drop within the bed. In this primary reactor design, select values were chosen as independent variables to create a packed bed reactor that could carry out the adsorption and regeneration steps while using the feed flow provided by an external geothermal power plant in the Salton Sea Region.

The independent variables for primary reactor design were the number of beds that accept feed at a given time, superficial velocity of the fluid feed, and adsorption capacities of lithium and sodium ions in iron (III) phosphate. The number of beds selected determined the volumetric flow rate of the feed to each bed, as shown in *Equation 3.1-7*, where $\dot{V}_{bed}$ is the volumetric flow rate

of the feed to one primary reactor (m^3/hr) and $\dot{V}_{overall}$ is the original volumetric flow rate of the brine.

$$\dot{V}_{bed} = \frac{\dot{V}_{overall}}{number\ of\ beds} \textit{ (E 3.1-7)}$$

The next value needed was superficial velocity of the fluid feed, which was selected as 0.0025 m/s due to optimization between industrial standard fluid velocity recommendations, bed diameter, and lithium capture (Gabelman, 2017). Using $\dot{V}_{bed}$ and the chosen superficial velocity, u (m/s), the diameter of one individual packed bed reactor, d_{bed} (m) was found using *Equation 3.1-8.*

$$d_{bed} = \sqrt{\frac{\dot{V}_{bed}}{\pi u}} \textit{ (E 3.1-8)}$$

The height and volume of the primary reactor were found by changing the length to diameter (L/D) ratio of the packed bed reactor and ensuring the pressure drop within the bed did not surpass 10 bar. Industry standard packed bed reactors typically use L/D ratios of 2-5, which provided a range in which to start testing L/D ratios versus pressure drop. Pressure drop was calculated in *Equation 3.1-9* below, where dP is the overall pressure drop (Pa), f_f is the dimensionless friction factor, ρ is the density of the brine (kg/m^3), u is the superficial velocity of the fluid (m/s), d_p is the diameter of the sorbent particle (m), and dz is the length of the reactor (m).

$$-\frac{dP}{dz} = \frac{f_f \rho u}{d_p} \textit{ (E 3.1-9)}$$

Dimensionless friction factor, f_f, was found with *Equations 3.1-10* and *3.1-11*, in which $\overline{\varepsilon}_b$ is the porosity of the iron (III) phosphate sorbent particles, and the Reynolds number, Re , is calculated using previously defined variables and the viscosity of the brine (Pa·s), μ.

$$f_f = \frac{(1-\overline{\varepsilon}_b)}{\overline{\varepsilon}_b}\left[1.75 + \frac{150(1-\overline{\varepsilon}_b)}{Re}\right] \textit{(E 3.1-10)}$$

$$Re = \frac{\rho u d_p}{\mu} \textit{(E 3.1-11)}$$

The density of the brine was found by adding the concentration of solids and liquid in the brine using the component mass flow rates in Table 3.0-1 and the total volumetric flow. The viscosity of the brine was assumed to be that of water at a temperature of 75 C.

After optimizing the bed height based on pressure drop and using the equations described above, the volume of the packed bed reactor, V_{bed} (m^3), was calculated with *Equation 3.1-12*.

$$V_{bed} = \pi\left(\frac{d_{bed}}{2}\right)^2 dz \textit{(E 3.1-12)}$$

The amount of iron (III) phosphate sorbent needed to fill one primary reactor was assumed to be the same as V_{bed}. After setting the volume of sorbent required equal to V_{bed}, the mass of sorbent in each bed, $m_{sorbent}$ (kg), was found in *Equation 3.1-13*, where $\overline{\varepsilon}_b$ is the porosity of the iron (III) phosphate sorbent particles, $V_{sorbent}$ is the value of V_{bed} (m^3), and $\rho_{sorbent}$ is the bulk density of the sorbent (kg/m^3).

$$\mathrm{m_{sorbent}} = \mathrm{V_{sorbent}}(1-\overline{\varepsilon}_\mathrm{b})\rho_\mathrm{sorbent} \textit{(E 3.1-13)}$$

3.1.3.2 Primary Adsorption and Regeneration Times

The variables used in the previous section also apply to this section. After primary reactor design, the adsorption and regeneration times could be determined using previously discovered values and assuming that the flow rate of stripping solution, iron (III) chloride, is an independent variable.

Using $m_{sorbent}$ and the sorbent capacities of lithium and sodium ions ($Li^+\ capacity$ and $Na^+\ capacity$ in mmol/g) provided by a personal communication, the theoretical amount of lithium and sodium ions obtained in the bed ($Li^+\ adsorbed$ and $Na^+\ adsorbed$ in mmol) per $m_{sorbent}$ was found using *Equations 3.1-14a and 14b* (J. Wang, personal communication, 2024).

$$Li^+\ adsorbed\ =\ Li^+\ capacity \cdot m_{sorbent} \cdot 1000 \quad \textit{(E 3.1-14a)}$$

$$Na^+\ adsorbed\ =\ Na^+\ capacity \cdot m_{sorbent} \cdot 1000 \quad \textit{(E 3.1-14b)}$$

It was assumed that 99% of $Li^+\ adsorbed$ is captured in the primary reactor to account for realistic losses. Finally, using the given mass flow rate of lithium ions in brine, $\dot{m}_{Li^+,feed}$ (kg/hr), the amount of time needed to provide 99% of $Li^+\ adsorbed$ was used to find the necessary adsorption time, t_{ads} (hr), in *Equation 3.1-15*.

$$\dot{m}_{Li^+,feed} = \frac{0.99 \cdot Li^+ adsorbed}{t_{ads}} \quad \textit{(E 3.1-15)}$$

To regenerate the adsorbed lithium and sodium ions in the primary reactor, one mole of iron (III) ions is required per mole of $Li^+\ adsorbed$ and $Na^+\ adsorbed$. Therefore, the total molar amount of iron (III) ions in the regeneration fluid, $Fe^{3+}\ in\ regneration\ fluid$ (mol), is the sum of $Li^+\ adsorbed\ and\ Na^+\ adsorbed$ (mol) seen in *Equation 3.1-16*. The molar flow

rate of iron (III) ions, $\dot{n}_{Fe^{3+}}$, is a chosen design variable that determined the regeneration time, t_{regen}, in *Equation 3.1-17.*

$$Fe^{3+}\ in\ regneration\ fluid\ =\ Li^{+}\ adsorbed\ +\ Na^{+}\ adsorbed \quad (E\ 3.1\text{-}16)$$

$$\dot{n}_{Fe^{3+}} = \frac{Fe^{3+}\ in\ regeneration\ fluid}{t_{regen}} \quad (E\ 3.1\text{-}17)$$

3.1.3.3 Secondary Reactor Design Process

Designing the secondary reactor followed a process like the one seen in *Section 3.1.3.2*, with a few differences in the amount of lithium and sodium ions absorbed on the bed and thus changes to the adsorption and regeneration scheduling time. While the primary reactors obtain most of the lithium ions delivered throughout one cycle of this process, the secondary reactors work to achieve the desired molar ratio of 100:1 lithium to sodium ions in the feed going to electrodialysis. Choosing to design secondary reactors that are smaller than the primary reactors decreased sorbent material costs and provided a convenient scheduling block for equipment maintenance, both of which are explained further in the *Economics* and *4.1.2 Scheduling* sections of the report, respectively.

The volumetric flow rate to the bed relied on the previous assumption that the concentration of iron (III) chloride in the regeneration fluid to the primary bed was 1 M. *Note 3.1-1: Although this metric changed once the electrodialysis block was designed after this unit and determined the recycle stream of iron (III) chloride to be approximately 0.5 M, the original sizing of the secondary beds was still sufficient and therefore was left as is.* After the regeneration fluid passes through the primary bed during primary regeneration, the iron (III) ions are reduced to iron (II) ions and flow with stripped lithium and sodium ions to the first secondary adsorption step. Assuming that the molar amount of lithium and sodium ions adsorbed was equal

to the molar amount of iron (III) ions reduced to iron (II) ions in the primary regeneration phase and that the regeneration solution is a 1 M aqueous solution of iron (III) chloride *(refer to Note 3.1-1 above)*, an overall volumetric flow rate to first secondary adsorption, $\dot{V}_{bed,2}$ (L/min) was determined using the molar flow rate of iron (III) chloride, $\dot{n}_{FeCl_3}$ (mol/min), depicted in *Equation 3.1-18*.

$$\dot{V}_{bed,2} = \frac{\dot{n}_{FeCl_3}}{1\ M} \textit{ (E 3.1-18)}$$

After the volumetric flow rate to one secondary bed was determined, the design process proceeded in the same manner as the primary design process did from the steps involving *Equations 3.1-1 to 3.1-13*. The difference between primary and secondary bed design was due to a change in the original $Li^+\ capacity$ and $Na^+\ capacity$. The original sorbent capacity for lithium and sodium ions was provided by a personal research communication who studied lithium uptake in iron (III) phosphate sorbent when the adsorption feed was at a 1:78 molar ratio of lithium to sodium ions (J. Wang, personal communication, 2024). However, using the selectivity value for lithium in the iron (III) phosphate sorbent, the molar ratio of lithium to sodium ions in the regenerated solution exiting the primary reactor and entering the secondary reactor is 5:1. The same source mentioned previously found that when the concentration of lithium to sodium ions in solution increased to a 1:1 molar ratio, $Li^+\ capacity$ increased and $Na^+\ capacity$ decreased. In a solution concentrated solely with lithium ions, the sorbent capacity change was negligible. Through this phenomenon, the secondary reactor was able to provide a highly purified solution during its regeneration step of approximately 2000:1 molar ratio of lithium to sodium ions. *Equation 3.1-19* depicts the relationship between sorbent capacity and selectivity provided by a personal communication, in which S is the dimensionless

selectivity towards lithium adsorption in the sorbent, $\frac{c_{Li^+,sorbent}}{c_{Na^+,sorbent}}$ is the relative concentration of lithium to sodium ions adsorbed on the sorbent, and $\frac{c_{Li^+,feed}}{c_{Na^+,feed}}$is the relative concentration of lithium to sodium ions in the feed that is to be adsorbed (J. Wang, personal communication, 2024).

$$S = \frac{\left(\frac{c_{Li^+,sorbent}}{c_{Na^+,sorbent}}\right)}{\left(\frac{c_{Li^+,feed}}{c_{Na^+,feed}}\right)} \textit{(E 3.1-19)}$$

3.1.3.4 Secondary Adsorption and Regeneration Times

The combination of changing design values and sorbent capacities in the secondary reactor led to variances in adsorption and regeneration times and incoming and outgoing flow rates. Using *Equation 3.1-14*, $Li^+ \, adsorbed$ and $Na^+ \, adsorbed$ were found. The first secondary adsorption is the same amount of time as primary regeneration, because the primary regeneration expenditure fluid becomes the adsorption feed for the first secondary adsorption. In other words, secondary adsorption cannot begin until feed is provided from the primary regeneration step.

While primary adsorption and primary wash are undergoing and the secondary bed is waiting for more feed, the feed that was not adsorbed onto the sorbent during first secondary adsorption is sent to a holding tank and recycled for 4 more subsequent adsorptions. These adsorptions are kept at 15 hours based off recommendation from a personal communication (J. Wang, personal communication, 2024). The t_{regen} for material captured during the secondary adsorptions was found using *Equations 3.1-16* and *3.1-17* among the same previously mentioned assumptions for that calculation.

3.1.4 Kinetic and Equilibrium Considerations

3.1.4.1 Electrochemical Cell Potential and Gibbs Free Energy of Reaction

The overall reversible reaction occurring in the packed bed reactor is also known as a redox reaction. One redox reaction is composed of an oxidation and reduction step, both called half reactions. The forward (adsorption) and reverse (regeneration) reactions separated into their subsequent half reactions are as follows:

Forward reaction (adsorption)

Reduction: $Li^+(aq) + Fe^{3+}PO_4(s) + e^- \rightarrow LiFe^{2+}PO_4(s)$ *(R.3-6)*

Oxidation: $Fe^{2+}(aq) \rightarrow Fe^{3+}(aq) + e^-$ *(R.3-7)*

Reverse reaction (regeneration)

Reduction: $Fe^{3+}(aq) + e^- \rightarrow Fe^{2+}(aq)$ *(R.3-8)*

Oxidation: $LiFe^{2+}PO_4(s) \rightarrow Li^+(aq) + Fe^{3+}PO_4(s) + e^-$ *(R.3-9)*

For the above redox process to occur, the half reactions must be spontaneous. Reaction spontaneity depends on the rate of electron transfer, which is discovered using electrochemical cell potential. Electrochemical cell potential, or E^o_{cell}, determines the voltage at which electron transfer occurs in a redox reaction. In other words, it quantifies the "driving force" between the half reactions in Volts (LibreTexts). The E^o_{cell} of the reaction at standard conditions is calculated as follows in *Equation 3.1-20*:

$$E^o_{cell} = E^o_{reduction} - E^o_{oxidation} \text{ (Eq. 3.1-20)}$$

$E^{o}_{reduction}$ and $E^{o}_{oxidation}$ are the electrochemical cell potentials (V) of the reduction and oxidation half reactions, respectively, for either the forward or reverse reaction. These values are found in cyclic voltammetry experiments with respect to a standardized anode and cathode. Standardized electrochemical cell potentials for the half reactions occurring between the anode and the cathode provide a basis for the difference in voltage between the known standard reaction and an unknown, experimental redox reaction. In this section of the report, values found were with respect to Ag^{+} and AgCl.

The E^{o}_{cell} values are used further to compute the non-standard electrochemical cell potential with the Nernst equation, since this reaction system is held at non-standard temperature and pressure. The Nernst equation is depicted in *Equation 3.1-21* below for both the forward and reverse reactions:

Forward reaction (adsorption)

$$E_{cell} = E^{o}_{cell} - \frac{RT}{nF}\ln\left(\frac{[Fe^{3+}]}{[Fe^{2+}]}\right) \textit{ (E 3.1-21a)}$$

Reverse reaction (regeneration)

$$E_{cell} = E^{o}_{cell} - \frac{RT}{nF}\ln\left(\frac{[Fe^{2+}]}{[Fe^{3+}]}\right) \textit{ (E 3.1-21b)}$$

In *Equation 3.1-21*, R is the ideal gas constant (J/mol·K), T is the temperature of the system (K), n is the number of electrons transferred from the reducing agent to the oxidizing agent, and F is Faraday's constant (Coulombs/mol). The Nernst equation for the forward reaction includes the ratio of the concentration of iron (III) ions to iron (II) ions because the electron is being driven to the iron (III) ions, which are reduced while acting as the oxidizing agent. The opposite occurs in the reverse reaction and leads to the inversion of the fraction in the natural log component of the formula.

An innate problem with the forward reaction in this system is that the transfer of an electron from iron (II) to iron (III) isn't spontaneous unless a redox mediator is added. In other words, the "driving force" between iron (II) and iron (III) is too low to reduce iron (III) phosphate if a redox mediator isn't added into the feed that is to be adsorbed (J. Wang., personal communication, 2024). However, the forward reaction in this system is spontaneous when using potassium citrate redox mediator (J. Wang., personal communication, 2024). It decreases the potential of the $E^{o}_{oxidation}$ value of the forward reaction by acting as an unreactive "driving force". Thus, potassium citrate is added to the feeds for both the primary adsorptions and first secondary adsorptions in this system.

Despite the addition of potassium citrate to the feed, the E^{o}_{cell} values in this system change with the concentrations of iron (II) and iron (III) ions in the brine. These changes are found in the $E^{o}_{oxidation}$ value of the forward reaction and consequently change the Nernst potential for adsorption depending on the iron (II) and iron (III) ion concentrations in the brine. To determine such changes in the $E^{o}_{oxidation}$ values, a colleague provided a graph depicting the electrochemical cell potential (V vs. Ag/AgCl) of the forward reduction reaction versus iron (II) ion percentage in brine with a molar ratio of 1:78 Li^{+}:Na^{+} (A. Hawkins, personal communication, February 14, 2024). The graph was created from data that studied the forward reduction reaction after EDTA, a redox mediator, was added to the feed. Therefore, the $E^{o}_{oxidation}$ values for the forward reaction involving citrate were approximated from this graph by subtracting the voltage difference between the two half reactions vs. Ag/AgCl. The paper reported that the half-cell voltage difference between the two redox mediators, EDTA and citrate, was 0.04 V. Therefore, any $E^{o}_{oxidation}$ value found on the graph at the respective iron (II)

ion percentage in the primary and secondary adsorption feeds was decreased by 0.04 V and used as an approximation.

The Nernst potential was used to discover Gibbs' Free Energy of the forward and reverse reactions and subsequently prove their spontaneity. The Gibbs Free Energy of reaction was calculated using *Equation 3.1-22,* where ΔG is Gibbs Free Energy (J/mol), n is the number of electrons transferred, and F is Faraday's constant (coulombs/mol).

$$\Delta G = -nFE_{cell} \text{ (E 3.1-22)}$$

From finding the standard electrochemical cell potential of the overall forward and reverse reactions, applying the Nernst equation to discover how non-standard conditions affects the reaction potential, and using the Nernst cell potentials to discover Gibbs Free Energy, the reactions were deemed spontaneous.

3.1.4.2 Equilibrium Constant

After acquiring Gibbs Free Energy values for the forward and reverse reactions described in the previous section, the equilibrium constant of the overall reversible reaction was found in *Equation 3.1-23*, where R is the ideal gas constant (J/mol·K), and T is temperature (K).

$$K_{eq} = e^{\left(-\frac{\Delta G}{RT}\right)} \text{ (E 3.1-23)}$$

All the K_{eq} values for the forward and reverse reactions at each step in the process were magnitudes of tens of thousands to millions, indicating fast and favorable forward reactions. The forward and reverse reaction are assumed to proceed at the same rate as first order reactions (G. Koenig, personal communication, Jan. 2024). A personal communication provided data on the change in iron (III) ion concentration in regeneration fluid during the reverse reaction of this

process on a laboratory scale. Using the changing concentrations in iron (III) ions in this experiment and assuming the reverse reaction is first order with respect to iron (III) ions, *Equations 3.1-24 to 3.1-26* were used to find an average reverse rate constant.

$$\frac{d[Fe^{3+}]}{dt} = k_{regen}[Fe^{3+}] \text{ (E 3.1-24)}$$

$$\int \frac{d[Fe^{3+}]}{[Fe^{3+}]} = k_{regen} \int dt \text{ (E 3.1-25)}$$

$$\ln([Fe^{3+}]) = k_{regen}t + \ln([Fe_0^{3+}]) \text{ (E 3.1-26)}$$

Using the relationship between K_{eq} and the rate constants depicted in *Equation 3.1-27* below, the forward rate constants, k_{ads} could be found.

$$K_{eq} = \frac{k_{ads}}{k_{regen}} \text{ (E 3.1-27)}$$

3.1.5 Diffusion Considerations

3.1.5.1 Biot Number

The extent to which diffusion affects the adsorption and regeneration reactions can be investigated by the Biot number. The Biot number is a dimensionless number representing the relationship between the internal and external mass transfer resistances (Carta, 2021). In other words, it is the ratio of the internal diffusive resistance to the external convective resistance, with its magnitude signifying which resistances are dominant. The Biot number was found by using *Equation 3.1-28* where k_c is the external convective mass transfer coefficient, R is the radius of the FP sorbent, $D^e_{A,B}$ is the effective diffusivity of the solute A in solvent B, and K_c is the distribution coefficient.

$$Bi = \frac{k_c \cdot R}{D^e_{A,B} \cdot K_c} \text{ (E 3.1-28)}$$

For adsorption, it was aimed to determine if the diffusion of lithium ions, either from the bulk fluid to the surface of the adsorbate or from the surface of the adsorbent through its pores, hindered the rate of the adsorption reaction in a significant way. The Biot numbers calculated for each adsorption stage are shown in *Table 3.1-1*. It is seen that all values were found to be relatively smaller than one, signifying that the external convective resistances are dominant. In other words, due to the high favorability of adsorption and the dilute nature of each stream, lithium ions have a greater difficulty diffusing through the bulk fluid than diffusing through the FP pores.

Table 3.1-1. Biot Number for each Stage.

Stage	Biot Number
Primary adsorption	0.000000206
1st Secondary Adsorption	0.000000834
2nd Secondary Adsorption	0.0000235
3rd Secondary Adsorption	0.000122
4th Secondary Adsorption	0.000397
5th Secondary Adsorption	0.00104
Regeneration	0.0000272

The regeneration stage differs in that it focuses on the diffusion of iron (III) ions, and diffusion limitations were taken into consideration by evaluating the Biot number for all regeneration steps as described above. Due to the parameters needed, reasonable approximations were able to be made such that all regeneration steps were able to be considered as having the same Biot number. The one Biot number for regeneration is shown at the bottom of *Table 3.1-1*. Like adsorption, the external convective resistances are dominant.

Although each bed in the PBR network was sized without the influence of diffusion limitations and focused on other parameters, such as pressure drop, the idea that external mass transfer resistances influence the adsorption and regeneration reactions can still be utilized. More specifically, it may be wished in future iterations of this work that the amount of lithium ions obtained in one of the PBRs is increased. One way this might be done is to increase bed length, however, it can be seen in *Equation 3.1-9* that pressure drop has a direct relationship with PBR length. The increase in pressure drop may be balanced by increasing the FP pellet size, with a larger pellet size leading to a smaller pressure drop. The influence of FP size, or diameter, on Biot number must then be examined. By increasing pellet diameter, the influence of internal resistances grows. Thus, it is important to realize that although diffusion limitations did not directly influence the above PBR network, they can be useful in improving upon the methods suggested above.

3.1.6 Ancillary Equipment Design

Operating the packed bed reactors requires ancillary equipment, including pumps, holding tanks, silos, and heat exchangers. The following section details the steps and calculations behind the design for each of these pieces of supplementary equipment.

3.1.6.1 Pump Design

Pumps are designed to transport a volumetric flow rate of fluid while accounting for the possible pressure drop the fluid will experience in the subsequent unit. The steps and calculations used to design the centrifugal pumps in this process are detailed in the following. First, the volumetric flow rate expected to pass through the pump was found. Next, the differential pressure that the pump must account for was found. The differential pressure includes the pressure drop, frictional losses, and gravitational pressure changes that a fluid may experience

when moving from one place to another. If the fluid to be pumped is going to pass through a unit and experience a pressure drop, *Equation 3.1-9* is used to calculate dP . If the fluid is to be pumped through a pipe or heat exchanger, 0.5 atm is added as frictional loss for each that applies. Since all pumps used in this process are centrifugal, 1/3 of frictional losses are due to a control valve. Finally, the gravitational pressure change due to height was calculated in *Equation 3.1-29* where ρ_{fluid} is the fluid density (kg/m^3), g is the gravitational constant (m/s^2), and dz is the height of what the fluid will pass through (m):

$$gravity\ head\ =\ \rho_{fluid} \cdot g \cdot dz \text{ (E 3.1-29)}$$

The addition of pressure drop, frictional losses, and gravity head provides the differential pressure. Next, the power consumed by a pump was found in *Equation 3.1-30*, where *P* is power (W) and $\dot{V}_{fluid,pump}$ is the volumetric flow rate of fluid traveling through the pump (m^3/s):

$$P = differential\ pressure \cdot \dot{V}_{fluid,pump} \text{ (E 3.1-30)}$$

3.1.6.2 Holding Tank and Silo Design

The steps and calculations used to design holding tanks and silos in this unit are detailed as follows. The size of a holding tank depends on the amount of material that is to be stored inside. In this process, the holding tanks for the subsequent brine stored for adsorption and the lithium enriched brine sent to electrodialysis were sized for one cycle's worth of material. The holding tanks for aqueous iron (III) chloride regeneration solution were sized for 24 hours' worth of material due to frequent usage of the material and the large requirement for one cycle. The amount of material held in a tank for a given amount of time was found in *Equation 3.1-31*,

where m_i is the mass of component i in the tank (kg), $\dot{m}_i$ is the mass flow rate of component i into the tank (kg/min), and $t_{flow,\,i}$ is the time that component i is flowing out of the tank (min).

$$m_i = \dot{m}_i \cdot t_{flow,i} \text{ (E 3.1-31)}$$

Following, the total volume of holding tank needed to hold $m_i$was found in *Equation 3.1-31*, where $V_{HT,\,i}$ is the volume of the holding tank for component i (m^3), m_i is as defined in the last paragraph, and ρ_i is the density of component i (kg/m^3).

$$V_{HT,\,i} = \frac{m_i}{\rho_i} \text{ (E 3.1-32)}$$

The total $V_{HT,\,i}$ found was compared with the volumes of industrial holding tanks that are currently for sale. Several holding tanks greater than or equal to $V_{HT,\,i}$ were designed and fit to realistic holding tank dimensions using published industrial recommendations for holding tanks. More details are provided in the *4.1.4.3 Holding Tanks* section.

Silo design followed the exact same steps as those above, but they were sized off 30 days' worth of solid material. Silos were designed for storage of iron (II) chloride, potassium citrate, and iron (III) chloride solid powders. Each silo was also fitted to an industrially available silo, which consequently determined the total amount of silos needed for storage of each solid component. Further information on the size of the silos is also available in the *4.1.4.3 Holding Tanks* section.

3.1.6.3 Heat Exchanger design

The brine from the geothermal power plant is 110 C, or about the temperature of saturated steam under such conditions (G. Geise, personal communication, November 13th, 2023). After potassium citrate and additional iron (II) chloride are added to the brine, the feed

enters a heat exchanger that decreases the temperature to 75 C before entering the primary beds for adsorption. The heat exchanger is a countercurrent shell and tube model where cooling water is used to absorb heat from the hot brine. The cooling water enters the heat exchanger at 30 C and exits at 45 C (E. Anderson, personal communication, March 18th, 2024).

The heat exchanger was designed using a HEATER block on Aspen. The inputs included the mass flow rates of lithium chloride, sodium chloride, and water entering the heat exchanger and the desired temperature decrease in the hot fluid. The HEATER block results reported the heat duty (kW), which was used to find the mass flow rate of cooling water in *Equation 3.1-33* where $\dot{m}_c$ is the mass flow rate of cooling water entering the heat exchanger (kg/s), Q_c is the heat duty absorbed by the cool fluid (J/s), $C_{p,c}$ is the specific heat capacity of water (J/kg·C), and ΔT_c is the difference in temperature between the fluid entering and exiting the heat exchanger (C):

$$\dot{m}_c = \frac{Q_c}{C_{p,c}\Delta T_c} \textit{ (E 3.1-33)}$$

Following, the logarithmic mean temperature difference was found to acquire the heat exchanger area. *Equation 3.1-34* defines the logarithmic mean temperature difference, where ΔT_{lm} is the logarithmic mean temperature difference (C), ΔT_1 is the difference between the temperature of the hot and cold fluid when they enter the heat exchanger (C), and ΔT_2 is the difference in temperature between the hot and cold fluid when they exit the heat exchanger (C):

$$\Delta T_{lm} = \frac{\Delta T_1 - \Delta T_2}{\ln\left(\frac{\Delta T_1}{\Delta T_2}\right)} \textit{ (E 3.1-34)}$$

The area where heat is transferred between fluids in the exchanger was found in *Equation 3.1-35*, where A is the area of heat transfer (m^2), Q is the heat duty (kJ/s), U_0 is the overall heat transfer coefficient ($W/m^2 \cdot C$), and ΔT_{lm} is the logarithmic mean temperature difference (C).

$$A = \frac{Q}{U_0 \Delta T_{lm}} \quad (E\ 3.1\text{-}35)$$

3.2 Electrodialysis Discussion

3.2.1 Ion Exchange Membrane

The overall reaction depicts lithium chloride being separated into its respective ions, with the chloride ion forming iron (III) chloride, and the lithium ion forming lithium hydroxide. The lithium ion can be transferred between anions due to the applied electric field driving force. Lithium is attracted to the negatively charged cathode and can pass through the ion-exchange membrane (IEM), or specifically, a cation-exchange membrane (CEM). An IEM is a semipermeable membrane that transports specific ions while blocking the passage of others. A CEM has negative fixed charge groups in the polymer that allow cations to pass through while opposing the passage of anions due to their like charges. Using a CEM in the system, lithium is driven by the electric field and allowed to pass through the negatively charged membrane while chlorine ions remain on the anode side of the cell. The redox reactions as well as the movement of lithium are driven by the electric field while the ions are separated using a membrane to create both the stripping solution and hydroxide form of the product.

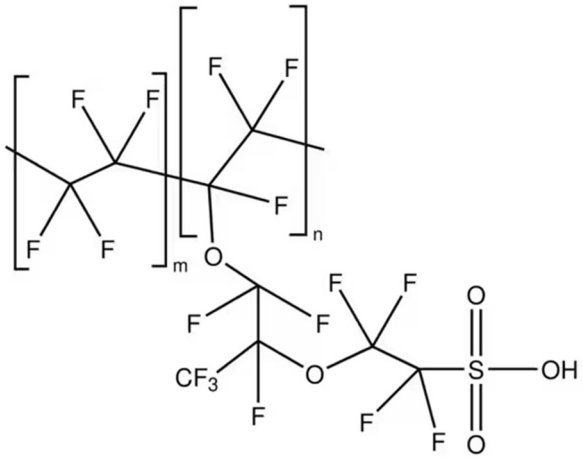

Figure 3.2-1. Structure of Nafion-117 Cation Exchange Membrane.

The chosen IEM is Nafion- 117, which is a perfluorinated membrane with sulphonic functional groups that boast high chemical and thermal stability (Stenina, 2004). An important parameter for electrodialysis membranes is ionic conductivity. Nafion is a well-studied membrane with extensive data available on ionic conductivity, permeability, and diffusion. Estimating conditions like those described in the study by Volkov, an ionic conductivity of $1.3 \cdot 10^{-2}$ S/cm was assumed (Volkov, 2021). Nafion is manufactured at a thickness of 0.0183 cm, which was assumed for calculations.

3.2.2 Reactions Overview

Electrodialysis is the separation of ions using an Ion Exchange Membrane (IEM) and an electric field driving force. Electrolysis is the redox reaction driven by an electric field. In the proposed system, both occur in a split cell with the anolyte and catholyte separated by an IEM to form lithium hydroxide. The aqueous feed from the packed bed reactor system contains primarily lithium chloride and iron (II) chloride as well as trace amount of iron (III) chloride and sodium chloride. The goal of the electrodialysis unit is to use redox reactions to convert iron (II) chloride into iron (III) chloride to regenerate the stripping solution while simultaneously generating lithium hydroxide. The following reactions are required at the anode and cathode, respectively:

$$2Fe^{2+} \rightarrow 2Fe^{3+} + 2e^{-} \text{ (R. 3.2.1)}$$

$$2H_2O + 2e^{-} \rightarrow 2OH^{-} + H_2 \text{ (R. 3.2.2)}$$

These two reactions together, with counter ions included, lead to the following overall reaction:

$$2LiCl\,(aq) + 2FeCl_2\,(aq) + 2H_2O\,(aq) \rightarrow 2LiOH\,(aq) + 2FeCl_3\,(aq) + H_2\,(g) \text{ (R. 3.2.3)}$$

The oxidation reaction shown in *Reaction 3.2.1* has a standard redox potential of 0.770 V, while the reduction presented in *Reaction 3.2.2* has a standard redox potential of –0.827 V (LibreTexts, 2021). In addition to the desired reactions for this process, two additional reactions are possible at the anode:

$$2Cl^- \leftrightarrow 2e^- + Cl_2 \text{ (R. 3.2.4)}$$

$$2H_2O \leftrightarrow 4H^+ + O_2 + 4e^- \text{ (R. 3.2.5)}$$

However, their higher redox potentials of 1.358 V for *Reaction 3.2.4* and 1.229 V for *Reaction 3.2.5* make these reactions less likely to occur (Grageda, 2020). More voltage is required for these secondary reactions to take place, which supports the decision to neglect their effect on the material balance despite a lack of experimental data for the proposed setup. A personal communication with an industry expert further supported this decision as it was stated the lower voltage "in conjunction with its already rapid kinetics means you should not have much difficulty selectively producing Fe^{3+} as opposed to chloride or water oxidation" (A. Rassoolkhani, personal communication, Feb. 7, 2024). It was also stated that if a secondary reaction were to occur, it would be "predominantly chlorine evolution" which can react with "residual Fe^{2+} to indirectly cause the formation of Fe^{3+}" (A. Rassoolkhani, personal communication, Feb. 7, 2024). For these reasons, only *Reactions 3.2.1* and *3.2.2,* which yield *Reaction 3.2.3,* have been considered in the material balance calculations in the electrodialysis unit.

3.2.3 Operating Voltage

In electrodialysis, one important parameter is the operating voltage of the system. Adequate voltage is required for the redox reactions at the anode and cathode, and additional

overpotential is required for ion mobility to overcome transport resistance in the system. The operating potential is a function of the equilibrium potential (ΔEe), anodic and cathodic overpotentials (ηa and ηc), and potential drops across the anolyte, catholyte, and membrane ((IR)a, (IR)c, and (IR)m) according to the following equation (Grageda, 2020).

$$Vcell = \Delta Ee + \eta a + |\eta c| + (IR)a + (IR)c + (IR)m \quad (E\ 3.2\text{-}1)$$

Using the standard redox potentials of the desired reactions, the equilibrium potential is 1.597 V. Anodic and cathodic overpotentials were calculated based on data for the chosen materials presented in the *Handbook of Chlor-Alkali Technology* and were adjusted based on the desired current density leading to values of 0.051 V and 0.368 V for the anode and cathode respectively (O'Brien et al., 2005 pg. 206). Potential drops for the anolyte and catholyte were found to be 0.55 V and 0.79 V based on average potential drops at the desired current density in a similar system (Grageda, 2020). The potential drop across the membrane was calculated based on the conductivity, area, and thickness of the membrane, as well as the current density, resulting in a value of 0.338 V. Using these values and *Equation 3.2-1*, an operating voltage of 3.693 V was calculated.

3.2.4 Current

In addition to the operating voltage, the current the system is operated at greatly affects electrodialysis in production capabilities and power requirements. To determine the required current, Faraday's Law of Electrolysis (*Equation 3.2-2*) was used to correlate the flow of lithium ions to the theoretical current requirement.

$$\frac{n_{theor}}{t} = \frac{I}{z \cdot F} \quad (E\ 3.2\text{-}2)$$

The theoretical molar flowrate of lithium ions is equal to the current (I) in amperes divided by the number of electrons per ion (z) times Faraday's constant (F), equal to 96484.5 A·s/mol. Using the flowrate of lithium ions entering the system from the adsorption and regeneration process and adjusting to run the electrodialysis unit as continuous, the inflow of lithium ions is approximately 56 g/s. Converting to a molar flowrate and utilizing Faraday's Law with a z value of 1 electron per ion, a theoretical current of approximately $7.8 \cdot 10^5$ A is obtained. $7.8 \cdot 10^5$ A represents the current required to move the lithium ions assuming all the current applied is used to move lithium ions. However, this is unrealistic, as current efficiency must be taken into consideration. Data does not yet exist on current efficiencies of this exact system, but data is currently being collected for a similar system in which the only alteration is the use of iron sulfates rather than iron chlorides. This system was found to have an average current efficiency of 70% (C. Morin, personal communication, Feb. 14, 2024). This value was assumed for the proposed system as a conservative estimate when considering the more favorable kinetics of iron oxidation in the chloride form, which will limit side reactions more than the currently studied system. Using this current efficiency, $1.1 \cdot 10^6$ A is recommended as the total current for the system.

3.2.5 Fuel Cell

While the main target of the electrodialysis unit is to regenerate the iron (III) chloride stripping solution and create lithium hydroxide, the ED reaction also produces a notable amount (~29 kg/hr) of hydrogen gas as a side product. This side product, if harnessed and fed into a proton-exchange membrane (PEM) fuel cell, can be quite valuable to generate electrical energy and recycle water back into the system.

Hydrogen fuel cells convert chemical energy into electrical energy via a redox reaction between diatomic hydrogen and oxygen, producing water as the only byproduct:

$$H_2\ (g) + ½\ O_2\ (g) = H_2O\ (l)\ \textit{(R. 3.2.6)}$$

Compared to traditional combustion engines, which are typically less than 20% efficient in converting the chemical energy in gasoline into power, standard hydrogen fuel cells achieve efficiencies between 40 and 60% (U.S. Department of Energy, 2015). Based on these values and the ~7:4 hydrogen to water molar ratio in the fuel cell feed stream, a 50% fuel cell efficiency was assumed. Given this efficiency, and the 33.6 kWh/kg energy content of H_2, it was determined that the hydrogen gas fed from ED into the fuel cell has a power generation capacity of 492 kW. This electric power generated from the fuel cell can be used to reduce the amount of external electrical power necessary to sustain operation. Additionally, operation of the hydrogen fuel cell produces approximately 131 kg/hr of water byproduct. This water can be fed back into the electrolysis cells to recover some of the ~22,000 kg/hr of water exiting from the cathode either with the hydrogen gas into the fuel cell or in solution with LiOH being fed to the crystallizer.

EH group engineering, a leading hydrogen fuel cell production company based out of Switzerland outlines the design specification for a 15 kW PEM fuel cell stack (EH Group Engineering AG, 2024). To consume and convert all the available H_2 gas, 33 15 kW fuel cell stacks are required.

Ambient air at a volumetric flow rate of approximately 215 L/s is utilized to supply the required O_2 to the system. This air flow rate corresponds to the molar flow rate of oxygen needed to sustain a stoichiometric oxygen/hydrogen ratio. To facilitate optimal mass transfer across the proton exchange membranes, feed gases (hydrogen and air) are typically pressurized to a

pressure between 3 and 4 bar (Hoeflinger & Hofmann, 2020). As such, the hydrogen and air streams, which are initially at atmospheric pressure (~1.01 bar) are pressurized to 3.5 bar before entering the fuel cell stack. The power required for this pressure change was determined by modeling the gas compressions in Aspen Plus V14 using a Peng-Robison equation of state and assuming isentropic compression.

3.2.6 Mass Balance

Having established the operating voltage and current for the system, a material balance can be completed. Having used Faraday's Law and current efficiency data to find the operating current, the design allows for all lithium ions flowing into the system to be transported across the membrane. Additionally, the selected overpotential allows for complete oxidation of iron with no assumed side reactions. If more data were to be collected, an optimal operating voltage would be chosen specifically to oxidize all the iron (II) chloride and transport all the incoming lithium across the membrane while using minimal voltage. Assuming the chosen operating voltage does exactly this, the mass balance can be completed by assuming all lithium that enters the anode passes through to the cathode, and all iron leaving the system comes out of the anode in the form of iron (III) chloride. Lithium and sodium are transported across the Nafion membrane, but iron and chloride are kept on the anode side of the unit. For every two cations that cross the CEM, two moles of water are reduced to produce two hydroxide ions and one mole of hydrogen gas. The stream coming into the anode side of the electrodialysis unit is at about 0.5 M concentration of lithium and iron ions based on the stripping solution used in the second regeneration cycle. In commercial electrodialysis units, solution is typically fed and removed to both sides of the cell at approximately the same flow rate. In addition to keeping flowrates on both sides of the cell rather constant, it is important to keep the ionic concentrations close to provide similar osmotic

pressures. This ensures minimal ionic concentration gradient and adequate solution conductivity on both sides of the cell. Due to the elevated amount of chlorine ions present in the anolyte, a recycle stream is added to the cathode side of the reactor to increase solution conductivity and ionic concentration. According to the Van't Hoff approximation, osmotic pressure can be estimated as a function of molar ionic concentration of species in solution (c_T) and temperature (T) according to the *Equation 3.2-3:*

$$\pi \cong c_T RT \quad \textit{(E 3.2-3)}$$

With an equal temperature and ideal gas constant, ionic concentration should be kept close to constant between the two sides. On the anode side, c_T averages to approximately 2.3 M between the inlet and outlet streams as lithium and sodium leave the anolyte. To reach a similar average ionic concentration on the cathode side of the cell, a recycle stream equal to 61% of the liquid leaving the cathode is employed. This recycle stream is met with pure water to further dilute it before it enters back into the electrodialysis unit. Pure water is added to compensate for the water sent to the crystallizer and the water vapor that leaves the system with the hydrogen gas. Some of this water is derived from an external source; however, almost 95% of the water required is recycled from both the hydrogen fuel cell (which produces water as a product) and the crystallizer unit (which evaporates off steam to be condensed and sent back to the electrodialysis cell).

Because the electrodialysis units are operated at about 75 C and atmospheric pressure, a significant amount of water vapor is lost with the hydrogen gas. To find the vapor fraction of water lost, the osmotic pressure was related to the activity of water according to *Equation 3.2-4*

where π is the osmotic pressure, a_w is the activity of water, R is the ideal gas constant, T is Temperature in Kelvin, and $\overline{V_w}$ is the molar volume of water.

$$\pi = -\ln(a_w)\frac{RT}{\overline{V_w}} \quad \textit{(E 3.2-4)}$$

Using *Equation 3.2-3* for osmotic pressure, a_w is found to be a function of ionic concentration and molar volume. a_w is equal to the fraction of water in the liquid phase (x_i) times the activity coefficient (γ_i). Using Raoult's Law, displayed in *Equation 3.2-5*, the calculated activity, saturation vapor pressure at the specified temperature, and operating pressure can be used to calculate the vapor fraction.

$$y_i P = x_i \gamma_i P_i^{sat}[T] \quad \textit{(E 3.2-5)}$$

In this case, a_w was found to be 0.95 and the saturation vapor pressure of water at 75 C is 0.38 atm (*Water,* n.d.). This leads to the vapor phase going to the fuel cell containing 36 mole % water. This, along with water molecules that are used to produce hydroxide, explains the discrepancy between the moles of liquid water fed into the cathode and that that leaves through the liquid stream.

3.2.7 Sizing

A current density of 2400 A/m^2 was chosen to maximize lithium hydroxide production and minimize energy consumption based on the data indicating minimal increase in lithium hydroxide production at power requirements above 2400 A/m^2 (Grageda, 2020). Dividing the necessary current by the current density gives 324 m^2 of necessary electrode area. The expected cell size is based on the commercially available chloro-alkali systems that have electrode dimensions of 3.4 m^2 and a membrane effective area of 3.4 m^2 (Budiarto et al., 2017). Like the

lab scale set up, the unit is a cube with the length, height, and width of the total system equal to 1.84 m and a volume of 6.3 m^3. Based on these dimensions, 96 cells are necessary, but 100 will be installed.

3.2.8 Power Requirements

The equation for electrical current is presented in *Equation 3.2-6*.

$$P = \frac{I}{\eta}V \quad (E\ 3.2\text{-}6)$$

Using the set operating voltage and total current for the electrodialysis units in parallel, the power required is 4.1 MW. However, from the assumed current density, only 70% of the power is being used to transport cations which means a portion of the power will be turned into heat. This accounts for approximately 1.2 MW of power that is turned into heat. If the electrodialysis units are heated beyond 75 C, more water will be lost as vapor, the membrane's anion rejection effectiveness can decrease, and materials of construction may be more expensive. Thus, cooling is necessary to keep the temperature constant. Luckily, with 100 cells with a volume of 6.2 m^3 each, the generated heat can be more easily dissipated than for a single larger unit.

Since the cells are positioned on the ground, heat can be dissipated from 5 of the 6 sides through forced convection of air. Heat transfer from convection can be modeled in *Equation 3.2-7* where Q is the heat transfer rate in watts, A is the surface area over which convection occurs, h_{air} is the convective heat transfer coefficient, and ΔT is the difference in temperature between the ambient air and the surface of the electrodialysis unit.

$$Q = Ah_{air}\Delta T \quad (E\ 3.2\text{-}7)$$

In this case, Q is equal to the approximately 1.2 MW of heat created that must be dissipated and A is equal to the combined surface area of all 100 cells. Some heat is lost to passive dissipation through the latent heat of vaporization of water, leading to approximately 1.1 MW of heat needed to be actively dissipated. Setting the ambient air temperature to 30 C by considering the climate of the Salton Sea region, the required heat transfer coefficient of air is about 15 W/m^2˙C *(Salton Sea,* n.d.*).* This corresponds to air flowing at about 0.5 m/s (Van Brecht et. al). To calculate the number of fans needed, the mass of air required was found using *Equation 3.2-8*:

$$Q = m_{air} C_p \Delta T \quad (E\ 3.2\text{-}8)$$

While Q is the same as previously, ΔT is the difference in the air temperature. Based on the specific heat capacity (C_p), the air is assumed to leave around 65 C, which gives a required mass flow of air of 32 kg/s. Converting to volume using the density of air divided by the linear flow (0.5 m/s), an area of 65 m^2 of fans can be used to adequately cool the additional heat created by the current inefficiency. This can be accomplished using 5 commercially available fans of 14 ft in diameter with a total energy requirement of 10 kW (Big Ass Fans, 2020). The total energy requirement of the electrodialysis unit, excluding pumps, is 4.12 MW. Approximately 0.5 MW of this energy requirement is generated internally by the fuel cell, and the remaining 88% of the energy needed is sourced externally.

3.2.9 Ancillary Equipment

Because the electrodialysis units are continuously operating at 75 C and 1 atm, no holding tanks or heat exchangers are required within this block. Material is fed into the system at the same temperature and pressure as the operating specifications, so material simply must be

pumped through the system. Since there are no pressure changes within the electrodialysis units and no significant height changes within the block, pumps are used solely to overcome the frictional losses associated with fluid flow through piping and valves. Estimating approximately 0.5 bar of frictional losses for piping and the standard 1/3 of the overall pressure drop for valving associated with centrifugal pumps, approximately 0.75 bar pressure drop must be overcome by the pumps to continuously move the fluid. Pumps are designed for the calculated volumetric flowrates and the associated pressure drop. As described in *Section 3.1.3.1*, using the volumetric flowrate and pressure drop according to *Equation 3.1-9*, the theoretical power can be calculated. To account for the expected pump efficiency of 70% and the electrical driving efficiency of 90%, the theoretical power is divided by both efficiencies to find the actual necessary power. Energy for the year can be found by multiplying power by the total operating hours considering plant operation time of 90%. Large pumps were used to move the total quantity of fluid for all 100 units. Streams are then divided, yet this results in negligible frictional losses and does not require the usage of additional pumps. Power requirements for electrodialysis unit pumps are detailed in *Table 3.2-1.*

Table 3.2-1. Pump and Compressor Power Requirements.

Pumps/ Compressors	Volumetric flow rate (m^3/s)	Pressure drop (bar)	Pressure drop (Pa)	Theoretical Power (W)	Power accounting for inefficiencies (kW)	Annual operating time (hr)	Power (kWh)
201	0.01599	0.75	75000	1199.61	1.90	7884	15012
202	0.01599	0.75	75000	1199.61	1.90	7884	15012
203	0.01585	0.75	75000	1188.42	1.89	7884	14872

3.3 Crystallization Discussion

3.3.1 Reaction Overview

After the electrodialysis, the lithium hydroxide solution enters the crystallization block to crystallize the product, lithium hydroxide monohydrate, at the minimum required 99.12 wt.% purity. Crystallization is defined as producing solid crystals from either a melt, vapor, or solution. In this process, lithium hydroxide monohydrate is crystallized from solution, which involves altering the solution equilibrium such that the solute reaches supersaturation and precipitates out. The overall reaction is displayed in *Reaction 3.3.1*:

$$Li^+\,(aq) + OH^-(aq) + \ H_2O\ (aq) \rightarrow LiOH \cdot H_2O\ (s) \quad \textit{(R. 3.3.1)}$$

3.3.2 Solubility Considerations

Achieving supersaturation can be done multiple ways. On the laboratory scale, crystals are formed either by adding salt or "antisolvent" to the solution. Salting-out crystallization is defined as increasing the salt concentration in a solution so that the desired product is no longer soluble, resulting in precipitation (Hyde et al., 2017). Similarly, antisolvent crystallization is the addition of another solvent, commonly an alcohol or organic solution, that the desired solid is sparingly soluble in, resulting in supersaturation (Nowee et al., 2008). These processes, while effective, are difficult to scale up to the commercial level due to limited material recovery, resulting in high costs.

On the commercial scale, either evaporative, cooling, or vacuum crystallization is used. Evaporative crystallization involves vaporization of the solvent until the solubility limit of the solute is reached, resulting in precipitation. This method is effective for solids where the solubility is not greatly affected by an increase in temperature. For solids where the solubility

greatly decreases as temperature decreases, the solvent can be cooled until the solubility limit is reached. In some cases, evaporation must be done to induce crystallization, but low operating temperatures are required- thus, evaporating off the solvent adiabatically at low pressures, or vacuum crystallization, can be employed (Skindzier et al., n.d.).

Our process uses vacuum crystallization due to the large volume of water entering the system and the decreasing solubility of lithium hydroxide monohydrate as temperature decreases, as shown in Figure 3.3-1 (Monnin & Dubois, 2005). Additionally, vacuum crystallization is easily scalable to commercial-scale operations. In addition to operating the crystallizer at lower temperatures, a recirculation stream is employed to further induce crystallization. The addition of pre-formed crystals to the crystallizing solution promotes nucleation- this process is called seeding (Parambil & Heng, 2017).

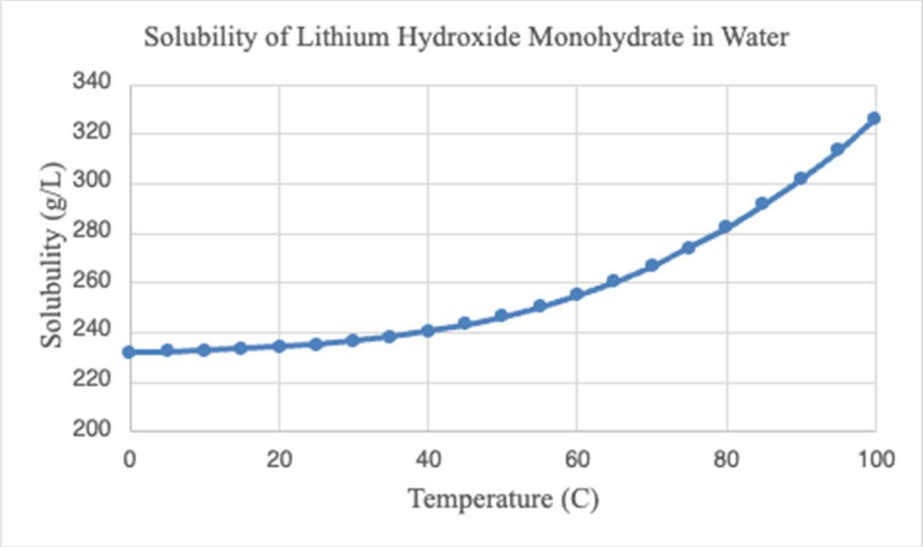

Figure 3.3-1. Solubility of Lithium Hydroxide Monohydrate in Water as a Function of Temperature (Monnin & Dubois, 2005).

The slurry exiting the crystallizer is pumped to a rotary vacuum filter to separate the lithium hydroxide monohydrate crystals. It is important that the crystals do not redissolve as the

pressure rises entering the unit; thus, the slurry will be further cooled before increasing the pressure prior to entering the filter. The wet solids then enter a rotary vacuum dryer via a belt feeder. Like the filter, it is crucial to ensure the solids do not redissolve into the solvent as they enter the dryer. The dryer operates below ambient pressure in 1-hour batches to prevent melting. To account for the batch operation of the dryer, the wet solids are held in a silo between batches. The output product is held in a silo in a 30-day supply quantity.

3.3.3 Crystallizer Sizing and Operating Conditions

Our process uses a forced circulation crystallizer (FCC), a continuous crystallization method commonly used in large-scale production (see *Figure 3.3-2*). Slurry is continuously recirculated through the system, mixing with the slurry in the tank, causing boiling at the surface. Simultaneous cooling and boiling promotes supersaturation, and the precipitated crystals leave through a circulating pipe (Genck et al., 2019).

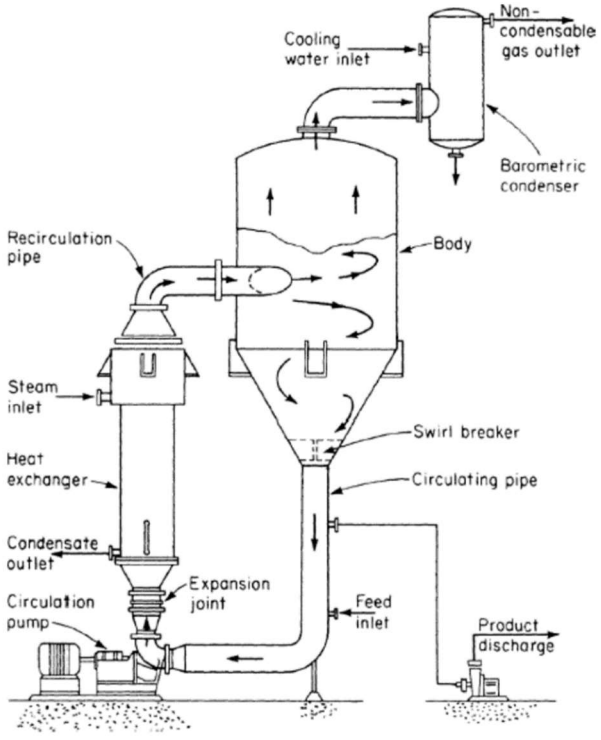

Figure 3.3-2. FCC Diagram. (Genck et al., 2019)

To model the crystallizer, the FLASH2 block in Aspen was used, along with the specified reaction chemistry using the ELECNRTL method. The reactions predicted by the Aspen model, in addition to *Reaction 3.3.1*, were as follows:

$$Li^+(aq) + OH^-(aq) \rightarrow LiOH(s) \text{ (R. 3.3.2)}$$

$$Na^+(aq) + OH^-(aq) \rightarrow NaOH(s) \text{ (R. 3.3.3)}$$

$$Na^+(aq) + OH^-(aq) + H_2O\,(aq) \rightarrow NaOH \cdot H_2O(s) \text{ (R.3.3.4)}$$

Presently, no literature exists on vacuum crystallization methods for lithium hydroxide monohydrate- the only data available was laboratory-scale antisolvent crystallization. Thus, the crystallizer was modeled by using appropriate assumptions to obtain the highest production of lithium hydroxide monohydrate. It was found that a pressure of 0.2 bar and a set vapor fraction of 92% were the optimal operating conditions for this unit, resulting in an operating temperature of 67.9 C. The low-pressure steam exiting the crystallizer is condensed and heated to 75 C before being sent back to the electrodialysis unit to help meet water requirements. It was assumed that a recirculation stream would be employed inside the crystallizer.

Sizing of the crystallizer was based on the inlet volumetric flowrate. A conservative residence time assumption of 15 minutes was made based on the crystallization of other simple salts (Ravichandran et al., 2019). Using the total inlet volumetric flowrate (including the feed from the electrodialysis block and the recycle stream), a required volume of 6.8 m^3 was calculated. Generally, it is recommended to oversize by 60% to account for vapor formation (Orehek et al., 2020) leading to a crystallizer volume of 10.8 m^3. Using a length/diameter ratio of 3, *Equation 3.3-1* was used to determine the required diameter of 1.65 m, or 5.5 ft, and the final

crystallizer specifications are documented in *Table 3.3-1*. A length of 5.25 m was determined based on the vendor.

$$D = \sqrt[3]{\frac{4V}{3\pi}} \rightarrow 1.65\ m \text{ (E 3.3-1)}$$

Table 3.3-1. Crystallizer Operating Specifications.

Parameter	Value
Temperature	67.9 C
Pressure	0.2 bar
Diameter	1.65 m
Length	5.25 m
Volume	10.65 m^3
Power Required	14 MW
Material of Construction	Stainless Steel

To prevent corrosion inside the unit, the crystallizer will be constructed out of 316 stainless steel. The power requirement for the unit is 14 MW- it will be heated with internal steam coils and electrical power to operate the vacuum. During start-up, some initial lithium hydroxide monohydrate crystals would need to be added to the crystallizer to initiate the reaction.

3.3.4 Filter Sizing and Operating Conditions

The slurry exiting the crystallizer is cooled and pumped up to 1.25 bar before entering a rotary vacuum filter- the additional cooling is to ensure the solids do not re-dissolve as the pressure rises. As the drum rotates, it is partially submerged in the slurry and a vacuum draws up the liquid through a cloth filter medium. The solids in the slurry are retained on the filter medium while the vacuum continues to draw liquid and air through the slurry. The wet solids are then scraped onto a conveyor belt for transfer into the dryer (Genck et al., 2019b).

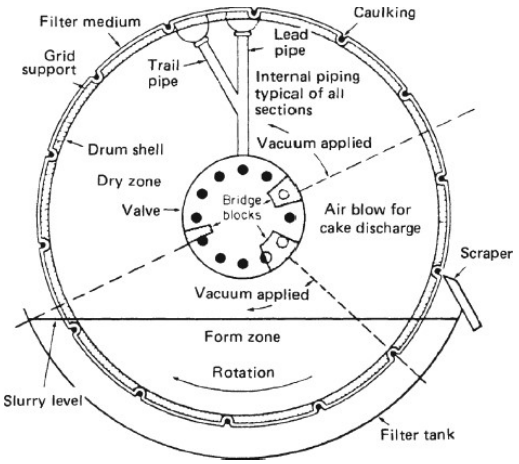

Figure 3.3-3. Rotary Vacuum Filter Schematic. (Genck et al., 2019b)

Modeling of the filter was done using the FILTER block in Aspen. The solid outlet was set to 0.99 of the inlet solids, and the liquid outlet was set to 0.89 of inlet liquid. These parameters were chosen based on what would give the most reasonable results for the wet cake exiting the filter. The resulting flow rates were used to calculate the filter area required. The area requirement was calculated using the following equation, assuming the solid is incompressible:

$$A = m_s \left(\frac{a_0 \mu}{2c\Delta P f}\right)^{\frac{1}{2}} \text{(E 3.3-2)}$$

Where m_s is the mass flow rate of the solid entering the filter, a_0 is the specific cake resistance, approximated as the same literature value as magnesium hydroxide at $1.35 \cdot 10^{10}$ m/kg, μ is the viscosity of water at the filter operating temperature, 50 C, equal to 0.0005474 Pa·s, c is the concentration of the solids in the filtrate, equal to 225 kg/m^3, ΔP is the differential pressure in the filter, equal to 25,331.25 Pa, f is the fraction of the drum submerged, assumed to be 0.3, and n is the rotational frequency of the drum, assumed to be 0.0833 s^{-1}. The required filter area was calculated to be 5.05 m^2, or 54.4 ft^2. Komline-Sanderson can accommodate this size with a filter area of 56 ft^2, or 5.2 m^2 (Komline-Sanderson, n.d.), constructed out of 316 stainless

steel. The hydraulic power requirement, calculated from the pressure drop and inlet volumetric flowrate, was calculated to be 35 W.

Table 3.3-2. Rotary Filter Operating Specifications.

Parameter	Value
Differential Pressure	0.25 bar
Hydraulic Power	35 W
Drum Diameter	1.37 m
Filter Area	5.2 m^2
Fraction Submerged	0.3
Rotational Speed	0.5 RPM
Material of Construction	Stainless Steel

3.3.5 Dryer Sizing and Operating Conditions

The wet cake from the filter is transferred to a rotary vacuum dryer. In these dryers, wet cake is placed in the drum in batches, the drum is sealed, and a vacuum is created while the drum rotates. In some cases, such as this process, heat is applied to the drum to aid in drying. The remaining solvent evaporates and is vented from the drum (Applied Chemical Technology, n.d.). To model the dryer, the FLASH2 block in Aspen was used- initially, the block was set to high temperatures at atmospheric pressure to simulate a hot air dryer, but it was found that due to the high moisture content remaining in the cake, the lithium hydroxide monohydrate crystals redissolved and precipitated again as lithium hydroxide solids. The flash was then run below atmospheric pressure to circumvent this issue, resulting in an operating pressure of 0.35 bar and operating temperature of 87.5 C. To size the dryer, it was estimated that the approximate holdup time per batch would be 1 hour, resulting in an inlet cake volume of 1.23 m^3. The volume of cake inside the dryer was assumed to be 1/3 of the total dryer volume, resulting in a required volume of 2.03 m^3. Based on other general dryer designs, the calculated diameter of the dryer was 0.6 m, while the length of the dryer was 7.2 m, resulting in a heating area of 14.14 m^2. The total power

requirement of the dryer is 2.69 kW. The dryer is constructed out of 316 stainless steel to prevent corrosion.

Table 3.3-3. Rotary Dryer Operating Specifications.

Parameter	Value
Operating Temperature	87.5 C
Operating Pressure	0.35 bar
Power Required	2.69 kW
Volume	2.03 m^3
Heat Area	14.14 m^2
Holdup Time	1 hour
Material of Construction	Stainless Steel

Inside the dryer, the cake undergoes further crystallization due to the amount of remaining solvent, resulting in an output production of 1,222 kg per batch at 99.6% purity. Assuming each batch takes exactly an hour and operates all day, the annual production would be 10,710,154 kg or 11,805 US tons. With an assumed plant uptime of 90%, or 7,884 hours of operating time per year, the annual production is 10,625 kg. This corresponds to a 99.8% conversion of lithium hydroxide entering the unit from ED. The water vapor evaporated from the dryer is compressed to 1 bar and vented into the atmosphere.

3.3.6 Ancillary Equipment Sizing and Operating Conditions

3.3.6.1 Heat Exchanger Design

The steam exiting the reactor cannot be used for heating within the system because of its low temperature and pressure (67.9 C and 0.2 bar, respectively); thus, the steam is condensed and sent to the electrodialysis unit to aid in water requirements. As outlined in section 3.1, the counter-current heat exchangers were modeled using the HEATER block in Aspen. The resultant heat duty was used to calculate the mass flow rate of cooling water required using *Equation 3.1-33* and using *Equations 3.1-34* and *3.1-35*, the heat transfer area was calculated. After the steam

is condensed, it is pumped to 1 bar and heated to 75 C for use in ED. To calculate the steam required for heating, *Equation 3.3-3* was used:

$$\dot{m_{steam}} = \frac{Q}{\Delta H_v} \quad (E\ 3.3\text{-}3)$$

Where ΔH_v is the heat of vaporization of steam at 100 C and 1 bar, assumed to come from the geothermal plant after electricity generation. Both heat exchangers used in condensing and heating the steam are constructed with basic carbon steel to minimize costs. Another heat exchanger is implemented to cool the slurry exiting the crystallizer after it is pumped to above atmospheric pressure- this is to further induce crystallization as well as ensure the solids do not re-dissolve from the increased pressure. While designed similarly to the other two exchangers in this block, this heat exchanger was constructed with Monel 400 to prevent corrosion from the hydroxide slurry.

3.3.6.2 Pump Design

As outlined in the prior sections, each pump was designed using the pressure drop, volumetric flowrate, and efficiency factors (see *sections 3.1.6.1 and 3.2.8*). The steam exiting the crystallizer, after it is condensed, must be pumped to 1 bar before it can be heated and sent to electrodialysis. The pressure drop through the heat exchanger was assumed to be 0.5 atm, and the pressure drop through the control valve and pipe was assumed to be an additional 1 atm. This pump was constructed with carbon steel to minimize costs. Similarly, the slurry exiting the crystallizer must be pumped to 1.25 bar prior to entering the vacuum filter to create a pressure differential for filtration- the gravity head from exiting the crystallizer was calculated using *Equation 3.1-29* and added to the assumed pressure drops from the heat exchanger, control valve, and pipe. To prevent corrosion from the slurry, the pump was constructed with stainless

steel; additionally, a slurry pump should be used in place of a generic centrifugal pump due to the high solids content of the slurry.

3.3.6.3 Compressor Design

Exiting the dryer is steam at 0.35 bar- to safely vent to the atmosphere, the steam must be expanded to 1 bar. The compressor was modeled using the COMPRESSOR block in Aspen to calculate the resulting volumetric flow rates and hydraulic power requirements- assuming 80% efficiency, the power requirement is 7.15 kW. The compressor is constructed with generic carbon steel to minimize costs.

3.3.6.4 Silo Design

The rotary dryer operates in 1-hour batches- thus, a silo is required for the exiting wet cake from the filter in between batches. As mentioned in *Section 3.1.6.2*, the volume of the silo is dependent on the amount of material entering and the duration of which the material needs to be held- assuming the holding time is an hour, and upsizing the required volume by 50%, the required volume for the silo is 2 m^2. The product exiting the dryer are dispensed into another silo, assumed to be held for 30 days prior to packaging and shipment, resulting in a required volume of 898 m^3. Both silos are constructed with 316 stainless steel to prevent corrosion.

3.3.6.5 Belt Conveyor Design

To transport the wet cake from the filter to the silo and out of the silo to the dryer, two conveyors are required. Using the inlet volumetric flowrate (m^3/s) of cake required for the filter, as well as equipment specifications from MonTech, the belt was designed to operate at 10 ft/min, or 0.05 m/s, a belt length of 10 m, and belt width of 0.3 m. The belt is constructed with rubber and stainless steel (MonTech, n.d.).

Section 4: Design

4.1 Lithium Adsorption and Regeneration

4.1.1 Packed Bed Reactor Network and its Non-Steady State Streams

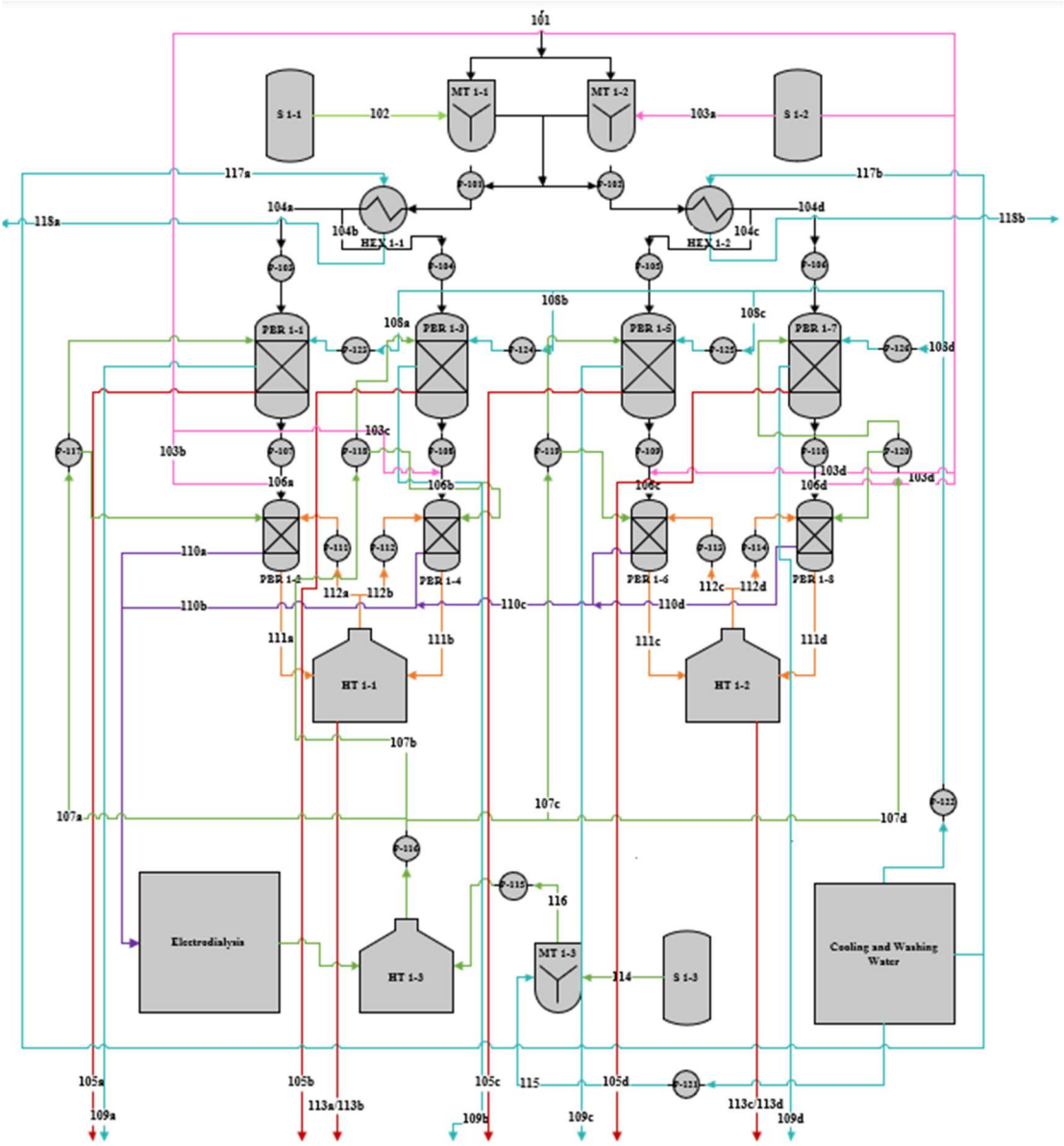

Figure 4.1-1. Packed Bed Reactor Network PFD.

Table 4.1-1 Packed Bed Reactor Stream Titles

Stream Number	Stream Title	Stream Color in Table 4.1-1
101	Brine from geothermal power plant	Black
102	Iron (II) chloride (s)	Green
103 a, b, c, d, e	Potassium citrate (s)	Pink
104 a, b, c, d	Brine cooled to 75 C	Black
105 a, b, c, d	Reinjected brine	Red
106 a, b, c, d	Brine sent to secondary adsorption	Black
107 a, b, c, d	Iron (III) chloride (aq)	Green
108 a, b, c, d	Wash water	Blue
109 a, b, c, d	Used wash water	Blue
110 a, b, c, d	Lithium enriched brine	Purple
111 a, b, c, d	Brine stored for subsequent adsorptions	Orange
112 a, b, c, d	Recycled brine	Orange
113 a, b, c, d	Reinjected brine	Red
114	Iron (III) chloride (s)	Green
115	Water added to iron (III) chloride powder	Blue
116	Iron (III) chloride (aq)	Green
117 a, b	Cooling water	Blue
118 a, b	Used cooling water	Blue

Figure 4.1-1 displays a detailed overview of the packed bed reactor network. *Table 4.1-1* supplements *Figure 4.1-1* by providing the names of the individual streams within the depiction. Brine is sent from the geothermal powerplant, at approximately 6,000 gal/min, and is first mixed with iron (II) chloride and potassium citrate. The iron (II) chloride is added such that there exists an equimolar amount of iron (II) ions and lithium ions and the potassium citrate is added such that the favorability of the adsorption reaction increases. The final design of the mixing tanks is described in further detail in *section 4.1.3*.

The inlet brine is then split to be sent to two of the primary PBRs, such as PBR-1 and PBR-5 in *Figure 4.1-1*. Focusing on just PBR-1, 99% of the inlet lithium ions (by mass) are absorbed onto the FP. The brine from which the lithium ions were obtained is then reinjected into the well. Before the primary bed can be regenerated, it is washed with externally sourced

water to remove any impurities in the small spaces of the FP sorbent. A stripping solution, which contains 0.5 M iron (III) chloride, is then sent through PBR-1 for the regeneration step. At this point, the solution leaving PBR-1 has a molar ratio of lithium to sodium ions of 5:1. Once the stripping solution exits PBR-1, it is sent directly to its secondary bed, PBR-2, for its first adsorption. Rather than being reinjected, such solution is sent to a series of holding tanks (grouped into two main tank blocks, HT-2 and HT-3, in *Figure 4.1-1*) and the adsorption/regeneration process is repeated four more times. There are no washing steps in between each secondary adsorption and regeneration step. The stripping solution for the five regeneration cycles in PBR-2 is sent to a holding tank as well, but this is done because such streams are destined for the electrodialysis unit, and it operates in a steady-state manner. All five streams sent to the electrodialysis unit are equivalent with a molar ratio of lithium to sodium ions of 2000:1. Overall, as stated previously, the initial adsorption recovers 99% of the lithium ions in the inlet brine. However, to achieve a ratio of lithium to sodium ions greater than 100:1, such that our final product is of battery-grade purity, adsorption steps were separated into primary and secondary beds. Furthermore, to recover as many of the lithium ions from primary adsorption as possible, multiple secondary adsorption steps were performed and lead to an overall recovery of 81% in the adsorption and regeneration block.

It should be noted that no additional iron (II) chloride is added for any of the adsorption steps in the secondary bed, as it is assumed that a fraction of the iron (III) ions in the initial stripping solution used for the regeneration of the primary bed were converted to iron (II) ions as the regeneration process proceeded. However, potassium citrate is added before the initial stripping solution is sent to the secondary PBR for reasons detailed in *Section 3.1.4.1*. It is

assumed that no further additions of potassium citrate are necessary for the subsequent adsorption steps in the secondary bed as it does not participate in the reactions.

Table 4.1-2a. Overall Stream Table.

Stream		101	102	103a	103b	104a	105a	106a	107a
Pressure (bar)		1.013	-	-	-	1.019	1.013	1.021	1.013
Component Mass Flow (kg/hr)	Na	79642.85	-	-	-	39821.42	39694.10	226.34	-
	Ca	36783.19	-	-	-	18391.59	18391.59	-	-
	K	20329.41	-	-	-	10164.71	10164.71	-	-
	Fe (2+)	1564.43	-	-	-	782.22	1624.42	3271.39	-
	Fe (3+)	-	-	-	-	-	50.96	79.31	-
	Mn	1396.81	-	-	-	698.41	698.41	-	-
	Sr	591.43	-	-	-	295.72	295.72	-	-
	Ba	291.63	-	-	-	145.81	145.81	-	-
	B	452.43	-	-	-	226.22	226.22	-	-
	Li	391.11	-	-	-	195.55	5.31	338.22	-
	Mg	1002.98	-	-	-	501.49	501.49	-	-
	Cl (-)	210666.59	-	-	-	105333.30	106467.25	-	-
	FeCl2	-	4054.25	-	-	2027.13	-	-	-
	H2O	969407.22	-	-	-	484703.61	484703.61	107671.51	107671.51
	Potassium citrate	-	-	20909.16	919.19	10454.58	10454.58	919.19	-
	FeCl3	-	-	-	-	-	-	-	9731.70

Stream		108a	109a	110a	114	115	116	117a	118a
Pressure (bar)		1.013	1.013	1.013	1.013	1.013	1.013	1.013	1.013
Component Mass Flow (kg/hr)	Na	-	-	0.68	-	-	-	-	-
	Ca	-	-	-	-	-	-	-	-
	K	-	-	-	-	-	-	-	-
	Fe (2+)	-	-	3278.56	-	-	-	-	-
	Fe (3+)	-	-	72.14	-	-	-	-	-
	Mn	-	-	-	-	-	-	-	-
	Sr	-	-	-	-	-	-	-	-
	Ba	-	-	-	-	-	-	-	-
	B	-	-	-	-	-	-	-	-
	Li	-	-	407.23	-	-	-	-	-
	Mg	-	-	-	-	-	-	-	-
	Cl (-)	-	-	6381.00	-	-	-	-	-
	FeCl2	-	-	-	6937.45	-	6937.45	-	-
	H2O	987155.27	4588961.61	107671.51	-	51544.64	51544.64	1208681.3	1208681.3
	Potassium citrate	-	-	-	-	-	-	-	-
	FeCl3	-	-	-	-	-	-	-	-

Table 4.1-2b. Stream Table for Each Stream Involved in the Secondary PBR Recycling.

Stream		111a.1	111a.2	111a.3	111a.4	112a.1	112a.2	112a.3	112a.4	113a
Pressure (bar)		1.013	1.013	1.013	1.013	1.021	1.021	1.021	1.021	1.013
Component Mass Flow (kg/hr)	Na	226.25	814.16	813.82	813.48	814.50	814.16	813.82	813.48	1379.40
	Fe (2+)	2838.93	8580.86	6941.57	5302.29	10220.14	8580.86	6941.57	5302.29	3350.70
	Fe (3+)	511.77	3481.66	5120.95	6760.23	1842.38	3481.66	5120.95	6760.23	3350.70
	Li	284.50	820.59	616.98	413.36	1024.21	820.59	616.98	413.36	416.40
	Cl (-)	6381.00	22971.60	22971.60	382.86	22971.60	22971.60	22971.60	22971.60	2127.00
	H2O	107671.51	107671.51	107671.51	107671.51	107671.51	107671.51	107671.51	107671.51	107671.51
	Potassium citrate	919.19	3309.07	3309.07	3309.07	3309.07	3309.07	3309.07	55.15	18383.70

The process describes just one primary and secondary bed sequence. In the next section, the schedule for each bed is described in further detail. *Tables 4.1-2a and 2b* depict the stream tables for the respective streams in *Figure 4.1-1*, but streams such as *103b-e*, *104a-b*, etc. include a letter along with a number because they are from the perspective of one primary and one secondary reactor unit. Therefore, streams with letters apply to all four reactor units. It is also of note that these mass flow rates are based on the unit of time specified in their corresponding section of the schedule, detailed in *section 4.1.2* below. For example, the streams in *Table 4.1-2b* are only flowing at that mass flow rate for the number of hours that secondary PBR recycling occurs and according to the schedule provided in the next section.

4.1.2 Scheduling

The process described in the previous section is outlined in *Table 4.1-3*, including the time required for each adsorption, washing, and regeneration stage.

Table 4.1-3. Time Required for Each Adsorption, Washing, and Regeneration Stage.

Step	Time (hrs)
Primary Adsorption	96
Washing	1.5
Primary Regeneration	54
1st Secondary Adsorption	54
1st Secondary Regeneration	7.5
2nd Secondary Adsorption	15
2nd Secondary Regeneration	7.5
3rd Secondary Adsorption	15
3rd Secondary Regeneration	7.5
4th Secondary Adsorption	15
4th Secondary Regeneration	7.5
5th Secondary Adsorption	15
5th Secondary Regeneration	7.5

With the initial brine being split between two primary beds, the steps outlined below will be operated by two sets of PBRs. In other words, a set of PBRs is one primary and secondary bed which operate in series, and two sets of beds will be conducting the steps outlined in *Table 4.1-3* at the same time in parallel. There are four additional PBRs that will operate offset from the aforementioned beds. More specifically, *Table 4.1-3* shows that it takes the same amount of time,

97.5 hours, to complete the first two steps and the last nine steps. Taking advantage of such an idea, the schedule will operate such that while two secondary beds are undergoing the first through fifth regeneration steps, the other two primary beds, the primary PBRs not in series with the operating secondary PBRs, will be undergoing their adsorption and then washing steps. Once the two operating secondary PBRs reach the end of the cycle, rather than their primary beds immediately beginning again, there will be a time delay. Such an idea is better described by examining *Table 4.1-4*. As shown below, the delay is equal to the time required for the primary regeneration and first secondary adsorption, and this is due to the idea that the first two steps and the last nine steps are of equal length. Moreover, the 54-hour delay allows for necessary actions that may need an extended period of downtime, such as bed maintenance.

Table 4.1-4. Packed Bed Reactor Network Schedule.

Hours Passed	PRB-1	PBR-2	PRB-3	PRB-4
97.5	Primary Adsorption			
	Washing			
151.5	Primary Regeneration	1st Secondary Adsorption		
249		1st Secondary Regeneration - 5th Secondary Regeneration	Primary Adsorption	
			Washing	
303			Primary Regeneration	1st Secondary Adsorption
400.5	Primary Adsorption			1st Secondary Regeneration - 5th Secondary Regeneration
	Washing			
454.5	Primary Regeneration	1st Secondary Adsorption		

4.1.3 Steady State Iron (II)/Iron (III) Chloride Streams for the Packed Bed Reactor Network

The stream table in *Table 4.1-2a* relating to the adsorption bed unit is based off non-steady state material balances, as described in *Section 4.1.2*. Due to the different time scales at which adsorption, washing, and regeneration take place between the primary and secondary adsorption beds, the mass flow of material reported in *Tables 4.1-2a* and 2*b* is with respect to the length of time at which it's taking place. For example, the flow of iron (III) chloride added during primary regeneration flows for 54 hours, whereas the flow of iron (III) chloride added

during each secondary regeneration takes place for 7.5 hours. The numerical value for flow is the same in each of the previously listed cases, but the time at which they are flowing is different. The stream tables for the electrodialysis and crystallizer units provided in upcoming sections of the report are reported at steady state. In other words, the flow of material in and out of those units is averaged over the total time in one complete cycle (151.5 hours). Iron (III) chloride is regenerated in the electrodialysis unit from the iron (II) chloride provided in *Stream 110a (as well as 110b, 110c, and 110d detailed in Figure 4.1-1 and Table 4.1-1)* of *Table 4.1-2a* that is sent from the adsorption unit. Therefore, it was necessary to perform a steady state material balance for the total iron (III) chloride needed for primary and secondary regeneration in comparison to the amount that is recycled from the electrodialysis unit. The following process was used to discover how much iron (III) chloride was needed in addition to that which is recycled from the electrodialysis unit to the adsorption unit.

$n_{Fe^{3+},overall}$ is the moles of iron (III) ions needed for 2 primary and secondary beds in one overall cycle, $\dot{n}_{Fe^{3+},p}$ and $\dot{n}_{Fe^{3+},s}$ are the flow of iron (III) ions to the primary and secondary bed during regeneration (mol/hr), respectively, and $t_{regen,p}$ and $t_{regen,s}$ are the times for primary and secondary regeneration (hr), respectively. $\dot{n}_{Fe^{3+},supplement}$ is the steady state molar flow of iron (III) ions added to the system (mol/hr), $t_{overall}$ is the total time in one overall cycle (hr), and $\dot{n}_{Fe^{3+},ED}$ is the steady state molar flow of iron (III) ions recycled from the electrodialysis unit (mol/hr). $\dot{m}_{Fe^{3+},supplement}$ is the steady state mass flow of iron (III) ions added to the system (kg/hr) and MW_{FeCl_3} is the molecular weight of iron (III) chloride.

$$n_{Fe^{3+},overall} = 2\left(\dot{n}_{Fe^{3+},p} \cdot t_{regen,p} + \dot{n}_{Fe^{3+},s} \cdot t_{regen,s} \cdot 5\right) \quad \textit{(E 4.1-1)}$$

$$\dot{n}_{Fe^{3+},supplement} = \frac{n_{Fe^{3+},overall}}{t_{overall}} - \dot{n}_{Fe^{3+},ED} \quad \textit{(E 4.1-2)}$$

$$\dot{m}_{Fe^{3+},supplement} = \dot{n}_{Fe^{3+},supplement} \cdot MW_{FeCl_3} \cdot \left(\frac{1\,kg}{1000\,g}\right) \quad \textit{(E 4.1-3)}$$

Iron (II) chloride is added to the primary adsorption step, so the steady state stream value for the addition of iron (II) chloride to the feed per one overall cycle was added to complement the steady state iron (III) chloride stream provided above. The following process was used to discover how much iron (II) chloride was added to the feed stream per one overall cycle. $n_{Fe^{2+},overall}$is the total molar amount of iron (II) ions needed for primary adsorption in addition to those in the feed (mols), $n_{Fe^{2+},p}$ is the molar flow of iron (II) ions to one primary bed during adsorption (mol/hr), $\dot{n}_{Fe^{2+},overall}$is the molar flow of iron (II) ions to one primary bed during adsorption (mol/hr), $\dot{m}_{Fe^{2+},overall}$is the steady state mass flow of iron (II) ions added to the system (kg/hr), and $MW_{FeCl_2}$is the molar mass of iron (II) chloride (g/mol).

$$n_{Fe^{2+},overall} = 2 \cdot \dot{n}_{Fe^{3+},p} \cdot t_{ads,p} \quad \textit{(E 4.1-4)}$$

$$\dot{n}_{Fe^{2+},overall} = \frac{n_{Fe^{2+},overall}}{t_{overall}} \quad \textit{(E 4.1-5)}$$

$$\dot{m}_{Fe^{2+},overall} = \dot{n}_{Fe^{2+},overall} \cdot MW_{FeCl_2} \cdot \left(\frac{1\,kg}{1000\,g}\right) \quad \textit{(E 4.1-6)}$$

Figure 4.1-2 depicts the stream values for iron (II) chloride and iron (III) chloride on a steady state basis.

Stream		102	114
Pressure		-	-
Component Mass Flow (kg/hr)	FeCl2	9637.6396	-
	FeCl3	-	6937.4495

Figure 4.1-2. Steady State Stream Values for Iron (II)/Iron (III) Chloride.

The amount of iron (II) and iron (III) chloride that will be needed per year can be found by multiplying $\dot{m}_{Fe^{2+},overall}$ and $\dot{m}_{Fe^{3+},overall}$ by the total number of cycles per year, which is approximately 58 cycles times a theoretical 90% annual operation rate. Thus, the amount of iron (II) and iron (III) chloride bought per year is reported in *Table 4.1-5*.

Table 4.1-5. Amount of Iron (II) and Iron (III) Chloride Bought (kg) per Year .

Chemical	Supplemented amount (kg/yr)
Iron (II) chloride	76,217,345.3
Iron (III) chloride	54,863,431.9

4.1.4 Mixing Unit Final Design

Upon receiving brine from the geothermal power plant, it is mixed with iron (II) chloride and potassium citrate solid, which are held in several silos determined by the expected amount of material needed for 30 days. The final number of silos, which was based upon standard, industrial capacities, are detailed in *Table 4.1-6* below. Only details important for determining capital costs are also included in *Table 4.1-6*, however, it should be noted that all SS316 silos are designed with a 60° cone-bottom, or hopper, and all polyester silos are designed with a 70°

hopper. A steeper cone slant was desired, as the intended use is to transport powders which are harder to flow than other solid forms (Chicago Metal Rolled Products, n.d.). Furthermore, iron (II) chloride powder is stored in silos made of different material than the potassium citrate due to the incompatibility of such chemicals with most common metal materials.

Table 4.1-6. Iron (II) Chloride and Potassium Citrate Storage Specifications.

Material to be stored	Iron (II) chloride	Potassium citrate
Number of silos	4	6
Material of construction (MOC)	Polyester	Stainless Steel 316
Capacity per silo (m^3)	500	2566

The iron (II) chloride and potassium citrate are then delivered evenly to multiple mixing tanks by screw conveyers. Based upon the solubility of the chemicals in water and previously set concentrations, the capacity needed to mix each chemical with the calculated amount of brine allowed for the number of mixing tanks to be found. More specifically, the overall capacity was split into multiple mixing tanks by relating the capacity needed to that of producible, industrial tanks. Overall, the number of mixing tanks needed, among other important parameters for each tank, are outlined in *Table 4.1-7*. As stated in the previous discussion section, each tank has a common residence time of 10 minutes. Furthermore, as provided by the source used to find industrial tank sizes, each mixing tank will be manufactured in high density polyethylene (HDPE), with Stainless Steel 316 wetted mixer parts, such as the PBT impeller (Protectoplas, n.d.). To protect any parts made of 316 Stainless Steel from the chloride ions present in the brine, there are several options for coatings, such as Teflon (Protectoplas, n.d.).

Table 4.1-7. Iron (II) Chloride and Potassium Citrate Mixing Tank Specifications.

Material to be mixed	Iron (II) chloride	Potassium citrate
Number of mixing tanks	2	8
Tank MOC	HDPE	HDPE
Impeller MOC	SS316 with Teflon coating	SS316 with Teflon coating
Tank diameter (m)	0.58	3.10
Height (m)	1.17	5.49
Impeller diameter (m)	0.29	1.55
Minimum RPM required	500	190
Total power required (kW)	4	3,759

4.1.5 Other Ancillary Equipment Final Design

Other ancillary equipment involved in the Packed Bed Reactor Network include, in order of discussion, heat exchangers, silos for iron (III) chloride storage, iron (III) chloride mixing tanks, holding tanks for liquid storage, pumps, and motors.

4.1.5.1 Heat Exchangers

As exemplified by the Packed Bed Reactor Network PFD located in *section 4.1.1*, two heat exchangers were designed to cool the inlet brine from 110 °C to 75 °C. Utilizing the "heater block" in the Aspen Plus V14 software, the heat duty (kW) for each heat exchanger was determined. This aided in the discovery of the required heat transfer area and cooling water flowrate, assuming an inlet and outlet cooling water temperature of 30 °C and 45 °C (Peters, Timmerhaus & West, 2003). The parameters important to calculating capital and operating costs shown later in this report are represented in *Table 4.1-8*.

Table 4.1-8. Specifications for Each Heat Exchanger Involved in the PBR Network.

Material to be cooled	Inlet brine
Material of construction	Monel 400
Heat transfer area (m^2)	486
Cooling water flow rate (kg/min)	20,145
Heat duty (kW)	-21,051

4.1.4.2 Iron (III) Chloride Storage and Mixing

Despite the generation of iron (III) chloride solution within the ED unit, it was determined that additional iron (III) chloride solution must be obtained to meet the PBR network's needs. Thus, it was found that iron (III) chloride powder would be stored on site in five silos and split evenly among two mixing tanks. As discussed in *section 4.1.3*, the silos for iron (III) chloride storage were set to be made of polyester to avoid any chemical incompatibilities. Indeed, the number of silos for iron (III) chloride solid storage was based upon the same standard 500 m^3 polyester silo used to design the iron (II) chloride storage. Furthermore, the material of construction for the mixing tanks and impellers are as listed in *Table 4.1-8*. New values different from those of the inlet brine mixing unit are summarized in *Table 4.1-9* below.

Table 4.1-9. Specifications Unique to the Iron (III) Chloride Storage and Mixing Unit.

Material to be stored/mixed	Iron (III) chloride
Number of silos	5
Number of mixing tanks	2
Tank diameter (m)	2.29
Height (m)	2.97
Impeller diameter (m)	1.14
Minimum RPM required	250
Total power required (kW)	468

4.1.4.3 Holding Tanks

In the effort to increase the amount of lithium obtained, the PBR network was designed such that the solution that undergoes adsorption in the secondary beds is held in a liquid storage tank between subsequent adsorption steps. As the flowrate of such solution decreases with each following adsorption, due to lithium and sodium ions being adsorbed each time, the total

capacity needed was based upon the solution entering the first secondary adsorption. The total number of tanks was then determined based upon a standard tank size.

It was identified that liquid storage tanks would also be needed for the lithium-enriched solution destined for the ED unit and the iron (III) chloride solution, with both allowing the ED unit to operate at steady state while the PBR network operates in cycles. It should be noted that the storage of iron (III) chloride solution was designed based upon the amount produced by the ED and iron (III) chloride mixing unit. *Table 4.1-10* below provides further information for all holding tanks, including the material of construction and capacities.

Table 4.1-10. Specifications for all Holding Tanks Involved in the PBR Network.

Liquid stored	Solution to undergo multiple secondary adsorptions	Lithium-enriched solution for the ED unit	Iron (III) chloride solution
Number of holding tanks	58	8	2
MOC	PP	PP	PP
Capacity per tank (m^3)	227	227	227

4.1.4.4 Pumps and Motors

Overall, there are 70 pumps and motors inside the Packed Bed Reactor Network, including spares. The primary material of construction for each pump is Hastelloy C-4. Based on the volumetric flow rate of the inlet fluid and the expected pressure drop, the total power requirement for pumping was found to be 1,791,338 kWh/yr.

4.2 Electrodialysis

4.2.1 Electrodialysis Units and Material Balance

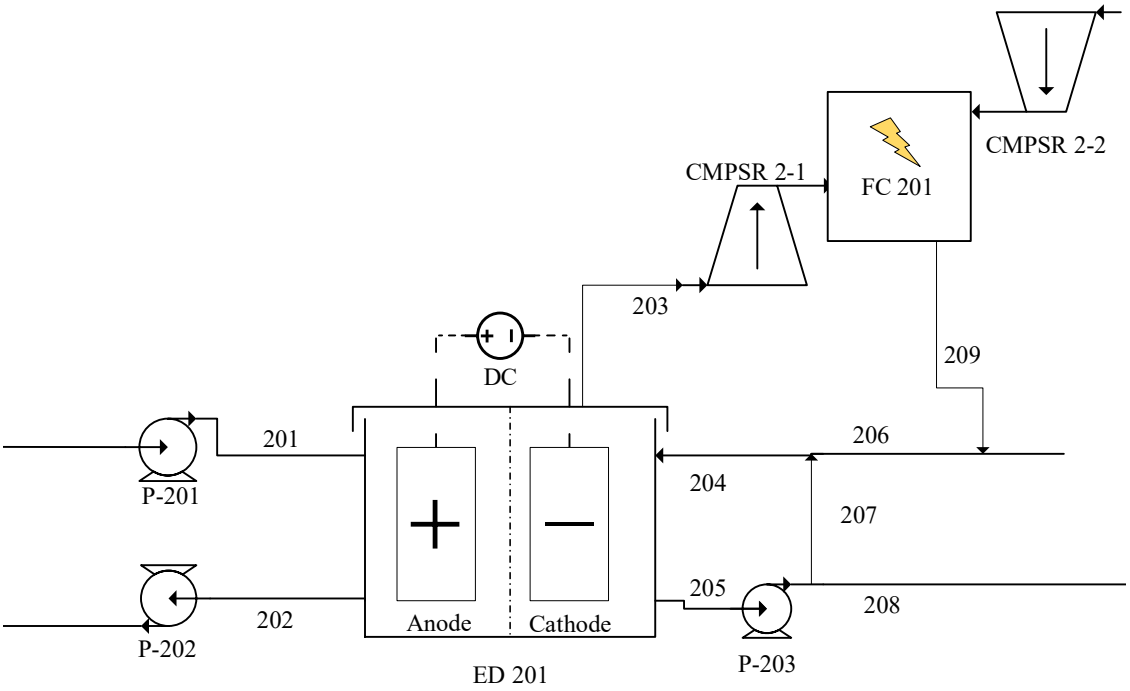

Figure 4.2-1. General Process Flow Diagram for Electrodialysis.

Electrodialysis is used to regenerate the iron (III) chloride stripping solution and create lithium hydroxide. A holding tank exists between the adsorption and stripping units and electrodialysis, allowing continuous electrodialysis operation. From the holding tank, a solution consisting of lithium chloride, iron (II) chloride, and trace amounts of iron (III) chloride and sodium chloride is fed to the anode side while a recycle stream of product diluted with additional water is fed to the cathode side of the units. Output from the anode is the regenerated stripping solution consisting solely of iron (III) chloride. Both saturated hydrogen gas and a solution of lithium hydroxide with trace sodium hydroxide leave the cathode side of the cell. The hydrogen gas produced the cathode of the electrolysis cell exits at 75 C in a ~7:4 molar ratio with water vapor in stream 203 before being compressed by CMPSR 2-1 to the desired 3.5 bar and fed into

a hydrogen fuel cell. To facilitate the reaction, ambient air at a temperature of 30 C is also pressurized to 3.5 bar by CMPSR 2-2 and pumped into the fuel cell at a rate of 9.61 mol/s. The mole balance for total streams shown in *Figure 4.2-1* are detailed in *Table 4.2-1* and the mass balance follows in *Table 4.2-2*.

Table 4.2-1. Molar Flow Rates Around Electrodialysis Units.

Stream		201	202	203	204	205	206	207	208
Temperature (C)		75	75	75	75	75	75	75	75
Pressure (Bar)		1.013	1.013	1.013	1.013	1.013	1.013	1.013	1.013
Mole Flow (mol/hr)		3263386	430363	22843	399560	3231752	125451	1956487	1275265
Phase		Liquid	Liquid	Vapor	Liquid	Liquid	Liquid	Liquid	Liquid
Component Flow (mol/hr)	Li+	29045	-	-	43567	72612	-	43567	29045
	OH-	-	-	-	43589	72648	-	43589	29059
	Fe2+	29064	-	-	-	-	-	-	-
	Fe3+	639	29703	-	-	-	-	-	-
	Cl-	89109	89109	-	-	-	-	-	-
	Na+	15	-	-	22	37	-	22	15
	H2	-	-	14530	-	-	-	-	-
	H2O	3115514	311551	8313	312382	3086455	125451	1869309	1217146

Table 4.2-2. Mass Flow Rates Around Electrodialysis Units.

Stream		201	202	203	204	205	206	207	208
Temperature (C)		75	75	75	75	75	75	75	75
Pressure (Bar)		1.013	1.013	1.013	1.013	1.013	1.013	1.013	1.013
Mass Flow (kg/hr)		61162	60960	179	57335	57359	22606	34729	22629
Phase		Liquid	Liquid	Vapor	Liquid	Liquid	Liquid	Liquid	Liquid
Component Flow (kg/hr)	Li+	202	-	-	302	504	-	302	202
	OH-	-	-	-	741	1236	-	741	494
	Fe2+	1623	-	-	-	-	-	-	-
	Fe3+	36	1659	-	-	-	-	-	-
	Cl-	3159	3159	-	-	-	-	-	-
	Na+	0	-	-	1	1	-	1	0
	H2	-	-	29	-	-	-	-	-
	H2O	56142	56142	150	56291	55618	22606	33685	21933

4.2.2 Material and Energy Requirements

100 electrodialysis units are operated in parallel with an applied potential of approximately 3.7 V and a total current of 1.1×10^6 A which accounts for a 70% current efficiency. This leads to 4.1 MW of electrical power required. Each cell has a current density of 2400 A/ m^2 with anode and cathode dimensions of 3.4 m^2 along with a Nafion-117 membrane with an effective area of 3.4 m^2. The anodes are constructed of graphite and the cathodes are made of nickel as recommended in literature (Grageda, 2020). The cells themselves are made of polyethylene. Air will be forced over the cells for cooling using 5 fans with 4.3 m (14 ft) diameter leading to an additional 10 kW of power required, and pumps used to move the fluid require an additional 5.7 kW. The power requirements for the hydrogen and air compressors respectively are 33.96 kW and 50.05 kW. With these inputs, fuel cell FC-201 will generate 492.1 kW of electrical power to be used within the plant. The more nuanced design of the hydrogen fuel cell was deemed beyond the scope of this project.

4.3 Crystallization

4.3.1 Crystallizer Units and Material Balance

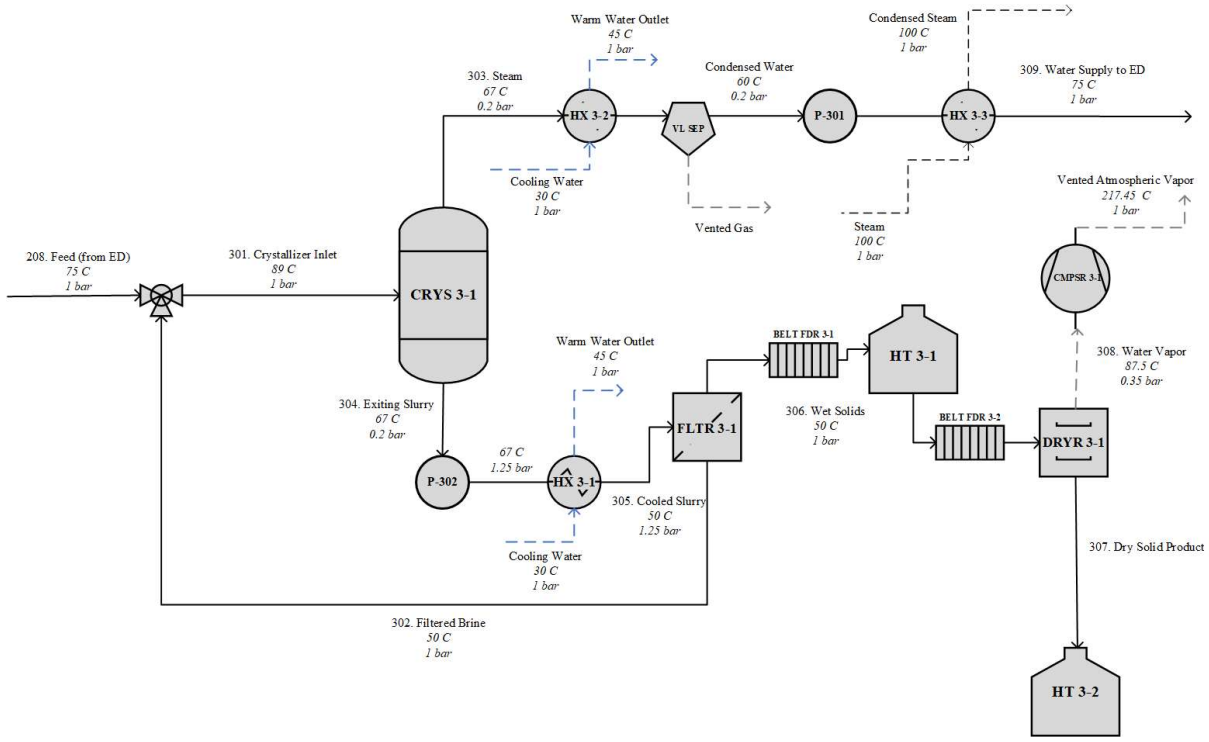

Figure 4.3-1. Process Flow Diagram for Crystallization Block.

The stream exiting the electrodialysis unit mixes with recycle stream 302 and enters the crystallizer CRYS 3-1 at 89 C and 1 bar. The crystallizer was sized based on the volume of slurry inside the unit, resulting in a volume of 10.65 m^3, length of 5.25 m, and diameter of 1.65 m. The crystallizer is obtained from Swenson Technologies and can be custom designed to meet our needs; thus, the crystallizer has the calculated diameter and is constructed with 316 stainless steel to prevent corrosion. Within the crystallizer, the solution is simultaneously cooled and evaporated at 67.9 C and 0.2 bar to crystallize the lithium hydroxide monohydrate product. Exiting stream 303 is low pressure steam at 0.2 bar, which is condensed in HX 3-2, pumped to 1 bar in P-301, and heated to 75 C in HX 3-3 before being sent to electrodialysis to meet the unit's water requirements. A vapor-liquid separator should be employed if any leftover gas from

electrodialysis remains in the stream. Stream 304 exits out of the bottom of the crystallizer and is pumped to 1.25 bar via P-302. It is assumed that within the crystallizer, a recirculation stream is employed for seeding to promote further nucleation.

Stream 304 is then sent to HX 3-1 to be cooled further to 50 C to induce further crystallization and prevent dissolution in the filter. The cooled stream is then sent to rotary vacuum filter FLTR 3-1 to separate the wet solids from the remaining brine. The filter was sized based on the properties of the wet solids and the inlet mass flow rate and density; thus, a filter area of 5.05 m^2 is required. Komline-Sanderson can accommodate this requirement with a filter area of 5.2 m^2, resulting in a diameter of 1.37 m. The remaining brine is recycled back to the crystallizer via stream 302, while the wet solids are scraped off the filter medium and are transported to silo HT 3-1.

The rotary dryer DRYR 3-1 operates in 1-hour batches; thus, the wet solids must be held in the silo while the previous batch dries. The dryer operates at 87.5 C and 0.35 bar to evaporate off the remaining water from the wet solids- operating below atmospheric pressure prevents the solids from redissolving into the brine and precipitating out as lithium hydroxide as determined by Aspen modeling. The dryer was sourced from Italvacuum- thus, the material of construction is 316 stainless steel. The evaporated water exits the dryer at 0.35 bar- to safely vent to the atmosphere, the low-pressure steam is sent through compressor CMPSR 3-1 to expand the steam to 1 bar. The hot steam exits into the atmosphere.

The dry solids in stream 307 are dispensed into silo HT 3-2 for storage until sale. The product exits the dryer at 99.6% purity, meeting the battery-grade specification of 99.12%. The annual production per year, assuming 90% plant uptime, is 9,639,139 kg, or 10,625 US tons. A detailed material balance is found in *Table 4.3-1*.

Table 4.3-1. Stream Table for Crystallization Block.

Stream		208	301	302	303	304	305	306	307	308	309
Temperature (C)		75	89	50	67	67	50	50	-	87.5	75
Pressure (Bar)		1	1	1	0.2	0.2	1.25	1	-	0.35	1
Mass Flow (kg/hr)		22803.78	24515.85	1712.07	21266.32	3254.09	3036.94	1357.70	1222.62	103.67	21266.32
Phase		Liquid	Liquid	Liquid	Vapor	Solid/Liquid	Solid/Liquid	Solid/Liquid	Solid	Vapor	Liquid
Component Flow (kg/hr)	H2O	21932.98	23037.53	1104.55	21266.32	1380.93	1234.47	136.51	3.00	103.67	21266.32
	Li+	201.63	297.13	95.54	-	163.77	107.35	11.81	0.31	0.00	-
	OH-	494.24	730.38	236.10	-	403.01	264.74	29.18	1.00	0.00	-
	LiOH*H2O	-	11.50	11.50	-	791.72	1132.87	1147.53	1217.06	0.00	-
	Na+	0.34	3.08	2.74	-	2.26	2.26	0.34	0.34	-	-

4.3.2 Material and Energy Requirements

The following section summarizes the equipment designed for the block. Only the main equipment details associated with capital costs are mentioned.

4.3.2.1 Primary Equipment Design and Power Requirements

The following table outlines the design and power requirements of the crystallizer, filter, and dryer. The filter is operated purely on electrical power, while the crystallizer and dryer will operate with a combination of heat and electrical power. The steam requirements to heat the crystallizer and dryer were not factored into the design process due to the complexity of the vacuum operation as well as a lack of specific data associated with the design process. Thus, the power requirements were calculated as solely electrical.

Table 4.3-2. Primary Equipment Specifications.

Equipment ID	Equipment Type	Size Specifications	Material of Construction	Annual Power Requirement (kWh)
CRYS 3-1	Crystallizer	10.6 m^3 in volume, 5.25 m length	316 Stainless Steel	110,376,000
FLTR 3-1	Filter	5.2 m^2 area	316 Stainless Steel + Cloth Medium	278
DRYR 3-1	Dryer	14.14 m^2 heating surface area	316 Stainless Steel	21,173

4.3.2.2 Heat Exchanger Design and Heat Duty

In total, 3 heat exchangers are used in this block as either heaters or coolers. Aspen modeling was used to determine the associated heat duty and aided in the calculation of utility stream requirements. As mentioned in *Section 4.1.5.1*, the cooling water was assumed to enter at 30 C and exit at 45 C, while the steam used for heating was assumed to condense in the exchanger.

Table 4.3-3. Heat Exchanger Specifications for Crystallization Block.

Equipment ID	Heater/Cooler	Heating Area Required (m^2)	Material of Construction	Heat Duty (kW)
HX 3-1	Cooler	36	Monel 400	-639
HX 3-2	Cooler	723	Carbon Steel	-16,170
HX 3-3	Heater	9	Carbon Steel	439

HX 3-1 was designed with Monel 400 to prevent corrosion from the slurry. Since the other two exchangers involve water, they were designed with generic carbon steel to minimize costs.

4.3.3.3 Additional Ancillary Equipment Design and Power Requirements

The remaining ancillary equipment and their associated specifications and power requirements are detailed in the following table.

Table 4.3-4. Ancillary Equipment Design and Power Requirements for Crystallization Block.

Equipment ID	Equipment Type	Specifications	Material of Construction	Annual Power Requirement (kWh)
P-301	Pump	2.32 bar differential pressure	Carbon Steel	27,417
P-302	Pump	2.33 bar differential pressure	316 Stainless Steel	9,007
BELT FDR 3-1	Conveyor Belt	0.05 m/s, 10 m length, 0.3 m width	Rubber + Carbon Steel	1,971
BELT FDR 3-2	Conveyor Belt	0.05 m/s, 10 m length, 0.3 m width	Rubber + Carbon Steel	1,971
HT 3-1	Silo	2 m^3 required volume	316 Stainless Steel	-
HT 3-2	Silo	898 m^3 required volume	316 Stainless Steel	-
CMPSR 3-1	Gas Compressor	493 m^3/s volumetric flow rate	Carbon Steel	56,492

4.3.3.4 Total Utility Stream and Electricity Requirements

Apart from the potential steam required to heat the crystallizer and dryer, the following table summarizes the annual electricity, cooling water, and steam requirements for this block.

Table 4.3-5. Utility Requirements for Crystallization Block.

Utility Stream	Total Annual Requirement
Electricity	110,494,309 kWh
Cooling Water at 30 C and 1 bar	2,112,435 kg
Steam at 100 C and 1 bar	5,507,047 kg

Section 5: Economics

5.1 Capital Costs

Where vendor pricing was not available, capital costs were estimated using E*quation 5.1-1* (Towler & Sinnott, 2022), where a, b, and n are constants defined by the type of equipment, and S is a size parameter with defined limits within which *Equation 5.1-1* is applicable.

$$C_e = a + bS^n \text{ (E 5.1-1)}$$

It should be noted that the equipment cost estimated through *Equation 5.1-1* does not account for inflation. Indeed, the textbook from which *Equation 5.1-1* was derived states that the equipment cost is what would be estimated in January 2010 (Towler & Sinnott, 2022). Thus, *Equation 5.1-1* is modified, where a Chemical Engineering Plant Cost Index (CEPCI) of 800 was divided by the January 2010 CEPCI as provided by Gavin Towler and Ray Sinnott in *Chemical Engineering Design: Principles, Practice and Economics of Plant and Process Design.* Furthermore, the equipment cost given by *Equation 5.1-1* is for equipment made of carbon steel. Due to the corrosivity of certain streams in this process, materials that are more resistant to chloride present in solution were modeled by further adjusting *Equation 5.1-1* with a factor based upon the material chosen. The final equation utilized to estimate the capital cost of equipment is shown below, where f represents the material cost factor as provided by Towler and Sinnott.

$$C = 1.5 f C_e \text{ (E 5.1-2)}$$

The overall fixed capital investment of the plant is based on the inside battery limits investment (ISBL) or the cost of the plant itself for the purposes of this project. ISBL plant costs include major and ancillary process equipment, bulk items, installation labor and supervision, and construction costs. Lang has proposed that ISBL fixed capital costs, a function of the total

purchased equipment cost and the total plant ISBL costs (including engineering costs), can be found by multiplying the equipment costs by what is now commonly referred to as a Lang factor. The Lang factor accounts for land, installation, construction, labor, and management costs during the construction phase. The factors are based on the type of processing plant. Identifying it as a mixed fluids-solids processing plant, capital cost estimations for the process described above have been calculated by multiplying equipment costs by a Lang factor of 3.63 (Towler & Sinnott 257).

5.1.1 Adsorption and Regeneration Capital Costs

The adsorption and regeneration unit requires a variety of equipment and materials to both capture lithium from geothermal brine and deliver an aqueous solution that is highly concentrated with lithium to the electrodialysis unit. The necessary equipment primarily includes adsorption beds, sorbent, pumps, motors, various holding units, impellers, and heat exchangers. The capital costs presented in Table 5.1-1 are categorized according to equipment type. The initial total capital costs are displayed as well as that with the consideration of the Lang Factor. The Lang Factor accounts for installation and space costs that come with plant construction. A Lang Factor of 3.63 was chosen according to recommendations for a solid and liquids processing plant (Towler & Sinnott, 2022).

Table 5.1-1. Breakdown of Capital Expenses by Equipment Type for Adsorption and Regeneration

Equipment/Material	Amount of Equipment/Material	Lifetime (Years)	Total Cost (USD)
Primary Beds	4	20	$634,002.79
Secondary Beds	4	20	$150,949.53
Sorbent	4,697,726 kg	20	$5,966,111.42
Pumps	70	20	$2,944,596.33
Motors	70	20	$1,282,439.81
Holding Tanks	68	20	$9,103,883.60
Silos	15	20	$6,909,951.35
Mixing Tanks	12	20	$378,942.07
Impellers	12	20	$42,745.00
Heat Exchangers	2	20	$586,559.60
		Total	$28,000,181.50
		Total with Lang Factor	$101,640,658.85

5.1.2 Electrodialysis Capital Costs

For electrodialysis, capital costs include membranes, electrodes, cell structures, pumps, motors, fans, and fuel cell components. Nafion 117 can be purchased from Chemours (Chemours personal communication, Mar. 19, 2024). For electrodes, assuming a cylindrical shape with 3.4 m^2 of exposed surface area and a thickness of 1 cm, electrode volumes were calculated and converted to mass based upon the density of the selected materials. Polypropylene is used to make the electrodialysis cell structures, requiring 3.4 m^2 per side of the cube-shaped cell and an assumed thickness of 2 cm. Pumps and motors have been priced as described above in *Equation 5.1-1* and have been constructed from Hastelloy C-4 to be resistant to chloride in the system. Cooling Fans have been priced by the vendor (Big Ass Fans, 2020).

Gas compressors were also priced as prescribed by *Equation 5.1-1* with the air and saturated hydrogen compressors being constructed using carbon and 316 stainless steels respectively. The cost of the hydrogen fuel cell stacks was estimated based on a 2018 per-kW capital cost estimate for Stationary PEM fuel cells published by a team at the National

Renewable Energy Laboratory (Hunter et al., 2021). As a contingency, 2 additional fuel cells were added.

Table 5.1-2. Breakdown of Capital Expenses for Electrodialysis and Fuel cell

Equipment	Amount of Equipment	Lifetime (Years)	Total Cost (USD)
Membranes	100	2	$557,000.00
Electrodes	200	3.5	$199,342.00
ED Cell Structure	100	20	$40,392.00
Pumps + motors	3	20	$99,058.60
Fans	5	20	$26,195.00
Gas Compressors	2	20	$1,047,276.00
Fuel Cell Stacks	35	20	$913,850.00
		Total	$2,883,110.00
		Total with Lang Factor	$10,465,700.00

5.1.3 Crystallization Capital Costs

The capital costs associated with the crystallization block include the vacuum crystallizer, rotary vacuum filter, rotary dryer, and various ancillary equipment. Since quotes from vendors were not readily available, the capital costs were estimated using the cost correlation curve described in *Equation 5.1-1.* The capital costs in Table 5.1-3 are categorized by equipment type and have been adjusted to account for the current CEPCI. The initial capital cost and adjusted Lang Factor cost are displayed as well. It was assumed that the lifetime of equipment would be 20 years

Table 5.1-3. Breakdown of Capital Expenses for Crystallization

Equipment	Amount of Equipment	Lifetime (Years)	Final Cost (USD)
Crystallizer	1	20	$116,586.74
Rotary Filter	1	20	$155,160.73
Rotary Dryer	1	20	$251,657.31
Pumps + Motors	2	20	$73,873.43
Silos	2	20	$392,116.86
Gas Compressors	1	20	$12,882.44
Belt Feeders	2	20	$145,017.83
Heat Exchangers	3	20	$382,476.73
		Total	$1,529,772.06
		Total with Lang Factor	$5,553,072.57

5.2 Operating Costs

5.2.1 Raw Materials

Various solid chemicals are needed to achieve the adsorption and regeneration process, including potassium citrate, iron (II) chloride, and iron (III) chloride. As the adsorption and regeneration process operates in a non-steady state manner, the cost per year for raw materials was estimated by first determining the amount of material needed per cycle, where a cycle was defined as 151.5 hours. The amount of material needed per year was then simply determined by multiplying the kg of material needed per cycle by the total number of cycles in one year. With the price per kg of each chemical determined from online vendors, the yearly costs associated with each raw material are outlined in *Table 5.2-1*. It should be reemphasized that due to this process being retrofitted to an existing geothermal power plant, there is no assumed cost with the 6,000 gal/min of brine that is received.

Table 5.2-1. Raw Material Costs for the Process

Raw Material	Amount needed per year (kg)	Cost (USD/Year)
Potassium Citrate	54,980,989.97	$60,606,149.76
Iron (II) Chloride	76,217,345.28	$7,621,734.53
Iron (III) Chloride	54,863,431.92	$10,972,686.38
Total	186,061,767.2	$79,200,570.68

5.2.2 Water and Steam Requirements

Water is required throughout the process for washing and mixing in the adsorption block, hydroxide production in the electrodialysis block, and cooling water for the multiple heat exchangers in the process. The price of utility water was found in a 2017 DOE report of water and wastewater prices in select cities in the United States- the paper reported a price of $5.85 USD per kilogallon in Valley Center, CA, in 2016 (Pacific Northwest National Laboratory,

2017). Adjusting to price per kilogram of water and accounting for inflation since 2016, a final cost of $0.0023 USD per kilogram of water was determined. The following table summarizes the water requirements for the process and the resultant cost of water per year, assuming a 90% plant uptime.

Table 5.2-2. Water Costs for the Process

Water Requirement	Feed Rate (kg/Year)	Cost (USD/Year)
Heat Exchangers - Adsorption	12,113,887,859	$28,005,161.04
Wash Water - Adsorption	359,315,694	$830,674.18
Mixing Water - Adsorption	407,630,508	$942,369.46
Production – Electrodialysis	9,533,346.3	$21,926.70
Heat Exchangers - Crystallization	2,112,435	$4,858.60
Total	12,892,479,842	$29,804,989.98

Note: The 'Feed Rate' was reported in kilograms per year to account for the batch cycles in the adsorption unit.

Steam is required in the crystallization block to heat the condensed water returned to the electrodialysis unit in a heat exchanger. The price of steam was estimated using a listed cost for LP steam without power credit from *Analysis, Synthesis, and Design of Chemical Processes, Fourth Edition* (Turton et al., 2012). The price was adjusted for inflation from 2012 (using a CEPCI of 584.6 (Maxwell, 2020)), resulting in a set price of $0.04008 USD per kilogram of steam. If the process was able to use steam at atmospheric pressure from the geothermal plant, however, it could be assumed that the cost of steam is negligible. However, this assumption would not be accurate for all plants, so the cost was accounted for.

Table 5.2-3. Steam Costs for the Process

Steam Requirement	Feed Rate (kg/hr)	Cost (USD/Year)
Heat Exchanger- Crystallization	628.66	$220,734.03
Total	628.66	$220,734.03

5.2.3 Energy Requirements

Energy is required for various processes within adsorption and regeneration, electrodialysis, and crystallization. These processes include pumping, mixing, cooling, drying, compressing, and moving various materials. The operations in the adsorption and regeneration and electrodialysis units are driven with electricity. In the crystallization unit, both electricity and heat in the form of steam are required to completely dry the final product. *Table 5.2-4* lists the category of equipment that requires power and its corresponding unit. The energy in kWh/year and resulting energy costs are also provided. The cost per kWh was set to $0.35 USD/kWh to match the price of electricity in Riverside County, CA, where a portion of the Salton Sea resides.

Table 5.2-4. Energy Costs by Unit and Process

Energy Requirement	Annual Energy Needed (kWh/year)	Cost (USD/year)
Pumps – Adsorption	1,791,338	$626,968.39
Mixing Tanks – Adsorption	4,861,684	$11,130,169.36
Pumps – Electrodialysis	78,840	$31,427.63
Fans - Electrodialysis	89,794	$27,594.00
Electrical Power - Electrodialysis	28,499,395	$9,974,787.99
Compressors- Fuel Cell	662,335	$231,817.19
Pumps - Crystallization	364,245	$12,748.56
Crystallizer - Crystallization	110,376,000	$38,631,600.00
Filter - Crystallization	278	$97.35
Belt Feeders - Crystallization	3,942	$1,379.70
Dryer - Crystallization	21,173	$7,410.56
Compressor - Crystallization	56,492	$19,772.06
Total	146,805,516	$60,695,772.79

Due to the production of hydrogen gas from the electrodialysis unit, a fuel cell was placed in the process to provide electricity back to electrodialysis. This helped decrease external energy usage and costs by providing over 3 million kWh per year and saving over $1 million in electricity costs. *Table 5.2-5* portrays the amount of electricity produced by the fuel cell and the

corresponding electricity costs saved as a result. The energy credited by the fuel cell was already factored into the total amount of power needed in *Table 5.2-4* above.

Table 5.2-5. Energy Provided by the Fuel Cell

Energy Credit Equipment	Annual Energy Produced (kWh/year)	Revenue (USD/year)
Fuel Cell	3,879,716.4	$1,357,900.74
Total	3,879,716.4	$1,357,900.74

5.2.4 Labor and Maintenance

Since the process is split into three major blocks, each block is expected to require 10 shift workers at a time. Assuming five shifts of workers are required for operation, it is necessary to employ 150 shift workers at the processing plant. Based on industry standards, each shift worker is estimated to receive a yearly salary of $50,000. In addition to shift workers, it is necessary to hire engineers. It is estimated that two engineers are required per unit, leading to a total of 6 engineers for the overall process. Due to elevated responsibility and training, and based on industry standards, each engineer will be paid $130,000 per year. Lastly, one plant manager is necessary to oversee all the operations and will be given a salary of $180,000 per year. In total, $8,460,000 will be spent yearly on labor.

Shift workers will be responsible for routine operations and some maintenance work. One routine maintenance order will be material replacement in the electrodialysis units. The Nafion membranes and the electrodes both have short lifespans in comparison to the anticipated 20-year lifespan of the plant. Membranes must be replaced every two years, but our operating schedule includes yearly replacement of half of the membranes. Electrodes should be replaced every 3.5 years. Instead of replacing all electrodes at once, every year 29 will be replaced to ensure no electrode is used beyond the 3.5-year mark. The cost of yearly replacement amounts to $335,455

and are considered in yearly maintenance costs. Additional maintenance expenses are estimated to be 2% of the total operating cost. Accounting for routine material replacement and other required maintenance, the yearly maintenance estimate is $3,740,605.

5.3 Process Viability

As of March 2023, Lithium hydroxide monohydrate is valued at $65/kg (About lithium, 2023). In our projections, we assume a 90% plant uptime to accommodate necessary maintenance, holidays, and other potential downtimes. Based on our designed operational model and considering this uptime, we anticipate an annual production of 10,625 tons of lithium. This production quantity, as determined by *Equation 5.3-1* below, translates to a corresponding annual revenue of $626,544,050.

$$Revenue = sale\ price \times \#\ of\ units\ sold \quad (E.\ 5.3\text{-}1)$$

Naturally, our financial projections must incorporate various factors, including capital investments, operational costs, and taxes. Relevant taxes to be considered include federal tax at 21%, state tax at 9%, and a product-specific lithium tax of $400 per ton (California Department of Tax and Fee Administration, 2024). A 20-year plant lifetime has been assumed, and the value reduction of capital investments is modeled as a 10-year straight-line depreciation. To assess the economic viability of our process design, two key economic indicators were considered: annual return on investment (ROI) and net present value (NPV).

ROI, calculated according to *Equation 5.3-2* below, provides a straightforward way to analyze the profitability of an investment in relation to its initial cost.

$$ROI = \frac{annual\ cash\ flow}{capital\ investment} \times 100 \quad (E.\ 5.3\text{-}2)$$

Generally, an ROI greater than 7% is considered to be a good investment (Birken, 2022). More narrowly in the context of a chemical plant, ROI's greater than 30% are deemed very desirable (Verret, 2020). The ROI for this project was calculated to be 162%.

Cumulative cash flows across the 20-year plant lifetime are plotted in Figure 5.3-1 below, with year zero reflecting the initial capital investment.

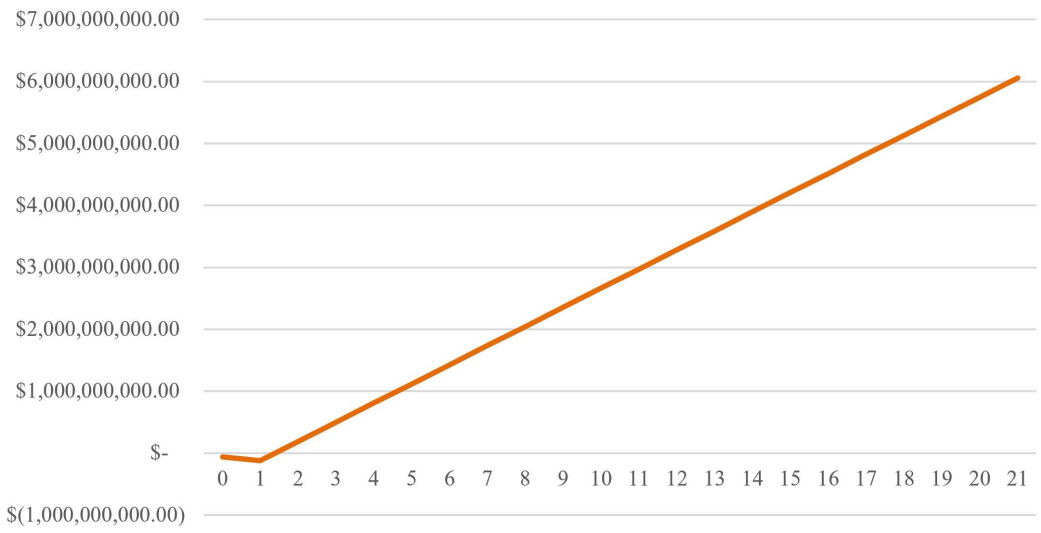

Figure 5.3-1. Cumulative Cash Flow Over Time.

Based on this plot, it is apparent that the plant will break even during the first year of operation. Though asset depreciation terminates at year 10, the difference in cash flow during and after the 10-year depreciation period is marginal, as operating costs significantly outweigh initial investments.

The net present value of the plant was calculated as prescribed by *Equation 5.3-3*, with CF_t representing the cash flow at time t, r representing the discount rate, and n representing the number of time periods.

$$NPV = \sum_{t=0}^{n} \frac{CF_t}{(1+r)^n} \quad (E.\ 5.3\text{-}3)$$

This financial metric represents the difference between the present value of cash inflows and the present value of cash outflows over a specific period, discounted at a specified rate. For this project, a discount rate of 8% was selected. NPV measures the net benefit or loss resulting

from an investment after accounting for the time value of money, and broadly an NPV greater than zero signifies project profitability (Fernando, 2024). Figure 5.3-2 below shows the NPV of investment across time.

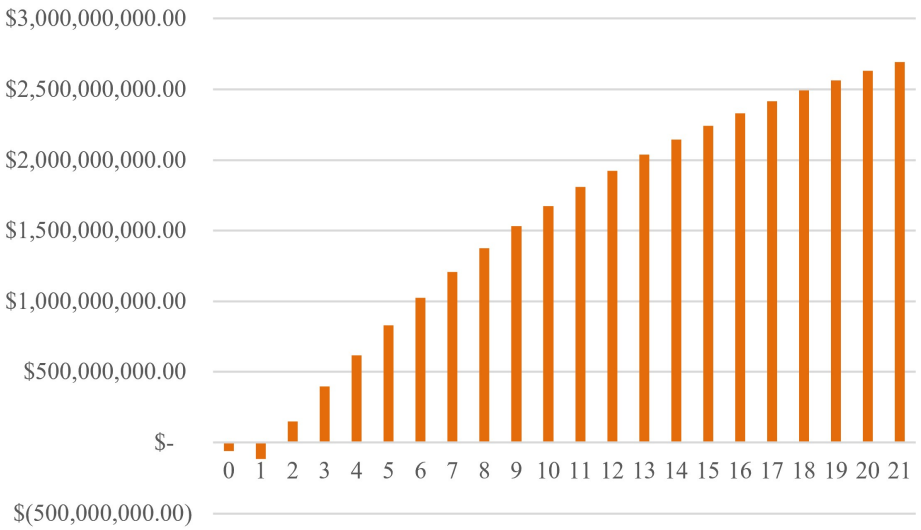

Figure 5.3-2. Net present value of Investment with an 8% Discount Rate.

As is clear in the figure above, by the 20th year of plant operation, an NPV of $2.6B is achieved, well surpassing the minimum NPV recommended for investment.

The robust ROI and NPV figures presented above unequivocally portray this project as a highly favorable investment opportunity, substantiating its viability and potential for lucrative returns.

Section 6: Environmental, Social, and Safety Considerations

6.1 Environmental Considerations

The primary concerns associated with this process are the water, power, and land requirements. In total, the process requires 13 billion kilograms of water a year to operate. Due to the high dissolved ion concentration and resulting osmotic pressure of the water within the process, a reverse osmosis (RO) system could not be implemented to recycle the water as the operating pressure required to generate flux would go beyond what commercially available RO systems can handle. As such, internal water recycling is limited. Although this process uses notably less water than traditional extraction methods (which would require almost 21 billion kilograms a year (Ahmad, 2020)), the quantity of water required is still significant. The state of California frequently experiences drought periods, the most recent occurring between 2020 and 2022. While larger cities are prepared to manage dry periods, smaller, rural communities are more vulnerable (Mount et al., 2021). Additionally, the *Pacific Institute* reported that the Salton Sea water level decreased by 11.4 ft from 2003-2022, and the inlet water flow decreased by over 9% from 2016-2022 (Pacinst, 2023). Thus, any operations in this area should be highly conscious of their water usage to not put nearby communities at risk, especially during drought seasons.

While the process is designed to retrofit to an existing plant, there are still significant land requirements, which contradict the original goal of reducing land requirements. The process in general has a large amount of equipment that will have to be constructed outside of the plant. Notably, the adsorption unit requires 68 holding tanks and 15 silos, which will require additional land outside of the plant. Within the electrodialysis block, 100 units are required, each unit

requiring 5 m^2 of land area to ensure proper air flow, which will also require about a football field's worth of space outside of the plant.

In addition to high water consumption, the process also requires 159,000 MWh a year to operate, which is 45% of the nameplate of the selected geothermal plant for construction. Although the electricity generated is from a renewable source, as well as a small amount supplied internally, the process would take away the amount of renewable energy supplied to the grid. Additionally, while geothermal energy is a renewable, there are still environmental hazards associated with the process, including the release of gas containing toxins such as ammonia and hydrogen sulfide, as well as water pollutants including toxic heavy metals (U.S. Fish & Wildlife Service, n.d.).

6.2 Social Considerations

It is estimated that the operation of the plant would provide 157 jobs, including operating personnel and site maintenance roles, generating economic benefits for the surrounding area. Additionally, the construction of a direct lithium extraction plant would increase domestic lithium production, allowing the country to decrease its reliance on imports. Presently, foreign imports, while not only costly, also pose several societal challenges, including the exploitation of local workers, displacement of communities and animals, and environmental negligence (Ahmad, 2020). Finally, the retrofitting of this plant to a geothermal plant has the potential to increase the attractiveness of geothermal energy as a primary driver in the renewables sector, potentially stimulating economic benefits for both the lithium and geothermal industries.

6.3 Safety Considerations

6.3.1 Lithium Adsorption and Regeneration

The primary chemical hazards in this process are associated with iron (II) chloride and iron (III) chloride powders that are added. According to the Fischer Scientific safety data sheets (SDS) for iron (II) chloride and iron (III) chloride, they are category 4 acute oral toxins, category 1 eye irritants, and toxic towards aquatic life. Iron (III) chloride is also a category 2 skin irritant. Both are incompatible with strong oxidizing agents and each other, while iron (III) chloride is additionally reactive with metals and strong bases. For storing purposes, they should be kept dry, cool, and receive adequate ventilation in an inert atmosphere. Potassium citrate powder does not have as many listed hazards as iron (II) chloride and iron (III) chloride, but it is also incompatible with strong oxidizing agents and should be stored in a dry environment with adequate ventilation at room temperature. Any of these powders may ignite with air or an oxidizing agent, resulting in a dust explosion, if they are not stored and maintained in the proper environment. Refer to the SDS for any of these chemicals for further information regarding storage recommendations.

6.3.2 Electrodialysis

One of the largest hazards associated with electrodialysis, and the process as a whole for that matter, is the production of chlorine gas. Although this is not expected based on the additional potential required to make chlorine gas in comparison to iron oxidation, the operating voltage is high enough that chlorine gas could be produced. While it is expected that any chlorine gas formed would interact with iron to produce iron (III) chloride anyways, some chlorine gas may escape, and it is vital to plan for the possibility of such. It is recommended that scrubbers are used to create bleach from any chlorine gas that is produced at the anode. Chlorine

gas is considered toxic and hazardous. It is a category 2 inhalation hazard with acute toxicity and a category 1 regarding skin corrosion *(Chlorine Gas MSDS*). It is fatal if inhaled and requires immediate medical attention if inhalation or contact occurs. Since it may not be possible to avoid chlorine gas completely with the current process, scrubbers should be used as engineering controls so any chlorine gas produced can be converted into a less harmful substance. To improve safety, an inherently safer design option is being considered at the laboratory scale utilizing iron sulfate rather than iron chloride. However, this has not been tested in the adsorption and regeneration units, and complete elimination of chlorine from the saline solution is unlikely, making the possibility of chlorine gas extremely difficult to avoid completely. Safety designs for chlorine gas have yet to be designed and have not been included in economic data and considerations, but safety equipment is recommended, and more research is required to better understand the associated hazards at the specified operating potential.

Though comparatively less harmful than chlorine gas, hydrogen gas – which is produced as a side product during electrodialysis and sent to the fuel cell for electricity generation – also poses risks that must be accounted for in this block. Though non-toxic, hydrogen is a category 1 flammable gas that can combust at concentrations from 4% to 74.2% by volume (*Hydrogen Gas MSDS)*. Hydrogen burns with a non-luminous flame, making it very difficult, if not impossible, to see in lighted conditions. Hydrogen's small molecular size allows for relatively easy permeation, and as such, containment materials of construction must be chosen wisely. Carbon steel is insufficient, as hydrogen permeation can cause embrittlement and loss of ductility especially at elevated temperatures. Instead, more corrosion and embrittlement-resistant alloys such as stainless steel should be used. As additional precautions, engineering controls such as

leak detection systems, pressure relief systems, ventilation systems, and flame arrestors should be installed and maintained regularly.

6.3.3 Crystallization

As with the other blocks, the crystallization block poses its own safety risks. One of the larger safety risks associated with the process is the equipment operating under a vacuum. Equipment that operates under a vacuum is highly prone to implosion, splattering chemicals, and fire, especially if any chemicals are drawn into the vacuum apparatus. Care should be taken to design the apparatus so that any potential leaks are prevented, and the system has an emergency ventilation procedure. Additionally, the vessels should not be suddenly opened to prevent a pressure surge, which could also lead to an explosion (High Vac Depot Staff, 2023). Additionally, the steam in this process, while not inherently dangerous, can be a safety hazard if not handled properly. The steam vented from the dryer into the atmosphere should be designed such that hot, condensed steam does not drop on and injure personnel (IChemE, 2004). Additionally, the hot steam in the exchangers can cause thermal expansion if not properly ventilated, resulting in an explosion. Proper risk mitigation should be employed during the design and construction process.

In terms of chemical hazards, lithium hydroxide monohydrate is a category 4 acute oral toxin, corrosive, and toxic to aquatic life. Special care should be taken to not inhale any dust from the process as the solids exit the dryer. Contact with the skin can cause permanent damage. Additionally, equipment should be frequently inspected for damage from corrosion. The SDS should be referred to regarding storage recommendations and accident mitigation.

Section 7: Conclusions and Recommendations

Overall, it has been shown that this process is a strong candidate for implementation and investment due to the favorable annual return on investment and net present value. That said, the initial motivation for this project was to improve upon the energy, water, and land requirements of traditional lithium extraction techniques. Section 6.1 outlined that 159,000 MWh are required per year to operate this process, equating to approximately 45% of the nameplate of an existing geothermal power plant. Furthermore, while this process demands considerably less water than traditional extraction methods, it still requires approximately 13 billion kg of water per year to operate in an area that frequently experiences periods of drought. The land requirements follow a similar pattern, where this process is indeed retrofitted to an existing geothermal power plant yet still requires additional land for various process equipment. Thus, it has been shown that this process can still improve, with specific recommendations for each block outlined below. It should be noted that an overarching recommendation is that data that is more relevant to the process and its conditions should be collected.

7.1 Conclusions and Recommendations for Adsorption and Regeneration

The first recommendation for the adsorption and regeneration unit is to find a replacement for the reaction "driving force", potassium citrate. Potassium citrate is an expensive chemical, standing currently at $1.10/kg. It is also minimally soluble in water, leading the unit to need eight 8,000 gallon mixing tanks just to dissolve the citrate in the flows going to adsorption. With adsorption happening for a total of 150 hours out of the 151.5-hour cycles, large amounts of potassium citrate were required and were consequently responsible for 56% of total annual chemical costs in this unit. A significantly less expensive chemical that could act as a "driving force" for adsorption would make the construction and operation of this theoretical plant much more feasible.

Furthermore, it is recommended to examine the favorability of the subsequent adsorptions in the secondary PBRs. During the secondary adsorption steps, it is assumed that the previously dissolved citrate will still increase the favorability of the subsequent adsorptions because it does not physically participate in the reaction. However, the concentrations of iron (II) and iron (III) ions are changing slightly with each subsequent adsorption. As lithium ions are continually adsorbed out of solution per each subsequent adsorption, the concentration of iron (III) ions increases relative to that of iron (II) ions. These two components are in the Nernst equation that determines whether the reaction will be favorable at non-standard conditions. It's recommended to test this strategy of recycling brine for subsequent adsorptions on a laboratory scale at the temperature of the brine. In this way, clearer discretion can be provided regarding how many times the brine can be recycled for subsequent adsorptions without adding iron (II) ions each step before the reaction fails to proceed forward.

The next recommendation is to decrease water and electricity usage in this unit as much as possible. This goal is universal in many processes and much easier said than done. The idea for this processing plant is built on the idea of sustainable lithium acquisition and decreased use of land, water, and other scarce resources. However, this unit uses 12.8 billion kg of water annually. Lithium extraction from salt flats is reported to use roughly 21 billion kg of water to produce an equivalent amount of product as seen in this design, meaning that water usage in the process was not even halved in comparison to current methods (Ahmad, 2020). Therefore, it is necessary to further advance this process such that it demands much less water.

Lastly, it's important to emphasize that while adsorption and regeneration is the costliest in terms of resources and money relative to the other units detailed earlier, it is one of the most crucial upstream operations in this process. Therefore, the adsorption and regeneration processes must be optimized to acquire as many lithium ions from the brine as possible while also maximizing product purity. As this is a newly researched operation, there are many ways adsorption and regeneration could be designed to achieve these two main goals. Further data collection on the adsorption and regeneration block is highly recommended to maintain the integrity of the product and meet the sustainability goals behind the process when on an industrial scale.

7.2 Conclusions and Recommendations for Electrodialysis

The lack of experimental data led the electrodialysis unit design to be based primarily on theory. It is recommended that more data is collected to optimize the operating voltage to a value in which all iron is oxidized, and no chlorine gas is produced. For purposes of this paper, many assumptions were made concerning the operating voltage and the expected reactions, yet experimental data would be instrumental in furthering the design and accuracy. A significant portion of the electrodialysis design was based on a system which lacked iron and intended to produce chlorine gas (Grageda, 2020). Current density and anticipated potential drops across the anolyte and catholyte were based on this system, which likely led to inaccuracies since not all components were represented. Current data was used for the current efficiency, but this data again did not include iron in the system and was not at the specified operating voltage. For the future of this work, it is important to collect data at the specified current density, voltage, temperature, electrode materials, anolyte and catholyte concentrations, and with all components accounted for. It is recommended that these variables be further optimized based on experimental data and results prior to implementation in the proposed processing plant.

7.3 Conclusions and Recommendations for Crystallization

The primary recommendation for the crystallization block is data collection on the solubility of lithium hydroxide monohydrate crystals. The specified reaction chemistry in Aspen Plus V14 indicated that crystallization was not possible at atmospheric pressure, resulting in the need for the unit to operate under a vacuum, ultimately increasing the energy requirement of the process. Literature data, however, states that the crystals should not have dissolved at the set temperature of the crystallizer (which was set to 110 C, or the approximate saturation point of the brine). A small-scale crystallization process should be employed to observe the reaction kinetics surrounding the formation of lithium hydroxide monohydrate to accurately predict operating specifications, particle size distribution, and growth rate to refine the crystallizer design. If crystallization is possible at atmospheric pressure, the operating cost would be reduced, and calculation of the steam requirements for the unit would be much more straightforward. Additionally, operation at atmospheric pressure would eliminate the need for one of the heat exchangers for the steam exiting the block (since the steam could be cooled and condensed in the same block) as well as the heat exchanger for the slurry exiting the crystallizer (since there would not be a concern for dissolution).

The same rationale applies for the rotary dryer design- again, if the thermodynamics of lithium hydroxide monohydrate solids drying was studied, there is a possibility that the dryer could operate continuously at atmospheric pressure rather than under a vacuum, lowering operating costs and eliminating the need for an additional belt feeder and holding tank. Additionally, calculation of the steam/air requirement for drying would make the operating cost calculations more accurate.

Finally, collection of literature values for lithium hydroxide monohydrate solid properties (including compressibility, cake resistance, etc.) would make design of the filter more accurate, resulting in higher accuracy in capital and operating costs for the filter.

Acknowledgements

We would like to thank University of Virginia Professors Geoff Geise, Gaurav "Gino" Giri, and Gary Koenig, part of Team TELEPORT, for sponsoring this project and their guidance throughout the design process. We would also like to thank the undergraduate and graduate members of their respective labs for providing research data to aid in design calculations. Finally, we would like to thank our technical advisor, Professor Eric Anderson, for his continual support and guidance throughout the completion of this project.

References

Ahmad, S. (2020, January 15). *The Lithium Triangle: Where Chile, Argentina, and Bolivia Meet*. Harvard International Review; Harvard International Review. https://hir.harvard.edu/lithium-triangle/

Applied Chemical Technology. (n.d.). *Rotary Vacuum Dryer*. Applied Chemical Technology. Retrieved March 23, 2024, from https://appliedchemical.com/equipment/rotary-drums/rotary-dryers/rotary-vacuum-dryer/

Ayranci, I. & Kresta, S. M. (2014). Critical analysis of Zwietering correlation for solids suspension in stirred tanks. *Chemical Engineering Research and Design, 92*(3). https://doi.org/10.1016/j.cherd.2013.09.005

Big Ass Fans. (2022, June 21). Cutsheet-es6.pdf. https://bigassfans.com/docs/es6/cutsheet-es6.pdf

Birken, E. G. (2022, September 28). *What Is Return On Investment (ROI)? – Forbes Advisor*. Forbes. Retrieved April 5, 2024, from https://www.forbes.com/advisor/investing/roi-return-on-investment/

Brecht, A. V., Hens, H., Lemaire, J.-L., Aerts, J. M., Degraeve, P., & Berckmans, D. (2005). Quantification of the heat exchange of chicken eggs. *Poultry Science*, *84*(3), 353–361. https://doi.org/10.1093/ps/84.3.353

Budiarto, T., Esche, E., Repke, J. U., & Leksono, E. (2017). Dynamic Model of Chloralkali Membrane Process. *Procedia Engineering*, *170*, 473–481.
https://doi.org/10.1016/j.proeng.2017.03.076

California Department of Tax and Fee Administration. (2024, January 4). *California Lithium Extraction Tax Study Report*. CDTFA. Retrieved April 5, 2024, from https://www.cdtfa.ca.gov/taxes-and-fees/LithiumTaxStudy.pdf

Carta, G. (2021). *Heat and mass transfer for chemical engineers.* (1st ed., pp.426-431). McGraw Hill.

Chao, J. (2020, August 5). *Geothermal Brines Could Propel California's Green Economy*. Berkeley Lab. https://newscenter.lbl.gov/2020/08/05/geothermal-brines-could-propel-californias-green-economy/

Chicago Metal Rolled Products. (2016, May 22). *What is the best angle design when rolling a metal cone for the bottom of a silo?* Retrieved March 21, 2024, from https://www.cmrp.com/blog/bending/angle-bending/what-is-the-best-angle-design-when-rolling-a-metal-cone-for-the-bottom-of-a-silo.html

Chlorine Gas MSDS. Airgas. (2021, February 11). https://www.airgas.com/msds/001015.pdf

Connor, N. (2021, June 29). *Graphite: Density, strength, hardness, melting point*. Material Properties. https://material-properties.org/graphite-density-strength-hardness-melting-point/

Convective Heat Transfer. Engineering ToolBox. (n.d.-a). https://www.engineeringtoolbox.com/convective-heat-transfer-d_430.html

Department of Energy. (n.d.). *Lithium*. Energy.gov. Retrieved November 28, 2023, from https://www.energy.gov/eere/geothermal/lithium

Earnshaw-Osler, M. (2023, February 24). *The social and environmental impacts of lithium mining*. Borrum Energy Solutions. https://borrumenergysolutions.ca/blogs/blog/the-social-and-environmental-impacts-of-lithium-mining#:~:text=The%20process%20of%20extracting%20lithium,to%20long%2Dterm%20ecological%20damage

Fernando, J. (2024, March 7). *Net Present Value (NPV): What It Means and Steps to Calculate It*. Investopedia. Retrieved April 5, 2024, from https://www.investopedia.com/terms/n/npv.asp

Gabelman, A. (2017, July). Adsorption basics: Part 1. *CEP Magazine*. https://www.aiche.org/publications/cep

Genck, W. J., Albin, B., Baczek, F. A., Dickey, D. S., Gilbert, C. G., Herrera, T., Laros, T. J., Li, W., McCurdie, P., McGillicuddy, J. K., McNulty, T. P., Moyers, C. G., Schoenbrunn, F., Wisdom, T. W., & Chen, W. (2019a). CRYSTALLIZATION FROM SOLUTION. In D. W. Green & M. Z. Southard (Eds.), *Perry's Chemical Engineers' Handbook* (9th Edition). McGrawHill Education. https://www.accessengineeringlibrary.com/content/book/9780071834087/tocchapter/chapter18/section/section21

Genck, W. J., Albin, B., Baczek, F. A., Dickey, D. S., Gilbert, C. G., Herrera, T., Laros, T. J., Li, W., McCurdie, P., McGillicuddy, J. K., McNulty, T. P., Moyers, C. G., Schoenbrunn, F., Wisdom, T. W., & Chen, W. (2019b). FILTRATION. In D. W. Green & M. Z. Southard (Eds.), *Perry's Chemical Engineers' Handbook* (9th Edition). McGrawHill Education. https://www.accessengineeringlibrary.com/content/book/9780071834087/tocchapter/chapter18/section/section51

Grageda, M., Gonzalez, A., Quispe, A., & Ushak, S. (2020). Analysis of a Process for Producing Battery Grade Lithium Hydroxide by Membrane Electrodialysis. *Membranes*, *10*(9). https://doi.org/10.3390/membranes10090198

High Vac Depot Staff. (2023, March 14). *Safety Considerations For Vacuum Systems*. High Vac Depot. https://highvacdepot.com/2023/03/14/safety-considerations-for-vacuum-systems/

Hyde, A. M., Zultanski, S. L., Waldman, J. H., Zhong, Y.-L., Shevlin, M., & Peng, F. (2017). General Principles and Strategies for Salting-Out Informed by the Hofmeister Series.

Organic Process Research & Development, *21*(9), 1355–1370. ACS Publications. https://doi.org/10.1021/acs.oprd.7b00197

Hydrogen Gas MSDS. Airgas. (2020, September 15). https://www.airgas.com/msds/001026.pdf

IChemE. (2004). *Hazards of Steam* (4th ed.). Institution of Chemical Engineers (IChemE). http://ndl.ethernet.edu.et/bitstream/123456789/42246/1/14.pdf

Iron (II) Chloride. ChemEurope. https://www.chemeurope.com/en/encyclopedia/Iron%28II%29_chloride.html

James, B. D., & Kalinoski, J. A. (2009, March 26). *Mass production cost estimation for direct H2 PEM fuel.* Mass Production Cost Estimation for Direct H2 PEM Fuel Cell Systems for Automotive Applications: 2008 Update. https://www.energy.gov/eere/fuelcells/articles/mass-production-cost-estimation-direct-h2-pem-fuel-cell-systems-0

King, M. (2022, Oct. 14). *Mixing* [Presenter]. CHE 3321, University of Virginia.

Komline-Sanderson. (n.d.). https://komline.com/wp-content/uploads/2024/02/KS-RDVF.pdf

Libretexts. (2021, December 17). *P1: Standard reduction potentials by element*. Chemistry LibreTexts. https://chem.libretexts.org/Ancillary_Materials/Reference/Reference_Tables/Electrochemistry_Tables/P1%3A_Standard_Reduction_Potentials_by_Element

London Metal Exchange. (2023, March). About lithium. www.lme.com/Metals/EV/About-Lithium

Maxwell, C. (2020, May 28). Cost Indices – Towering Skills. Toweringskills.com. https://toweringskills.com/financial-analysis/cost-indices/

MIT. (n.d.). Material type cost. https://web.mit.edu/course/3/3.11/www/modules/props.pdf

Monnin, C., & Dubois, M. (2005). Thermodynamics of the LiOH + H_2O System. *Journal of Chemical & Engineering Data*, *50*(4), 1109–1113. ACSPublications. https://doi.org/10.1021/je0495482

MonTech. (n.d.). *TB40 Belt Conveyor: Enhancing Fast and Precise Processes*. Retrieved March 23, 2024, from https://montech.com/us/en/belt-conveyors/tb40-conveyor/

Mount, J., Escriva-Bou, A., & Sencan, G. (2021, April). *Droughts in California*. Public Policy Institute of California. https://www.ppic.org/publication/droughts-in-california/

National Renewable Energy Laboratory. (2021, July 21). *Using Direct Lithium Extraction To Secure U.S. Supplies*. Www.nrel.gov. https://www.nrel.gov/news/program/2021/using-direct-lithium-extraction-to-secure-us-supplies.html .

Nowee, S. M., Abbas, A., & Romagnoli, J. A. (2008). Antisolvent crystallization: Model identification, experimental validation and dynamic simulation. *Chemical Engineering Science*, *63*(22), 5457–5467. ScienceDirect. https://doi.org/10.1016/j.ces.2008.08.003

Orehek, J., Teslić, D., & Likozar, B. (2020). Continuous Crystallization Processes in Pharmaceutical Manufacturing: A Review. *Organic Process Research & Development*, *25*(1), 16–42. https://doi.org/10.1021

O'Brien, T. F., Bommaraju, T. V., & Hine, F. (2005). *Handbook of Chlor-Alkali Technology* (Vol. 1). Springer.

Pacific Northwest National Laboratory. (2017). Water and Wastewater Annual Price Escalation Rates for Selected Cities across the United States. Department of Energy. https://www.energy.gov/sites/prod/files/2017/10/f38/water_wastewater_escalation_rate_study.pdf

Pacinst. (2024, Mar. 21). *Current Information on the Salton Sea.* Pacific Institute. https://pacinst.org/current-information-salton-sea/

Parambil, J. V., & Heng, J. Y. Y. (2017). Seeding in Crystallisation. *Engineering Crystallography: From Molecule to Crystal to Functional Form*, 235–245. Springer Link. https://doi.org/10.1007/978-94-024-1117-1_13

Peters, M. S., Timmerhaus, K. D., & West, R. E. (2003). Heuristics for process equipment design. In *Plant design and economics for chemical engineers* (5th ed., pp. 966-973). McGraw-Hill Education. https://elbunkerdequimica.files.wordpress.com/2020/09/plant-design-and-economics-for-chemical-engineers-by-max-peters-klaus-timmerhaus-ronald-west-max-peters-z-lib.org_.pdf

Perfluorinated membrane made of Nafion TM 117. Sigma-Aldrich. (n.d.). https://www.sigmaaldrich.cn/CN/zh/product/aldrich/292567

Protectoplas. (2022, October 20). *Industrial mixing tanks: Plastic mixing tanks with agitators & baffles*. Retrieved March 21, 2024, from https://protectoplas.com/industrial-mixing-tanks/

Ravichandran, S. A., Krist, J., Edwards, D., Delagah, S., & Pellegrino, J. (2019). Measuring sparingly soluble, aqueous salt crystallization kinetics using CSTRs in series: Methodology development and CaCO3 studies. *Separation and Purification Technology*, *211*, 408–420. https://doi.org/10.1016/j.seppur.2018.09.084

Salton sea climate info: What's the weather like in Salton Sea, California (U.S.A.). Salton Sea climate info | what's the weather like in Salton Sea, California (U.S.A.). (n.d.). https://www.whatstheweatherlike.org/united-states-of-america/california/salton-sea.htm

Towler, G. & Sinnott, Ray. (2022). *Chemical Engineering Design - Principles, Practice and Economics of Plant and Process Design (3rd Edition)*. Elsevier https://app.knovel.com/hotlink/pdf/id:kt012WN1S1/chemical-engineering/fixed-capital-investment

Turton, R., Bailie, R. C., Whiting, W. B., Shaeiwitz, J. A., & Bhattacharyya, D. (2012). Analysis, Synthesis, and Design of Chemical Processes (4th ed.). Prentice Hall. https://learning.oreilly.com/library/view/analysis-synthesis-and/9780132618724/?ar=. Chapter 8.3.

Shine, I. (2022, July 20). *The world needs 2 billion electric vehicles to get to net zero. But is there enough lithium to make all the batteries?* World Economic Forum. https://www.weforum.org/agenda/2022/07/electric-vehicles-world-enough-lithium-resources/

Skindzier, M., Kaplan, K., & Roberts, A. (n.d.). *Crystallizers – Visual Encyclopedia of Chemical Engineering Equipment*. Encyclopedia.che.engin.umich.edu. Retrieved March 23, 2024, from https://encyclopedia.che.engin.umich.edu/crystallizers/#4P8ZWTP0WJGU3JH020BP

Stenina, I. A., Sistat, P., Rebrov, A. I., Pourcelly, G., & Yaroslavtsev, A. B. (2004). Ion mobility in Nafion-117 membranes. *Desalination*, *170*(1), 49–57. https://doi.org/10.1016/j.desal.2004.02.092

U.S. Fish & Wildlife Service. (n.d.). *Geothermal Energy | U.S. Fish & Wildlife Service*. FWS.gov. https://www.fws.gov/node/265252#:~:text=Air%20and%20water%20pollution%20are

Verrett, J., Qiao, R., Barghout, R. A. (2020). Foundations of Chemical and Biological Engineering I. BCcampus.

Volkov, V. I., Chernyak, A. V., Gnezdilov, O. I., & Skirda, V. D. (2021, April 19). *Hydration, self-diffusion and ionic conductivity of Li+, Na+ and Cs+ cations in Nafion membrane studied by NMR*. Solid State Ionics. https://www.sciencedirect.com/science/article/abs/pii/S0167273821000801

Water - saturation pressure vs. temperature. Engineering ToolBox. (n.d.-b). https://www.engineeringtoolbox.com/water-vapor-saturation-pressure-d_599.html?vA=80&units=C

Ying Shan, L. (2023, August 29). *A worldwide lithium shortage could come as soon as 2025*. CNBC. https://www.cnbc.com/2023/08/29/a-worldwide-lithium-shortage-could-come-as-soon-as-2025.html

20.4 Cell Potential Under Standard Conditions. LibreTexts. https://chem.libretexts.org/Bookshelves/General_Chemistry/Map%3A_Chemistry_-_The_Central_Science_(Brown_et_al.)/20%3A_Electrochemistry/20.04%3A_Cell_Potential_Under_Standard_Conditions

Appendix A: Design and Operating Calculations

A.1 Sample Calculations for Equipment Design, Scheduling, and Operating

---

Mixing Unit Sizing and Operating Requirements

$\dot{m}_{solid}$ = 33,785 g/min	Mass flow rate of $FeCl_2$ (s) into one $FeCl_2$ mixing tank
$solubility$ = 1.057 g/mL	Solubility of $FeCl_2$ (s) in H_2O (l) at 100 C (ChemEurope)
$\dot{V}_{feed,mixing}$ = 0.03 m^3/min	Volumetric flow rate of feed sent to one $FeCl_2$ mixing tank
V_{mix} = 0.32 m^3	Volume of one $FeCl_2$ mixing tank
τ = 10 min	Residence time

(E 3.1-1) $\frac{\dot{m}_{solid}}{solubility} = \dot{V}_{feed,mixing} = \frac{33{,}785\ g/min}{1.057\ g/mL} * \left(\frac{1\ L}{1000\ mL}\right) * \left(\frac{1\ m^3}{1000\ L}\right) = 0.03\ m^3/min$

(E 3.1-2) $V_{mix} = \dot{V}_{feed,mixing} \cdot \tau = 0.03 \frac{m^3}{min} * 10\ min = 0.32\ m^3$

Impeller Sizing

$d_{impeller}$ = 0.29 m	Diameter of the impeller in 1 $FeCl_2$ mixing tank
d_{mixing} = 0.58 m	Diameter of 1 $FeCl_2$ mixing tank
N_{Re} = 1,841,082.27	Reynolds number for mixing $FeCl_2$ (s) in the brine
ρ_{fluid} = 974.89 kg/m^3	Density of the fluid to be mixed (brine in the case of the $FeCl_2$ mixing tank)
μ_{fluid} = 0.0003765 Pa s	Viscosity of the fluid to be mixed
N_P = 1.7	Power number for mixing $FeCl_2$ (s) in the brine
n = 8.33 rev/s	Impeller speed in the $FeCl_2$ mixing tank
P = 2,039.48 W	Power required for the impeller in one $FeCl_2$ (s) mixing tank

(E 3.1-3) $d_{impeller} = d_{mixing} \cdot 0.5 = 0.58\ m * 0.5 = 0.29\ m$

(E 3.1-4) $\frac{\dot{m_{solid}}}{2 \cdot \dot{V_{feed,mixing}} \cdot \rho_{fluid} + \dot{m_{solid}}} \cdot 100 = mass\ percent\ of\ solid$

(E 3.1-5) $N_{Re} = \frac{n d_{impeller}^2 \rho_{fluid}}{\mu_{fluid}} = \frac{8.33 \frac{rev}{s} * 0.29\ m^2 * 974.89 \frac{kg}{m^3}}{0.0003765\ Pa\ s} = 1{,}841{,}082.72$

(E 3.1-6) $N_P = \frac{P}{n^3 d_{impeller}^5 \rho_{fluid}} \rightarrow P = N_P n^3 d_{impeller}^5 \rho_{fluid} = 1.7 * (8.33 \frac{rev}{s})^3 * (0.29\ m)^5 *$

$974.89 \frac{kg}{m^3} = 2{,}039.48\ W$

Primary/Secondary Reactor Sizing

$\dot{V}_{bed}$ = 0.19 m^3/s	Volumetric flow rate of the brine to 1 primary bed
$\dot{V}_{overall}$ =23.04 m^3/min	Volumetric flow rate of the brine
$number\ of\ beds$ = 2	Number of primary beds operating per adsorption period
d_{bed} = 9.88 m	Diameter of one primary bed
u = 0.0025 m/s	Superficial velocity of the fluid to the bed
dz = 9.88 m	Height of one primary bed
f_f =22.45	Friction factor for the primary bed
ρ = 974.89 kg/m^3	Density of the feed
d_p = 0.003 m	Diameter of the sorbent particle
$\bar{\varepsilon_b}$ = 0.4	Porosity of the sorbent particle
Re = 19.42	Reynolds number for the fluid flow to the primary bed
μ = 0.0003765 Pa s	Viscosity of the brine
V_{bed} = *759.50 m^3*	Volume of one primary bed
$m_{sorbent}$ = 1,063,297.50 kg	Mass of sorbent in one primary bed
$V_{sorbent}$ = 759.50 m^3	Volume of sorbent in one primary bed
$\rho_{sorbent}$ = 1400 kg/m^3	Bulk particle density of the sorbent
$\dot{V}_{bed,2}$ = 1000 L/min	Volumetric flow rate of aqueous regeneration solution to one secondary bed (for sizing purposes)
$\dot{n}_{FeCl3}$ = 1000 mol/min	Molar flow of $FeCl_3$ to one secondary bed
S = 390	Initial selectivity for lithium versus sodium in the primary bed when adsorbing the brine
$C_{Li^+,sorbent}$ = 2.5 mmol/g	Theoretical concentration of lithium ions in the sorbent
$C_{Na^+,sorbent}$ = 0.5 mmol/g	Theoretical concentration of sodium ions in the sorbent
$C_{Li^+,feed}$ = 1 wt/vol (relative to Na^+)	Concentration of lithium ions in the feed with respect to sodium ions
$C_{Na^+,feed}$ = 78 wt/vol (relative to Li^+)	Concentration of sodium ions in the feed with respect to lithium ions

(E 3.1-7) $\dot{V}_{bed} = \frac{\dot{V}_{overall}}{number\ of\ beds} = \frac{23.04\ m^3/min}{2} * \left(\frac{1\ min}{60\ s}\right) = 0.19\ m^3/s$

(E 3.1-8) $d_{bed} = \sqrt{\frac{\dot{V}_{bed}}{\pi u}} = \sqrt{\frac{0.19\ m^3/s}{\pi * 0.0025\ m/s}} = 9.89\ m$

(E 3.1-9) $-\frac{dP}{dz} = \frac{f_f \rho u}{d_p} \rightarrow -dP = \frac{22.45 * 974.89 \frac{kg}{m^3} * 0.0025 \frac{m}{s}}{0.0025} * 9.89\ m = -647.45 \frac{kg}{m*s^2} = -0.006\ bar$

(E 3.1-10) $f_f = \frac{(1-\bar{\varepsilon}_b)}{\bar{\varepsilon}_b}\left[1.75 + \frac{150(1-\bar{\varepsilon}_b)}{Re}\right] = \frac{1-0.4}{0.4}\left[1.75 + \frac{150(1-0.4)}{19.42}\right] = 22.45$

(E 3.1-11) $Re = \frac{\rho u d_p}{\mu} = \frac{974.89 \frac{kg}{m^3} * 0.0025 \frac{m}{s} * 0.003\ m}{0.0003765\ Pa*s} = 19.42$

(E 3.1-12) $V_{bed} = \pi \left(\frac{d_{bed}}{2}\right)^2 dz = \pi(\frac{9.89\ m}{2})^2 * 9.89\ m = 759.50\ m^3$

(E3.1-13) $\mathrm{m_{sorbent}} = \mathrm{V_{sorbent}}(1 - \bar{\varepsilon}_\mathrm{b})\rho_{\mathrm{sorbent}} = 759.50\ m^3 * (1 - 0.4) * 1400 \frac{kg}{m^3} =$ 1,063,297.5 kg

(E 3.1-18) $\dot{V}_{bed,2} = \frac{\dot{n}_{FeCl_3}}{1\ M} = \frac{1000 \frac{mol}{min}}{1\ M} = 1000\ L/min$

(E 3.1-19) $S = \frac{\left(\frac{c_{Li^+,sorbent}}{c_{Na^+,sorbent}}\right)}{\left(\frac{c_{Li^+,feed}}{c_{Na^+,feed}}\right)} = \frac{\frac{2.5}{0.5}}{\frac{1}{78}} = 390$

Primary Adsorption and Regeneration Times

$Li^+\ adsorbed$ = 2,658,243,740 mmol	Total amount of lithium ions adsorbed in the primary bed
$Li^+\ capacity$ = 2.5 mmol/g sorbent	Lithium ion uptake capacity in the sorbent
$Na^+\ adsorbed$ = 531,648,748 mmol	Total amount of sodium ions adsorbed in the primary bed
$Na^+\ capacity$ = 0.5 mmol/g sorbent	Sodium ion uptake capacity in the sorbent
$\dot{m}_{Li^+,feed}$ = 3.26 kg/min	Mass flow rate of lithium ions in the brine to one primary bed during primary adsorption
t_{ads} = 96 hours	Time for primary adsorption (rounded)
$Fe^{3+}\ in\ regen.fluid$ = 3,189,893 mols	Moles of iron (III) ions that regenerate the primary bed

$\dot{n}_{Fe^{3+}}$ = 1000 mol/min	Molar flow rate of iron (III) ions to the primary bed during primary regeneration
t_{regen} = 54 hours	Time for primary regeneration (rounded)

(E 3.1-14a) $Li^+\ adsorbed\ =\ Li^+\ capacity \cdot m_{sorbent} \cdot 1000 = 2.5 \frac{mmol}{g\ sorbent} *$

$1{,}063{,}297.50\ kg * \left(\frac{1000\ g}{1\ kg}\right) = 2{,}658{,}243{,}740$ mmol

(E 3.1-14b) $Na^+\ adsorbed\ =\ Na^+\ capacity \cdot m_{sorbent} \cdot 1000 = 0.5 \frac{mmol}{g\ sorbent} *$

$1{,}063{,}297.50\ kg * \left(\frac{1000\ g}{1\ kg}\right) = 531{,}648{,}748\ mmol$

(E 3.1-15) $\dot{m}_{Li^+,feed} = \frac{0.99 \cdot Li^+ adsorbed}{t_{ads}} \rightarrow t_{ads} = \frac{0.99 \cdot 2{,}658{,}243{,}740\ \text{mmol} * \left(\frac{1\ \text{mol}}{1000\ \text{mmol}}\right) * \left(\frac{6.94\ \text{g}}{\text{mol}}\right) * \left(\frac{1\ \text{kg}}{1000\ \text{g}}\right)}{3.26\ kg/min} *$

$\left(\frac{1\ hr}{60\ min}\right) = 96\ hours$

(E 3.1-16) $Fe^{3+}\ in\ regneration\ fluid\ =\ Li^+\ adsorbed\ +\ Na^+\ adsorbed\ =$

$\left(\frac{2{,}658{,}243{,}740\ \text{mmol}}{1000}\right) + \left(\frac{531{,}648{,}748\ \text{mmol}}{1000}\right) = 3{,}189{,}893$ mols

(E 3.1-17) $\dot{n}_{Fe^{3+}} = \frac{Fe^{3+}\ in\ regeneration\ fluid}{t_{regen}} \rightarrow t_{regen} = \frac{3{,}189{,}893\ mols}{1000\ mol/min} * \left(\frac{1\ hr}{60\ \text{min}}\right) = 54\ hours$

Electrochemical Cell Potential, Nernst Potential, and Gibbs' Free Energy

E^o_{cell} = 0.442 V (vs Ag/AgCl)	Standard cell potential for the overall primary adsorption reaction
$E^o_{reduction}$ = 0.242 V (vs Ag/AgCl)	Standard cell potential for the reduction half reaction during primary adsorption
$E^o_{oxidation}$ = -0.2 V (vs Ag/AgCl)	Standard cell potential for the oxidation half reaction during primary adsorption
E_{cell} = 0.579 V (vs Ag/AgCl)	Nernst cell potential for the overall primary adsorption reaction
R = 8.314 J/mol*K	Ideal gas constant
T = 75 C	Temperature of the brine
n = 1	Number of electrons transferred during the reaction

F = 96,485 Coulombs/mol	Faraday's constant
$[Fe^{3+}]$ = 0.01 wt/vol (with respect to [Fe^{2+}])	Concentration of iron (III) ions in the brine relative to iron (II) ions
$[Fe^{2+}]$ = 0.99 wt/vol (with respect to [Fe^{3+}])	Concentration of iron (II) ions in the brine relative to iron (III) ions
ΔG = -55,947 J/mol	Gibbs' Free Energy for primary adsorption

(Eq. 3.1-20) $E^o_{cell} = E^o_{reduction} - E^o_{oxidation} = 0.242\ V - -0.2\ V = 0.442\ V$

(E 3.1-21a) $E_{cell} = E^o_{cell} - \frac{RT}{nF}\ln\left(\frac{[Fe^{3+}]}{[Fe^{2+}]}\right) = 0.352\ V - \frac{8.314\frac{J}{mol*K}*(75\ C+273.15)}{96{,}485\frac{Coulombs}{mol}} * \ln\left(\frac{[Fe^{3+}]}{[Fe^{2+}]}\right) =$

$0.579\ V$

(E 3.1-22) $\Delta G = -nFE_{cell} = -96{,}485\frac{Coulombs}{mol} * 0.579\ V = -55{,}947\frac{J}{mol}$

Equilibrium Constant

K_{eq} = 247,918,461.8	Equilibrium constant for primary adsorption
ΔG = -55,947 J/mol	Gibbs' Free Energy for primary adsorption
R = 8.314 J/mol*K	Ideal gas constant
T = 75 C	Temperature of the brine

(E 3.1-23) $K_{eq} = e^{\left(-\frac{\Delta G}{RT}\right)} = e^{\left(-\frac{-55{,}947\frac{J}{mol}}{8.314\frac{J}{mol*K}*(75\ C+273.15)}\right)} = 247{,}918{,}461.8$

Biot Number

k_c = 4.59 * 10^{-5} m/s	External mass transfer coefficient
R = 0.0015 m	Radius of FP particle
$D^e_{A,B}$ = 1.35 * 10^{-5} cm^2/s	Effective diffusivity coefficient for species A (Li^+) in fluid B (brine)
K_c = 2.48 * 10^8	Equilibrium constant for primary adsorption

(E 3.1-28) $Bi = \frac{k_c \cdot R}{D^e_{A,B} \cdot K_c} = \frac{4.59*10^{-5}\frac{m}{s} * 0.0015\ m}{1.35*10^{-5}\frac{cm^2}{s} * (\frac{1m}{100cm})^2 * 2.48*10^8} = 2.06 * 10^{-7}$

Pump Design and Operating Requirements

$gravity\ head$ = 94,488.29 kg/m^3	Pressure drop the fluid flowing through P-103 experiences from gravity
ρ_{fluid} = 974.89 kg/m^3	Density of the brine
g = 9.8 m/s^2	Gravity
dz = 9.89 m	Height of one primary bed
P = 26,153.04 W	Power required by P-103
$differential\ pressure$ = 272,414.97 Pa	Differential pressure for P-103
$\dot{V}_{fluid,pump}$ = 0.10 m^3/s	Volumetric flow of brine through P-103

(E 3.1-29) $gravity\ head = \rho_{fluid} \cdot g \cdot dz = 974.89 \frac{kg}{m^3} * 9.8 \frac{m}{s^2} * 9.89\ m = 94{,}488.29 \frac{kg}{m*s^2}$

(E 3.1-30) $P = differential\ pressure \cdot \dot{V}_{fluid,pump} = 272{,}414.97\ Pa * 0.10 \frac{m^3}{s} = 26{,}153.04\ W$

Holding Tank/Silo Sizing

m_i = 924851.17 kg	30 days' worth of $FeCl_2$ (s)
$\dot{m}_i$ = 33.79 kg/min	Mass flow rate of $FeCl_2$ (s) out of S 1-1
$t_{flow,i}$ = 5760 min*4.75	Time that $FeCl_2$ (s) flows out of S 1-1 within a period of 30 days (4.75 cycles/30 days)
$V_{HT,i}$ = 479.20 m^3	Volume of S 1-1
ρ_i = 1930 kg/m^3	Density of $FeCl_2$ (s)

(E 3.1-31) $m_i = \dot{m}_i \cdot t_{flow,i} = 33.79 \frac{kg}{min} * 5760\ min * 4.75 = 924{,}851.17\ kg$

(E 3.1-32) $V_{HT,\,i} = \frac{m_i}{\rho_i} = \frac{924{,}851.17\ kg}{1930\ kg/m^3} = 479.20\ m^3$

Counter-Current Heat Exchanger Sizing and Operating Requirements

$\dot{m}_c$ = ?	Rate of cooling water at 30 C (kg/s)
Q = -638,210 W	Heat Duty of HX 3-1
$C_{p,c}$ = 4,182 J $kg^{-1}K^{-1}$	Heat Capacity of Water at 30 C
ΔT_c = 15 C	Temperature difference of cooling water
ΔT_{lm} = *?*	Logarithmic mean temperature difference
ΔT_1 = 22.9 C	Temperature difference of entering slurry and exiting cooling water
ΔT_2 = 20 C	Temperature difference of exiting slurry and entering cooling water
A = *?*	Required heat exchanger area
U_0 = 850 W $m^{-2}K^{-1}$	Overall heat transfer coefficient, estimated for water-liquid exchanging

(E 3.1-33) $\dot{m}_c = \frac{-Q}{C_{p,c}\Delta T_c} = \frac{638210\ W}{\left(4182\ \frac{J}{kg\ K}\right)(15\ C)} = 10.17\ kg/s$

(E 3.1-34) $\Delta T_{lm} = \frac{\Delta T_1 - \Delta T_2}{\ln\left(\frac{\Delta T_1}{\Delta T_2}\right)} = \frac{22.9\ C - 20\ C}{\ln\left(\frac{22.9\ C}{20\ C}\right)} = 21.47\ C$

(E 3.1-35) $A = \frac{Q}{U_0 \Delta T_{lm}} = \frac{638210\ W}{(850\ \frac{W}{m^2 K})(21.47\ C)} = 35.06\ m^2$

Adsorption and Regeneration Steady State Iron (II) and (III) Chloride Mass Flows

$n_{Fe^{3+},overall}$ = *10,980,000 mols*	Moles of iron (III) ions needed per cycle
$\dot{n}_{Fe^{3+},p}$ = *1000 mol/min*	Molar flow of iron (III) ions to primary regeneration
$t_{regen,p}$ =*54 hours*	Time for primary regeneration
$\dot{n}_{Fe^{3+},s}$ = *1000 mol/min*	Molar flow of iron (III) ions to secondary regeneration
$t_{regen,s}$ = *7.5 hours*	Time for one cycle of secondary regeneration

$\dot{n}_{Fe^{3+},supplement}$ = *42,772.28 mol/hr*	Steady state supplementary molar flow of iron (III) ions to each cycle
$t_{overall}$ = *151.5 hours*	Time for one cycle
$\dot{n}_{Fe^{3+},ED}$ = *29,702.97 mol/hr*	Steady state molar flow of iron (III) ions from electrodialysis
$\dot{m}_{Fe^{3+},supplement}$ = *6937.45 kg/hr*	Steady state supplementary mass flow of iron (III) ions to each cycle
MW_{FeCl3} = *162.195 g/mol*	Molecular weight of $FeCl_3$
$n_{Fe^{2+},overall}$ = *11,520,000 mols*	Moles of iron (II) ions needed per cycle
$\dot{n}_{Fe^{2+},P}$ = *1000 mol/min*	Molar flow of iron (II) ions to primary adsorption
$t_{ads,p}$ = *96 hours*	Time for primary regeneration
$\dot{n}_{Fe^{2+},overall}$ = *76039.60 mol/hr*	Steady state mass flow of iron (III) ions per cycle
$\dot{m}_{Fe^{2+},overall}$ = *9637.64 kg/hr*	Steady state mass flow of iron (II) ions per cycle
MW_{FeCl_2} = *126.745 g/mol*	Molecular weight of $FeCl_2$

(E 4.1-1) $n_{Fe^{3+},overall} = 2\left(\dot{n}_{Fe^{3+},p} \cdot t_{regen,p} + \dot{n}_{Fe^{3+},s} \cdot t_{regen,s} \cdot 5\right) = 2\left(1000\frac{mol}{min} * 54\ hours * \frac{60\ min}{1\ hr} + 1000\frac{mol}{min} * 15.5\ hours * \frac{60\ min}{1\ hr} * 5\right) = 10{,}980{,}000\ mols$

(E 4.1-2) $\dot{n}_{Fe^{3+},supplement} = \frac{n_{Fe^{3+},overall}}{t_{overall}} - \dot{n_{Fe^{3+},ED}} = \frac{10{,}980{,}000\ mols}{151.5\ hrs} - 29{,}702.97\frac{mol}{hr} = 42{,}772.28\frac{mol}{hr}$

(E 4.1-3) $\dot{m}_{Fe^{3+},supplement} = \dot{n}_{Fe^{3+},supplement} \cdot MW_{FeCl_3} \cdot \left(\frac{1\ kg}{1000\ g}\right) = 42{,}772.28\frac{mol}{hr} * \frac{162.195\ g}{mol} * \left(\frac{1\ kg}{1000\ g}\right) = 6937.45\frac{kg}{hr}$

(E 4.1-4) $n_{Fe^{2+},overall} = 2 \cdot \dot{n}_{Fe^{2+},P} \cdot t_{ads,p} = 2 * \frac{1000\ mol}{min} * 96\ hours * \frac{60\ min}{1\ hr} = 11{,}520{,}000\ mols$

(E 4.1-5) $\dot{n}_{Fe^{2+},overall} = \frac{n_{Fe^{2+},overall}}{t_{overall}} = \frac{11{,}520{,}000\ mols}{151.5\ hours} = 76039.60\frac{mol}{hr}$

(E 4.1-6) $\dot{m}_{Fe^{2+},overall} = \dot{n}_{Fe^{2+},overall} \cdot MW_{FeCl_2} \cdot \left(\frac{1\,kg}{1000\,g}\right) = 76039.60\,\frac{mol}{hr} * 126.745\,\frac{g}{mol} *$

$\left(\frac{1\,kg}{100}\right) = 9637.64\ \frac{kg}{hr}$

Standard Reduction Potential of Electrodialysis Overall Reaction

$E^o_{oxd} = 0.77\,V$	Standard Redox Potential of Oxidation Reaction
$E^o_{red} = -0.827\,V$	Standard Redox Potential of Reduction Reaction
$\Delta Ee = ?$	Equilibrium Redox Potential

$E^o_{oxd} - E^o_{red} = \Delta Ee$

$\Delta Ee =$ 0.77 – (-0.827 V)

$\Delta Ee = 1.597\,V$

Membrane Potential Drop

$(IR)m = ?$	Potential drop across membrane
$J = 0.24\,A/cm^2$	Current Density
$A = ?$	Area
$l = 0.0183\,cm$	Path length or thickness of membrane
$k = 0.013\,S/cm$	Ionic conductivity

$(IR)m = J * A * \frac{l}{kA}$

$(IR)m$ = 0.24 $A/cm2$ * 0.0183 cm/ 0.013 S/cm

$(IR)m = 0.338\,V$

Required Operating Voltage

$\Delta Ee = 1.597\,V$	Equilibrium Redox Potential

$\eta a = 0.074\ V * \frac{2400\ A/m^2}{3500\ A/m^2} = 0.051\ V$	Anodic overpotential
$\eta c = 0.536\ V * \frac{2400\ A/m^2}{3500\ A/m^2} = 0.368\ V$	Cathodic overpotential
$(IR)a = 0.368\ V$	Potential drop across anode
$(IR)c = 0.55\ V$	Potential drop across cathode
$(IR)m = 0.338\ V$	Potential drop across membrane
V_{cell} =?	Operating Potential of the Cell

(E. 3.2-1) $V_{cell} = \Delta Ee + \eta a + |\eta c| + (IR)a + (IR)c + (IR)m$

$V_{cell} = 1.597 + (0.074\ V * \frac{2400\ A/m^2}{3500\ A/m^2}) + (0.536\ V * \frac{2400\ A/m^2}{3500\ A/m^2}) + 0.368 + 0.55 + 0.338$

$V_{cell} = 3.69$ V

Theoretical Current Needed for Production Rate of LiOH

$I_{theor} = ?$	Theoretical current required to move Li^+ ions
$m_{theory} = 56\ g$	Mass of Li^+ ions to be moved
$t = 1\ second$	Timescale
$z = 1$	Number of electrons per ion
$F = 96484.5 \frac{As}{mol}$	Faraday's constant
$Mw = 6.941\ g/mol$	Molecular weight

(E. 3.2-2) $I_{theory} = \frac{m_{theor}}{t} * z * \frac{F}{Mw}$

$I_{theor} = 56\ g\ Li/1\ s$ *1*96484.5 As/mol / 6.941 g/mol

$I_{theor} = 778433.5$ A

Osmotic Pressure and Activity of Water

$\pi = ?$	Osmotic Pressure
$c_T = 2.53\ mol/L$	Molar concentration of ions
$R = 0.08206\ L\ atm/\ mol\ K$	Ideal Gas Constant
$T = 348\ K$	Temperature
a_w =?	Activity of water
$\overline{V_w} = 0.018\ L/mol$	Molar Volume of water

(E. 3.2-3 & 3.2-4) $\pi \cong c_T RT = -\ln(a_w)\frac{RT}{\overline{V_w}}$

2.53 mol ions/L = $-\frac{ln(a_w)}{0.018\ L/mol}$

$a_w = 0.955$

Raoult's Law

$y_w = ?$	Fraction of gas phase that is water
$P = 1\ atm$	Pressure
$x_w = \frac{a_w}{\gamma_w}$	Fraction of liquid phase that is water
$\gamma_w = \frac{a_w}{x_w}$	Activity coefficient of water
$P_w^{sat}[T]$ =*0.3809 atm*	Saturation pressure at specified temperature
$a_w = 0.955$	Activity of water

(E. 3.2-5) $y_w P = x_w \gamma_w P_w^{sat}[T] = a_w P_w^{sat}[T]$

$y_w * 1 = 0.955 * 0.3809\ atm$

$y_w = 0.36$

Number of Electrodialysis Cells

I = *778433.5 A*	Operating Current
$J = 2400\ A/m^2$	Current Density
A_{cell} = 3.4 m^2	Electrode area per cell
$n = ?$	Number of cells

$J = \frac{I}{A_{cell} n}$

$2400 \frac{A}{m^2} = \frac{778433.5\ A}{3.4\ m^2 * n}$

$n = 95.4 \approx$ 100 cells

Power Calculation

P = ?	Electrical Power
I = 778433.5 A	Operating Current
$\eta = 0.70$	Current Efficiency
V = 3.69 V	Voltage

(E. 3.2-6) $P = \frac{I}{\eta} * V$

P = $\frac{778433.5\ A}{0.70}$ * 3.69 V

P = 4106939.454 W

Crystallizer Unit Sizing

$\dot{V} = 443.76\ L/min$	Inlet volumetric flowrate
$\tau = 15\ min$	Residence time
$\frac{L}{D} = 3$	Length/Diameter Ratio
$V = ?$	Volume required

$$V = 1.6(V)(\tau) = 1.6\left(443.76\ \frac{L}{min}\right)\left(15\ \text{min}\right)\left(\frac{1\ m}{1000\ L}\right) = 10.65\ m^3$$

(E 3.3-1) $D = \sqrt[3]{\frac{4V}{3\pi}} = \sqrt[3]{\frac{4(10.65 m^3)}{3\pi}} = 1.65\ m$

$L = 3D = 3(1.65\ m) = 4.95\ m$ → upsize to 5.25 m from vendor (Swenson Tech)

Rotary Filter Sizing

$n = 0.00833\ s^{-1}$	Filter speed
$f = 0.3$	Fraction of filter submerged in slurry
$\Delta P = 25331.25\ Pa$	Pressure drop in filter
$a_0 = 1.35 * 10^{10}\ \frac{m}{kg}$	Specific cake resistance
$\dot{m}_s = 0.315\ \frac{kg}{s}$	Mass flow rate of inlet solid
$c = 226\ \frac{kg}{m^3}$	Solid mass per volume filtrate
$\mu = 0.005474\ Pa * s$	Viscosity of water at 50 C
$\dot{V}_f = 0.00139\ \frac{m^3}{s}$	Flow rate of exiting filtrate
$A = ?$	Filter area required
$P = ?$	Power required

$$\textit{(E 3.3-2)}\ A = \dot{m}_s\left(\frac{a_0\mu}{2c\Delta Pf}\right)^{\frac{1}{2}} = \left(0.315\frac{kg}{s}\right)\left(\frac{\left(1.35*10^{10}\frac{m}{kg}\right)(0.005474\ Pa*s)}{2\left(226\frac{kg}{m^3}\right)(25331.25\ Pa)(0.3)(0.00833\ s^{-1})}\right)^{\frac{1}{2}} =$$

$5.06\ m^2 \rightarrow 5.2\ m^2\ from\ vendor$

$$P = \dot{V}_f * \Delta P = \left(0.00139\frac{m^3}{s}\right)(25331.25\ Pa) = 35$$

Rotary Vacuum Sizing

$t = 1\ hr$	Dryer holdup time
$\dot{V}_c = 1.227\ \frac{m^3}{hr}$	Volume of cake entering
$V = ?$	Required dryer volume
$\frac{L}{D} = 12$	Length/diameter ratio
$SA = ?$	Heating surface area

$$V = 1.66\dot{V}_c t = 1.66\left(1.227\frac{m^3}{hr}\right)(1hr) = 2.037\ m^3$$

$$D = \sqrt[3]{\frac{4V}{12\pi}} = \sqrt[3]{\frac{4(2.037m^3)}{12\pi}} = 0.6\ m$$

$$L = 12D = 12(0.6m) = 7.2\ m$$

$$SA = \pi DL + \frac{\pi}{2}D^2 = \pi(0.6m)(7.2m) + \frac{\pi}{2}(0.6m)^2 = 14.14\ m^2$$

Belt Feeder Sizing

$\dot{V}_c = 1.227\ \frac{m^3}{hr}$	Volume of cake entering
$L = 10\ m$	Belt length
$W = 0.301\ m$	Belt width
$u = 0.051\ m/s$	Belt velocity
$h = ?$	Est. cake height

$$h = \frac{\dot{V}_c}{u * W} = \frac{1.227\ \frac{m^3}{hr}}{(0.051\ \frac{m}{s})(0.301m)} = 0.022\ m$$

Silo Sizing- Crystallization Block

$\dot{V}_s = 0.8185\ \frac{m^3}{hr}$	Volumetric flow of solid
$t = 30\ days = 720\ hours$	Holding time
$\frac{L}{D} = 3$	Length/diameter ratio
$w = 0.05\ m$	Est. wall thickness
$V_{required} = ?$	Required volume
$V_{actual} = ?$	Actual volume

$V_{required} = 1.5\dot{V}_s t = 1.5\left(0.8185\frac{m^3}{hr}\right)(720\ hrs) = 884\ m^3$

(E 3.3-1) $D = \sqrt[3]{\frac{4V}{3\pi}} = \sqrt[3]{\frac{4(884m^3)}{3\pi}} = 7.21\ m$

$L = 3D = 3(7.21m) = 21.64\ m$

$V_{actual} = \pi(w + D)^2(w + L) = \pi(0.05m + 7.21m)^2(0.05m + 21.64m) = 898\ m^3$

Appendix B: Economic Calculations

B.1 Sample Calculations for Operating Costs

Chemical Cost Estimation

$\dot{m}_{PC}$ = 348.49 kg/min	Mass flow of potassium citrate added primary and the first secondary adsorption steps per cycle
t_{PC}= 9000 min	Time that potassium citrate is flowing into the cycle
N_{cycles}= 58	Number of cycles per year
f_o = 0.9	Plant operating fraction
$Price\ for\ Potassium\ Citrate$ = \$1.10/kg	

$$Final\ Cost = \dot{m}_{PC} * t_{PC} * N_{cycles} * f_o * \$1.10$$
$$= 348.49 \frac{kg}{min} * 9000\ min * 58 * 0.9 * \$1.10\ kg = \$60{,}606{,}149.76$$

Electricity Cost Estimation

$P_{required} = 7.165\ kW$	Power requirement of Compressor 3-1
$t = 7{,}884\ hrs$	Annual operating time
$Cost\ of\ Electricity = \$0.35\ per\ kWh$	

$$Final\ Cost = \$0.35 * (7.165\ kW)(7884\ hrs) = \$19{,}772.06$$

Cost of Water Estimation

$Reported\ Price\ of\ Water\ in\ 2016 = \$5.85\ per\ kilogallon$

$2016\ CEPCI$: 541.7

$Current\ CEPCI$: 800

$t = 7{,}884\ hrs$	Annual operating time
$\dot{m}_c = 267.93\ kg/hr$	Total water required for crystallizer block
$\rho = 995\ \frac{kg}{m^3}$	Density of water at 30 C

$$\frac{\$5.85}{kgal} * \frac{1\ kgal}{3.785\ m^3} * \frac{1\ m^3}{995\ kg} = \$0.00155\ per\ kg$$
$$\$0.00155 * \left(\frac{800}{541.7}\right) = \$0.0023\ per\ kg\ (current)$$

$$Annual\ Cost = \dot{m}_c t(\$0.0023) = \left(267.93\frac{kg}{hr}\right)(7884\ hr)\left(\frac{\$0.0023}{kg}\right) = \ \$4{,}858.60$$

B.2 Sample Calculations for Capital Costs

Capital Cost Estimation from Towler & Sonnett
Note: A table listing the variables associated with different equipment cost estimations can be found on page 253 of Chemical Engineering Design - Principles, Practice and Economics of Plant and Process Design (3rd Edition).

$S = 1.9827\ \frac{L}{s}$	Volumetric flow entering P-302 (size parameter)
$a = 8000$	
$b = 240$	
$n = 0.9$	
$f = 1.3$	Material cost factor for 316 stainless steel
2010 $CEPCI$: 532.9	
$Current\ CEPCI$: 800	

(E 5.1-1) $C_e = a + bS^n = 8000 + (240)(1.9827)^{0.9} = \$8{,}444.38$

(E 5.1-2) $C = \left(\frac{800}{532.9}\right) f C_e = 1.5(1.3)(\$8{,}444.38) = \$16{,}479.93$

$Accounting\ for\ spare\ pump$: $2 * C = \$32{,}959.85$

B.3 Additional Economic Calculations

Product Revenue

$P = \frac{\$65}{kg}$	Bulk price of lithium hydroxide monohydrate
$\dot{m}_p = 1222.62\ \frac{kg}{hr}$	Production rate
$t = 7{,}884\ hrs$	Operation time

$$R = (P)\left(\dot{m}_p\right)(t) = (\$65)(1222.62)(7{,}884) = \$626{,}544{,}045.90$$

Appendix C: Supplementary Files

File Name	File Type	Description
GLEP Calcs.xlsx	Excel Spreadsheet	Design and operating calculations for each block of the process
Plant Economics.xlsx	Excel Spreadsheet	Detailed economic calculations by block and for the whole process
Crystallization Final Design.bkp	Aspen Plus V14 Backup File	Full modeling of crystallization unit
Condensing Steam.bkp	Aspen Plus V14 Backup File	Modeling HX 3-2 and 3-3 to get respective heat duties
Compressor Modeling.bkp	Aspen Plus V14 Backup File	Modeling CMPSR 3-1 to get hydraulic power
InletBrineCooler.bkp	Aspen Plus V14 Backup File	Heat Exchanger modeling for HX 1-1 and 1-2
FC Compressors.bkp	Aspen Plus V14 Backup File	Gas (air, hydrogen) compressor modeling for fuel cell block